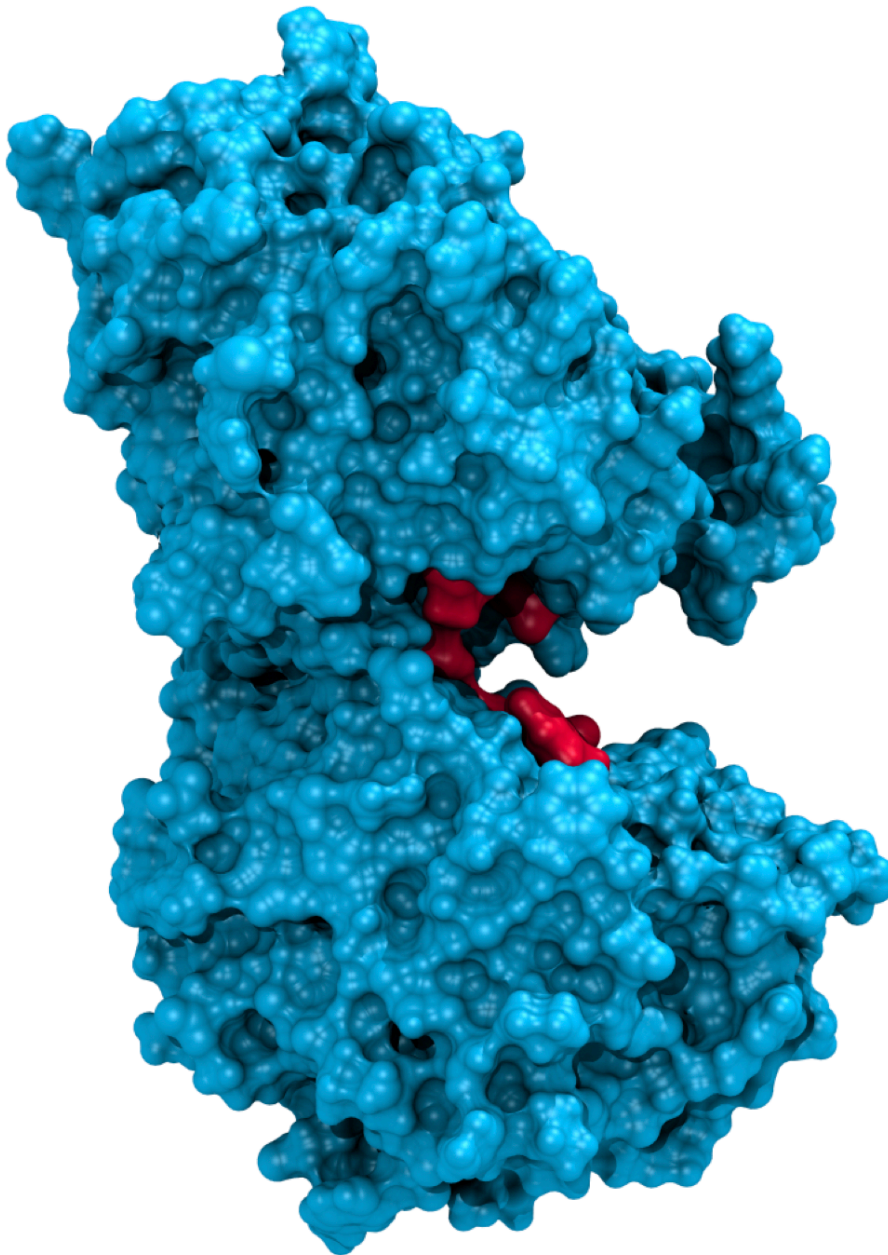UiT

THE ARCTIC
UNIVERSITY
OF NORWAY

Faculty of Health Sciences

Department of Medical Biology

Ligand binding and dynamics of the GABA$_B$ receptor Venus flytrap domain

—

Linn Samira Mari Evenseth
A dissertation for the degree of Philosophiae Doctor – October 2019

Contents

Acknowledgement

I would like to express my gratitude to my main supervisor Professor Ingebrigt Sylte for being an absolutely great mentor! You have given me so many opportunities, showed me a lot of trust by encouraging my work and by allowing me to attend conferences and represent the group on many locations. I am truly grateful for your continuous motivation and support. Thank you so much for always being available (and all the time you have used during these years) to discuss, answer question and share your knowledge!

Further I would like to address my outermost appreciation to my excellent co-supervisors Assoc.Prof. Mari Gabrielsen, Assoc. Prof. Kurt Kristiansen and dr. Imin Wushur. Mari, you have been a tremendous support and source of inspiration during these years. You have been available almost around the clock on countless occasions, especially while I've been abroad, regaining my confidence whenever necessary. Your detail-oriented mind, all our discussions and talks, and your knowledge has been crucial along this whole process. Imin, thank you for always listening to my ideas, numerous discussions and sharing your insight regardless of the hour and the place. I have so many good memories from the days and nights in the lab. Kurt, you got me into modelling during my M.Sc. when you enthusiastically supervised an *in Silico* lab. exercise in 2013. Thank you for sharing all your knowledge, discussions and for always being supportive!

I would also like to thank all the current and former fellow PhD/Master students at the group; Thibaud, Krishanti and Fatema, thank you for good discussions and advices. I would like to give a special thanks to you Fatema. Thanks for the years together in the office.

I would like to express my appreciation to Professor Andrezj Bojarski. Andrezj, you have kindly allowed me to visit your group multiple times, and from the first time I have felt included to the point that Krakow now feels like my second home. I am truly appreciative of our collaboration, your kindness, all our talks and discussions!

I would like to thank Dr. Dawid Warszycki. The first time I visited Krakow, I was told that you got angina and I thought you were dead. It turned out that the angina was toothache and luckily you came back to work. We have worked closely together for quite some time and along the course you have become a dear friend. A friendship that comes with a lot of scientific discussions, new ideas, a great deal of knowledge, work and vodka.

I would like to thank professor Andrea Cavalli for allowing me to join his excellent group in Bologna, supervising me on enhanced sampling, sharing knowledge and providing all necessary resources.

I would like to express my gratitude to Assoc.Prof Matteo Masetti for his extraordinary supervision. Matteo, with your passion and great amount of knowledge, you have been a source of inspiration. I am honored that I got to spend two periods with you at the lab!

List of Papers

This thesis is based on the three following papers:

I.   **In Silico Methods for the Discovery of Orthosteric GABA$_B$ Receptor Compounds,**
      Linn M. Evenseth, Dawid Warszycki, Andrzej J. Bojarski, Mari Gabrielsen and Ingebrigt Sylte,
      Molecules, 2019, DOI 10.3390/molecules24050934

II.   **Identification of orthosteric GABA$_B$ receptor compounds by Virtual Screening,**
      Linn S.M. Evenseth, Imin Wushur, Dawid Warszycki, Andrzej J. Bojarski, Mari Gabrielsen and Ingebrigt Sylte
      Manuscript, 2019

III. **Exploring the conformational dynamics of the extracellular Venus flytrap domain of the GABA$_B$ receptor: a path-metadynamics study,**
      Linn S.M. Evenseth, Riccardo Ocello, Mari Gabrielsen, Matteo Masetti, Ingebrigt Sylte, and Andrea Cavalli
      Manuscript, 2019

Abbreviations

AC – Adenylyl Cyclase

ADMET – Absorption, Distribution, Metabolism, Excretion and Toxicity

AMPA – α-amino-3-hydroxy-5-methyl-4-isoxazole proprionic acid

ATP – Adenosine Triphosphate

BBB – Blood-Brain-Barrier

BRET – Bioluminescence Resonance Energy Transfer

CaMKII – Calmodulin-dependent Protein Kinase II

cAMP – Cyclic Adenosine Monophosphate

CaSR – Calcium Sensing Receptor

cGMP – Cyclic Guanosine Monophosphate

CHO – Chinese Hamster Ovarian

cMD – Classical Molecular Dynamics

CNS – Central Nervous System

Cryo-EM – Cryogenic Electron Microscopy

CV – Collective Variable

GDP – Guanosine Diphosphate

DMSO – Dimethyl sulfoxide

EPSP – Excitatory Postsynaptic Potential

ERK 1/2 – Extracellular signal-regulated kinase 1/2

FDA – Food and Drug Administration

FES – Free Energy Surface

FF – Force Field

FP – Fluorescence polarization

fs – Femtoseconds

GABA – γ-aminobutyric acid

GAD –Glutamate decarboxylase

GAT – GABA Transporter

GHB – γ-hydroxybutyrate

GIRK - G-protein Coupled Inwardly Rectifying K^+ channel

GDP – Guanosine Diphosphate

GPCR – G-protein-coupled receptor

G-protein – Guanine nucleotide binding protein

GRKs – G-protein coupled receptor kinases

GTP – Guanosine Triphosphate

HBSS – Hank´s Balanced Salt Solution

HTS – High Throughput Screening

HTVS – High Throughput Virtual Screening

ICM – Internal Coordinate Mechanics

IFD – Induced Fit Docking

IPSP – Inhibitory Postsynaptic Potential

ITC – Isothermal titration calorimetry

KA – Kainate

KCTD – Potassium Channel Tetramerization Domain proteins

LB – Ligand Binding

LB1 – Lobe 1

LB2 – Lobe 2

LBDD – Ligand-based Drug Design

LBVS – Ligand-based Virtual Screening

LIA – Linear Interaction Approximation

LIE – Linear Interaction Energy

LTP - Long-Term Potentiation

MD – Molecular Dynamics

MetaD – Metadynamics

mGluR – Metabotropic Glutamate Receptor

MM – Molecular Mechanics

MM-GBSA – Molecular mechanics Generalized-born surface area

ms – millisecond

nAChR – Nicotine Acetylcholine Receptors

NAM – Negative Allosteric Modulators

NEM – N-ethylmaleimide

NMDA – N-methyl-D-aspartate

NMR - Nuclear Magnetic Resonance Spectroscopy

PAM – Positive Allosteric Modulators

PES – Potential Energy Surface

PDM – Post-docking minimization

PKA – Protein Kinase A

PKC – Protein Kinase C

PKG – Protein Kinase G

PLC – Phospholipase C

PNS – Peripheral Nervous System

PSA – Polar Surface Area

ps – Picosecond

QM – Quantum Mechanics

QSAR – Quantitative Structure Activity Relationship

RGS – Regulators of G-protein signaling

SAM – Silent Allosteric Modulator

SBDD – Structure-based Drug Design

SBVS – Structure-based Virtual Screening

smFRET – single-molecule Förster resonance energy transfer

SNARE – SNAP receptor, where SNAP – Soluble NSF attachment protein and NSF – N-ethylmaleimide sensitive factor

SP – Standard Precision

SPC – Simple Point Charge

SP**R** – Surface plasmin resonance

TIP3P – Transferable Intermolecular Potential 3P

TM – Transmembrane

VFT – Venus flytrap

VMD – Visual molecular dynamics

VGCC - Voltage-gated Ca^{2+} Channel

VS – Virtual Screening

VSW – Virtual Screening Workflow

WT – Wild type

WT-MetaD – Well-Tempered Metadynamics

XP – Extra Precision

μs – Microsecond

3D – Three dimensional

Abstract

The γ-amino-butyric-acid (GABA) is the main inhibitory neurotransmitter in the central nervous system (CNS) and exerts its physiological role by binding to the ionotropic $GABA_A$ and $GABA_C$ receptors and the metabotropic $GABA_B$ receptor ($GABA_B$-R). The $GABA_B$-R is an obligate heterodimer that belongs to class C of guanine-binding proteins (G-protein) coupled receptors (GPCRs). Each monomer, $GABA_{B1a/b}$ and $GABA_{B2}$, is comprised of an extracellular bi-lobed domain connected by a short loop to a heptahelical transmembrane domain (7TM). The extracellular domain is called the Venus flytrap (VFT) due to the architectural and mechanical resemblance to the carnivorous flower. The $GABA_{B1a/b}$ VFT contains the orthosteric GABA binding site, while the 7TM domain of $GABA_{B2}$ hosts an allosteric binding site and is responsible for binding of G-proteins.

Previous studies have shown that the $GABA_B$-R is associated with numerous neurological and neuropsychiatric disorders including learning and memory deficits, depression and anxiety, addiction and epilepsy. The role of $GABA_B$-R in pathophysiology makes it an exciting target for drug interventions, especially since there is only one drug on the market targeting the receptor, the agonist baclofen. At present, there are few known available orthosteric $GABA_B$-R ligands and the majority of them are analogues or derivatives of GABA. The low structural diversity of known ligands may indicate that the conformational space of orthosteric ligands and the orthosteric binding site is not fully explored. The complex activation mechanisms of the $GABA_B$-R and concepts such as ligand bias, where activation of GPCRs favors one intracellular signaling pathway, and allosteric modulation of signaling effects, emphasize the benefits of discovering new orthosteric ligands that can promote advantageous- and/or block potential adverse effects, either alone or in combination with allosteric modulators. The three dimensional (3D) structure of the full $GABA_B$-R has not been resolved, but nine crystal structures of the VFTs co-crystalized with agonists or antagonists have been published. Based on knowledge from other class C members, the receptor is presumed to undergo comprehensive structural rearrangements when activated, starting from stabilization of the extracellular $GABA_{B1a/b}$ VFT in a closed conformation and transduction of the signal to the 7TM of the $GABA_{B2}$ and binding of G-proteins.

On the background of the limited number of agonist and antagonist, we tested the applicability of both classical structure-based and ligand-based methods in a virtual screening (VS) workflow to discover novel orthosteric ligands targeting the $GABA_B$-R. The methods found to be reliable were further applied in a VS study to retrieve potential candidates from databases of altogether 8.2 million commercially available compounds. A total of 34 ligands were bought and tested in a functional cAMP assay using Wild Type (WT) Chinese hamster ovary (CHO) cells and CHO-K1 cells stably overexpressing the human $GABA_B$-R. All compounds have been tested in the wild type cells, while eight have so far been tested in the $GABA_B$-R cells, and two have showed antagonistic properties. In paper 3, classical

molecular dynamics (MD) simulations were used to gain insight into the structural movements of the VFT, and investigate potential stable receptor conformations in absence of ligands. Analysis and concatenation of the MD trajectories showed reaction coordinates for the open-close transition, but the transition could not be observed in individual simulations. Frames were extracted and connected to represent motions of the VFT as a path collective variable to study the free energy surface associated with the transitions in a Well-Tempered metadynamics stimulations. The results show that the barriers between the open/inactive and closed/active conformation is high, indicating that a ligand is needed for receptor transition.

1 Introduction

1.1 Neurotransmission and neurotransmitters

The nervous system can be separated into two major parts based on function and structure, the central nervous system (CNS) and peripheral nervous system (PNS). The CNS consists of the spinal cord and the brain, while the PNS is a collection of all nerves outside this area and is responsible for transmitting signals to the CNS (called afferent or sensory neurons) and from the CNS (called efferent or motor neurons) (Costanzo, 2010).

The nervous system is comprised of neurons (nerve cells) that are specialized in receiving and conducting electrochemical impulses from other neurons or cells. A neuron consists of a cell body, called soma, with dendrites and an axon extending from the soma (Fig. 1). The dendrites are branched extensions of the cell body capable of conducting impulses to the cell body, while the axon is a long extension of the cell body responsible for communication with other neurons by transmitting the received impulses from the dendrites (Barrett and Ganong, 2010).
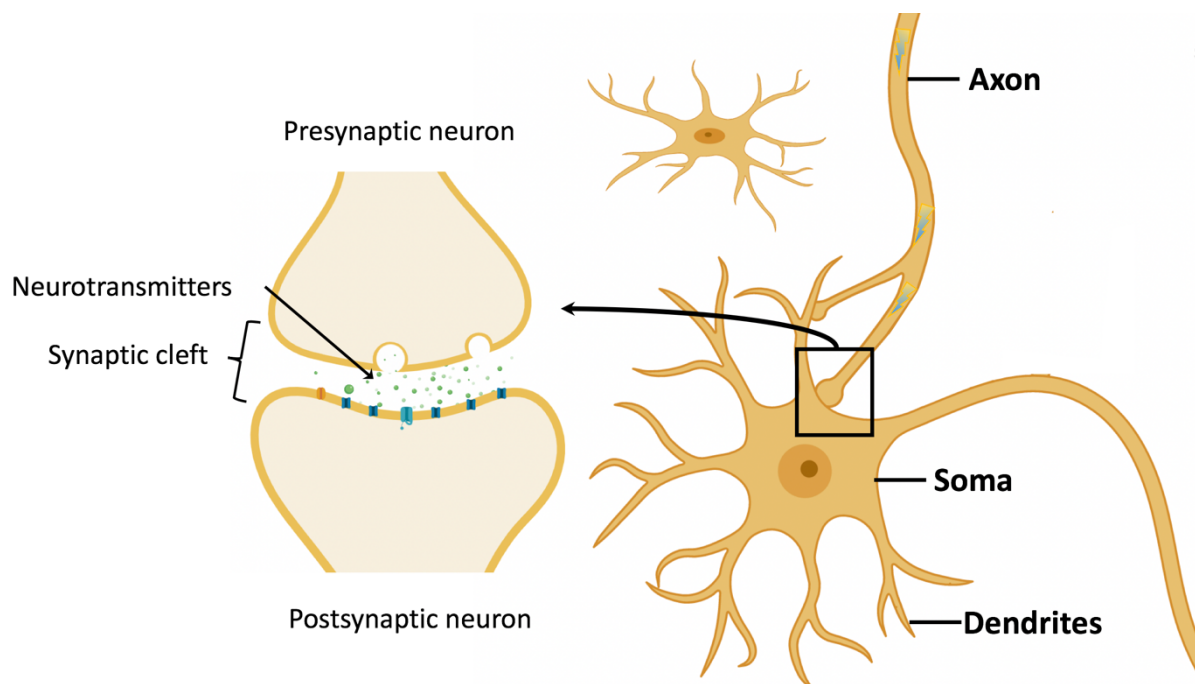
Figure 1 – An illustration of a network of neurons with typical neuron structures and the chemical synapses. Depolarization of a neuron causes an action potential to travel through the axon and causes vesicles filled with neurotransmitters to merge with the membrane and be released into the synaptic cleft.

The impulses are electrochemical waves travelling along the axon that can cause a release of molecules (ions, neurotransmitters) from terminals of the presynaptic cell into the synaptic cleft, that act on the postsynaptic cell (Battista et al., 2015). The impulses are triggered by voltage-gated sodium (Na^+) channels in the cell membrane of the neuron, and are called action potentials. The resting membrane potential of a nerve cell is -70 mV, and the sodium-potassium ion pump bound to adenosine triphosphate (ATP) is an important contributor to regulating and balancing the membrane potential (Battista et al., 2015). Action potentials occur when a stimulus, e.g. a neurotransmitter, causes influx of cations resulting in a more positive cell body, and when the current reaches the critical threshold of -55 mV the action potential is triggered (Battista et al., 2015). The event activates voltage-gated sodium channels at the axon closest to the cell body, which becomes depolarized and sends the signal further down the axon.

The impulses received by dendrites and the transmission conducted by axons are conveyed in the synaptic cleft. In the synaptic cleft, the plasma membrane of the presynaptic cell comes into close proximity with the membrane of the target neuron (postsynaptic cell) (Fig. 1). There are billions of neurons in the brain that communicate via chemical and electrical synapses. Electrical synapses are directly coupled by a physical connection between the pre- and postsynaptic neuron that allows ions to flow directly from one neuron to another (Pereda, 2014). Chemical synapses encompass release of the chemical messengers, neurotransmitters, from the presynaptic neuron to a receiving cell or neuron and are the most common type of synapses (Barrett and Ganong, 2010; Pereda, 2014).

Neurotransmitters themselves are produced by presynaptic neurons and stored in synaptic vesicles. More than 100 different neurotransmitters have been identified and divided into two main classes in humans; small-molecule neurotransmitters and neuropeptides (Barrett and Ganong, 2010). The small molecule neurotransmitters include amino acid transmitters like glycine, γ-aminobutyric acid (GABA), and glutamate, bioaminergic neurotransmitters such as dopamine, noradrenaline, adrenaline, histamine and serotonin synthesized from amino acid precursors, and purinergic neurotransmitters such as ATP and adenosine. Acetylcholine is also a small molecule neurotransmitter. The neuropeptides contain three or more amino acids and include substances such as the endorphins (Barrett and Ganong, 2010).

Following release of the neurotransmitters to the synaptic cleft, receptors present on surrounding postsynaptic cells can bind neurotransmitters released by presynaptic cells and either inhibit, excite or modulate the postsynaptic cell (Fig. 1) (Barrett and Ganong, 2010). The

nature of the neurotransmitter as inhibitory or excitatory depends on the target receptor. For example acetylcholine gives an excitatory function on neuromuscular junctions causing muscles to contract by binding to nicotinic acetylcholine receptors (nAChRs), while giving inhibitory effect in the heart causing the heart rate to slow down by binding to muscarinic acetylcholine receptors (mAChRs) (Battista et al., 2015). Termination of neurotransmitter binding to its receptor is accomplished by removal of neurotransmitters from the synaptic cleft. There are three main ways of removal depending on the neurotransmitter; enzymatic breakdown, reuptake and diffusion away from the synaptic cleft (Lodish, 2000). Monoamines like dopamine, serotonin and noradrenalin are mainly removed by reuptake of the intact molecule into the axon terminal that released the monoamines by specialized and selective transporter proteins. Acetylcholine and neuropeptides become enzymatically degraded in the synaptic cleft. Reuptake of amino acid neurotransmitters like GABA and glutamate is facilitated both post- and presynaptically by uptake through transporter proteins, in addition to diffusion and uptake by non-neuronal cells (Barrett and Ganong, 2010; Lodish, 2000).

Through binding to its receptor(s), a neurotransmitter can cause ion channels to open or close on the postsynaptic cell and thereby increases or decreases the likelihood of the postsynaptic neuron to fire an action potential. If the shift in synaptic potential makes the postsynaptic neuron less likely to generate an action potential (influx of anions), it is called hyperpolarization or inhibitory post-synaptic potential (IPSP), which is often associated with the main inhibitor neurotransmitter GABA. Excitatory postsynaptic potential (EPSP) is the depolarizing response from opening of channels ensuring influx of cations and sometimes multiple EPSPs are needed to trigger the action potential (Barrett and Ganong, 2010). Glutamate is the neurotransmitter most often associated with EPSP. A postsynaptic neuron may receive signals from multiple neurons of both excitatory and inhibitory character and if the sum of the signals causes the membrane potential to reach the threshold potential, the neuron fires and potentially release neurotransmitters from presynaptic terminus.

Neurotransmitter receptors can be divided into two broad categories, G-protein coupled receptors (GPCRs) and ligand-gated ion channels (ionotropic receptors) (Fig. 2). GPCRs are mainly responsible for slower synaptic responses (seconds) because binding of a neurotransmitter causes activation of intracellular G-proteins before these can activate intracellular signaling cascades and/or ion channels. Ligand-gated ion channels are responsible for fast synaptic responses (milliseconds to seconds) because binding of a neurotransmitter

causes immediate conformational changes allowing ions to cross the membrane (Barrett and Ganong, 2010; Lodish, 2000).
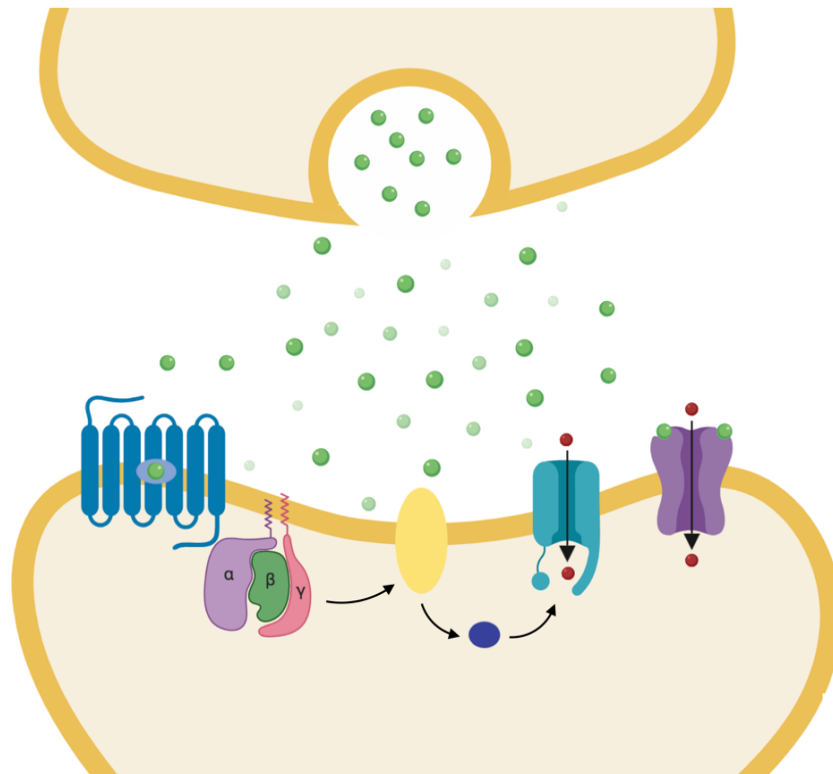

Figure 2 – A simplified representation of slow and fast neurotransmitter receptors at the postsynaptic neuron. Binding of a neurotransmitter to a G-protein coupled receptor (blue) can activate intracellular effectors affecting ion channels resulting in fluxion of ions across the membrane. Ligand gated ion channels (purple) bind neurotransmitters, inducing conformational changes of the receptor and allow ions to be translocated through the channel and thereby exhibit a fast responses in the millisecond range.

1.2 GABA and Glutamate in the CNS

GABA is the main inhibitory neurotransmitter in the CNS, while glutamate is the main excitatory neurotransmitter. The inhibitory function of GABA is closely regulated with the excitatory function of glutamate for maintaining normal brain function.

Glutamate is distributed throughout the brain and spinal cord. Glutamate signaling is conducted both by ionotropic and metabotropic receptors (Barrett and Ganong, 2010). Ionotropic glutamate receptors mediate fast excitatory transmission and can be divided into 3 different classes based on the agonist selectivity; N-methyl-D-aspartate (NMDA) that controls Ca^{2+} influx and kainate (KA) and α-amino-3-hydroxy-5-methyl-4-isoxazole proprionic acid (AMPA) that controls the influx of Na^+, K^+ and to some degree Ca^{2+} (Niciu et al., 2012). The

metabotropic glutamate receptors (mGluR) are responsible for slow synaptic activation and function by recruitment of intracellular heterotrimeric G-proteins and thereby activation of secondary signals and downstream signal transduction pathways. There are in total eight different mGluRs divided into three groups based on homology, signal transduction pathways and ligand binding (Niswender and Conn, 2010). The first group contains mGluRs 1 and 5, group 2 includes mGluRs 2 and 3 and the last group includes mGluRs 4, 6, 7 and 8. The receptors in these groups couple to different G-proteins and have different functions, most of them modulate voltage-gated calcium channels (Niciu et al., 2012; Wierońska and Pilc, 2019).

GABA is synthesized from glutamate by glutamate decarboxylase (GAD). GABA exerts its function by binding to the ionotropic $GABA_A$ receptor ($GABA_A$-R) and $GABA_C$ receptors ($GABA_C$-R) and the metabotropic $GABA_B$ receptor ($GABA_B$-R). Activation of the ionotropic $GABA_A$-R and $GABA_C$-R causes influx of Cl^- ions, leading to hyperpolarization of the cell (Chebib and Johnston, 1999). The $GABA_B$-R is found on neurons and glia cells and has a widespread distribution in the CNS (Gassmann and Bettler, 2012).

1.3 G-protein-coupled receptors

The GABA and glutamate metabotropic receptors are members of the GPCR superfamily of receptors that constitutes one of the largest protein superfamilies encoded by the mammalian genome (Katritch et al., 2013). GPCRs are involved in extensive physiological signaling processes in the human body from detecting external signals such as ions, photons and lipids, to signals such as hormones and neurotransmitters (Fredriksson, 2003). GPCRs play a substantial role in pathophysiology and are therefore among the most intensively studied drug targets (Hauser et al., 2017). More than 800 GPCRs are encoded by the human genome, which comprises 4 % of the total protein-coding genome (Fredriksson, 2003; Pándy-Szekeres et al., 2018). Approximately half of the GPCRs have sensory functions including mediating olfaction and taste, pheromone signaling and light, while the remaining are non-sensory GPCRs (Hauser et al., 2017).

All GPCRs are activated by binding of an agonist at an extracellular accessible site, and they share the common feature of seven transmembrane spanning (7TM) α helices connected by intra- and extracellular loops (Fig. 3). Ligand binding induces a conformational change in the intracellular part of the receptors resulting in binding of G-proteins or the adaptor proteins arrestins to the intracellular parts of the receptors (Erlandson et al., 2018). G-proteins and

arrestins are further responsible for activation, regulation and termination of intracellular signaling cascades (Erlandson et al., 2018). The signaling cascades lead to cellular responses where individual receptors exhibit unique combinations of signals due to the coupling to different G-proteins or arrestins. Constitutive activity without external stimulus present may also occur (Hilger et al., 2018; Luckey, 2014).
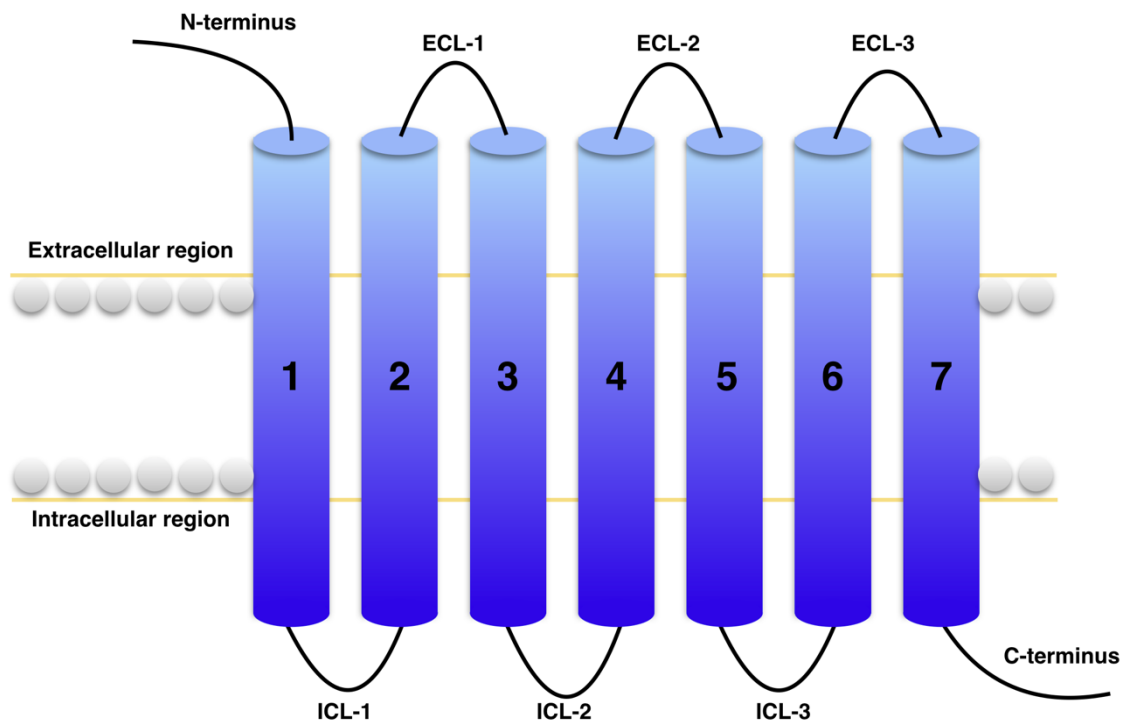

Figure 3 – An overview of the general architecture of the 7 transmembrane domain of a GPCR. The N-terminus and three loops (ECL1-3) are located on the extracellular side of the membrane and the C-terminus with three loops (ICL1-3) are located on the intracellular side.

Two main classification schemes exist for separating GPCRs into classes based on sequence homology and phylogenetic analysis; the clan system and the GRAFS classification (Fredriksson, 2003; Kolakowski, 1994). These schemes are partly overlapping by denoting the classes A-F or by their prototypical members; class A (Rhodopsin), class B (B1: Secretin and B2: Adhesion), class C (Glutamate), class F (Frizzled) and taste 2. Class D and E only exist in invertebrates and are encountered by the clan system, while the GRAFS system only includes classes identified in humans (Fredriksson, 2003; Kolakowski, 1994). The classes are further separated into subclasses based on pharmacological classification of their endogenous ligands (Davies et al., 2011; Fredriksson, 2003; Kolakowski, 1994). Class A (rhodopsin family) is the largest and the most studied class and contains approximately 700 receptors for amines, lipids,

and neuropeptides among others (Katritch et al., 2013). Peptide binding GPCRs are the biggest family within class A and are mainly receptors for hormone peptides which are important in physiological processes such as hormonal homeostasis (Hollenstein et al., 2014; Kobilka, 2007). Class B (secretin and adhesion family) GPCRs are more diverse with multiple physiological functions and are characterized by their long N-terminus that is capable of mediating contact with surrounding cells through cell-cell or/and cell matrix interactions (Paavola and Hall, 2012). Class C (glutamate family) is composed of 22 GPCRs and includes receptors for the main inhibitory and excitatory neurotransmitters GABA (GABA$_B$-R) and glutamate (mGluRs), respectively (Munk et al., 2016). In addition to the neurotransmitter binding receptors, the class is composed of calcium sensing receptors (CaSR) important for calcium homeostasis, pheromone receptors, taste 1 receptors and several orphan receptors (Chun et al., 2012).

The architecture of the entire receptor and localization of binding sites vary between the different classes of GPCRs. Members of class A have the simplest receptor architecture with both the orthosteric and a topologically distinct allosteric binding sites located in the 7TM (Lee et al., 2015). In contrast, the class C members have a large extracellular N-terminal that hosts the orthosteric binding site in a bi-lobed architecture, while the allosteric site is located within the 7TM (Basith et al., 2018; Geng et al., 2013).

1.3.1 GPCR signaling pathways

Agonist binding causes receptor activation and coupling to heterotrimeric G-proteins or arrestins that initiate intracellular signaling cascades (Hilger et al., 2018). The G-proteins consist of three subunits: Gα, Gβ and Gγ (Hilger et al., 2018). In the resting state, guanosine diphosphate (GDP) is bound to the Gα subunit (Hilger et al., 2018). Coupling of a heterotrimeric G-protein to a receptor induces a conformational change in Gα, which causes an exchange of the GDP to guanosine triphosphate (GTP), and a switch from inactive to active state (Hilger et al., 2018) (Fig. 4). Activation induces downstream effects by dissociation of the GTP-bound α subunit from the Gβγ dimer, and interactions of Gα and Gβγ with effectors (Hilger et al., 2018). The effectors include enzymes that modulate secondary messengers or ions channels such as calcium channels (Chang et al., 2013). The G-protein remains active as long as GTP is bound to the Gα subunit. The signaling process is inactivated by the α subunits

ability to hydrolysis of GTP to GDP and re-association of the G-protein subunits (Battista et al., 2015; Hilger et al., 2018).
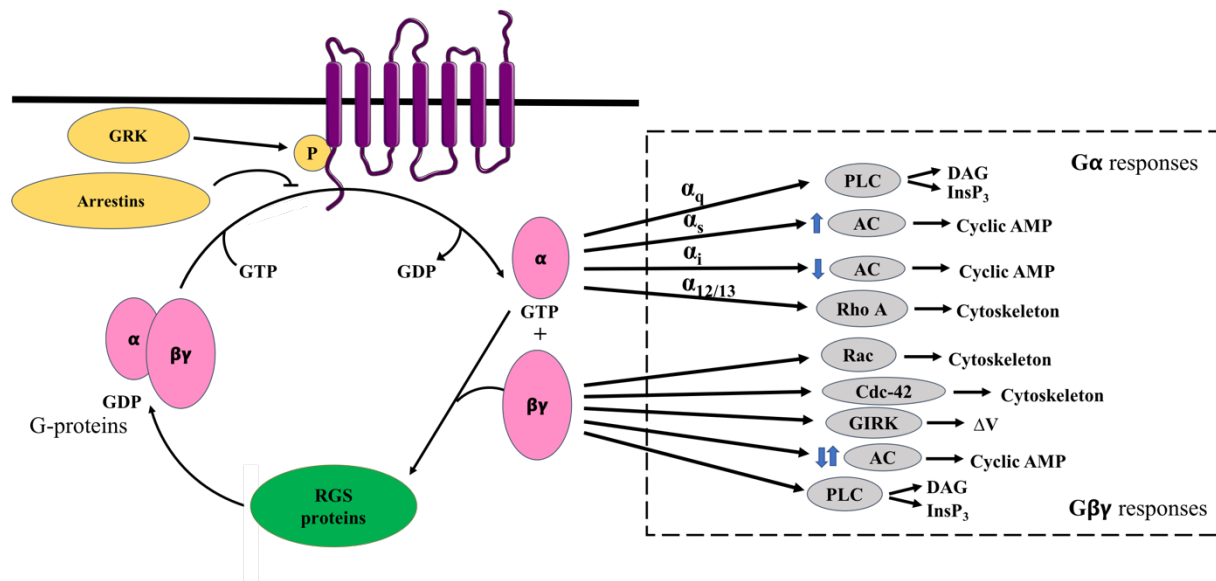

Figure 4 – A simplified scheme of signaling pathways for GPCRs. Activation of a receptor causes coupling to G-proteins or Arrestins. The Gα family are shown with their second messengers in addition to the targets of the Gβγ subunits. GIRK – G-protein Coupled Inwardly Rectifying K$^+$ channel, G-proteins – Guanine nucleotide binding protein, RGS – Regulators of G-protein signaling, PLC – Phospholipase C, AC – Adenylyl Cyclase, GTP – Guanosine Triphosphate, GDP – Guanosine Diphosphate, Cdc-42 – Cell division control protein 42, DAG – Diacylglycerol, InsP$_3$ – inositol (1, 4, 5) triphosphate, AMP – Adenosine monophosphate, ΔV – Voltage change. Rho A - a subfamily of small GTPases (modified from Watson, 2015).

G-proteins are separated into four main classes Gα$_s$, Gα$_{i/o}$, Gα$_{q/11}$ and Gα$_{12/13}$ based on sequence homology (Neves, 2002). Activation of each class is associated with inhibition or activation of a particular set of effector proteins. The Gα$_{i/o}$ subunit often targets and inhibits the enzyme adenylyl cyclase (AC) and thereby formation of the second messenger cyclic adenosine monophosphate (cAMP) from ATP and activation of protein kinase A (PKA) (Battista et al., 2015). This pathway is used by many neurotransmitters such as dopamine, acetylcholine and GABA (Gassmann and Bettler, 2012; Neves, 2002). Muscarinic acetylcholine receptors, coupled to G$_{i/o}$, are located in the heart to produce effects opposing the effects of the β-adrenergic receptors by decreasing the heart rate. Gα$_s$ stimulates the AC and thereby the cAMP production, and further activation of PKA which regulates ion channels and affect gene expression (Gassmann and Bettler, 2012). For instance in cardiac muscles the β-Adrenergic receptors are using this pathway, where the cAMP dependent PKA phosphorylates and opens calcium channels and thereby increases force and rate of the contraction (Battista et al., 2015).

The $G_{q/11}$ class activates the phospholipase C (PLC) pathway and second messengers such as inositol (1, 4, 5) triphosphate (IP_3) and diacylglycerol (DAG) (Neves, 2002). IP_3 triggers release of calcium from endoplasmic reticulum (ER) and can give effects such as smooth muscle contraction and increased hormone or transmitter release by depolarization (Battista et al., 2015). GPCRs that utilize this pathway include some of the muscarinic acetylcholine and serotonergic receptors (Battista et al., 2015). DAG activates and regulates one of the six PKC types which again can give over 50 different effects including neurotransmitter release, ion transport and inflammation (Battista et al., 2015; Neves, 2002). $G_{12/13}$ interacts via the Rho GTPase family, which is a part of the Ras superfamily (Kozasa et al., 2011). The cellular effects and interactions with effectors of this class are still under investigation, but there is strong evidence that it plays a large role in processes such as cell growth and polarity, apoptosis and immunity (Neves, 2002; Suzuki et al., 2009; Syrovatkina et al., 2016). The $\beta\gamma$ dimer can interact with G-protein-coupled receptor kinases (GRK), AC, PLC and multiple ion channels such as G-protein-mediated inwardly rectifying potassium channels (GIRK).

Activation of GPCRs can also lead to phosphorylation of intracellular amino acids by GRKs. The phosphorylated site can then act as a binding site for arrestins causing G-protein independent signaling and receptor desensitization (Hilger et al., 2018). Arrestins activate effector proteins such as mitogen-activated protein kinases (MAPKs), which regulate cellular processes including proliferation, differentiation and apoptosis, or the cytoplasmic non-receptor tyrosine kinases Src (Alberts, 2008). There are also some G-proteins, G_s and G_i that can activate Scr (Alberts, 2008). There are four different subtypes of arrestins that are suggested to be highly adaptable in terms of changing conformations to engage different downstream effectors (Hilger et al., 2018). Recruitment of arrestins also promotes internalization by endocytosis and the receptors becomes dephosphorylated and recycled or degraded in lysosomes (Benke, 2012).

1.3.2 Orthosteric and allosteric GPCR ligands

Ligands bind to the orthosteric binding site and act as agonists activating the receptor, or antagonists inhibiting the receptor function. The magnitude of agonist activation depends on the affinity and efficacy of the agonist. A full agonist is defined as a compound giving maximum (100 %) efficacy meaning maximum effect, while agonists with less efficacy are called partial agonists (Fig. 5). Inverse agonists exerts the opposite pharmacological effect of full or partial agonists and will turn-off the constitutive receptor activity (Fig. 5) (Salahudeen

and Nishtala, 2017). Antagonists can compete with agonists for the binding to the receptor (competitive), and in contrast to inverse agonists, antagonists do not turn-off the constitutive activity. Most antagonists bind in a reversible manner, but may also bind irreversibly to the receptor. In all cases the antagonist reduces the ability of agonists to bind (Salahudeen and Nishtala, 2017).
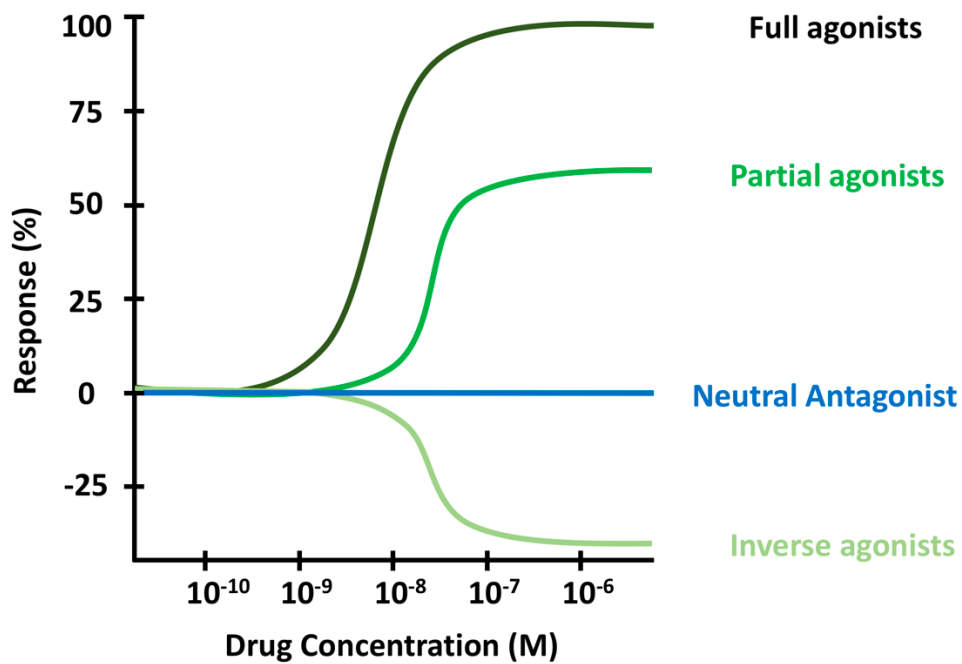

Figure 5 – Illustration of potential dose-response plots for agonists with different receptor efficacy (green) and for antagonists (blue).

Binding of modulators in the allosteric site can change the receptor efficacy, called efficacy modulation, and/or modify of the agonist association or dissociation rate, called affinity modulation (Conn et al., 2014; Gilchrist, 2010). Positive allosteric modulators (PAMs) bind to the allosteric site and potentiate receptor activation upon binding of an orthosteric agonist. Negative allosteric modulators (NAMs) inhibit or reduce responses normally produced by agonist, most probably by stabilizing the 7TM domain in an inactive conformation. In addition, some ligands binding in the allosteric binding site have intrinsic agonist activity, and are called agoPAMs, as they also potentiate the effect of agonists (Conn et al., 2014). Silent allosteric modulators (SAM) have no effect on the orthosteric agonists and behaves as a competitive antagonists of the allosteric binding site (Burford et al., 2013).

GPCR activation of a specific pathway depends on capability of the agonist to stabilize a particular active receptor conformation (Wootten et al., 2018). Agonists exhibiting pathway specific selectivity have been identified for several GPCRs, named biased agonists, while the phenomena is named biased agonism or functional selectivity (Wootten et al., 2018). Binding of an allosteric modulator can also contribute to stabilization of receptor conformations induced by the agonist and thereby contributing to activation of a specific signal pathway (Foster and Conn, 2017; Smith et al., 2018).

1.3.3 *In vitro* studies of ligand affinity and activity

In vitro ligand screening and characterization is a compulsory part of drug discovery and development, and requires assays for description of ligand activity (for example differentiation between agonist, antagonist or PAM, NAM, or SAM) assays for studying different signaling pathways for the receptor, and assays measuring affinity and potency. As previously described, GPCRs can activate multiple signal pathways, and concepts such as biased signaling needs to be taken into consideration when selecting or developing functional assays to avoid rejecting potential valuable drug candidates (Zhang and Xie, 2012).

Ligand-binding assays using radioactive ligands are commonly applied, alone or in combination with other ligands, in order to resolve which binding site the ligand occupies (orthosteric, allosteric), the binding affinity and kinetics among other purposes (Hulme and Trevethick, 2010; Miyano et al., 2014). A disadvantage of such assays is their hazardous nature and in addition the custom production and labeling of ligands with a radioisotope is time- and

cost expensive (Sykes et al., 2019). Fluorescence-based methods are emerging as an alternative to radioligand-based methods as they are not hazardous (Sykes et al., 2019). These types of binding studies require a fluorophore to be attached via a linker to the ligand(s) and the signal from the probe can then be detected upon ligand binding. A challenge with fluorescence labeling is that the molecular weight is increasing and can influence the physicochemical- and pharmacological properties of the ligands (Sykes et al., 2019). Time-resolved fluorescence resonance energy transfer (TR-FRET) assay is an example of a relatively new fluorescence based method that can be applied in a HTS where a distance-dependent transfer of energy from a donor (e.g. a tagged receptor) to an acceptor (e.g. a tagged ligand) results in a traceable signal (Zhang and Xie, 2012). This technology can be applied for multiple types of studies from kinetic measurements to protein-protein interaction, dynamics and trafficking (Vernall et al., 2014). There are multiple variants ligand binding assays, and they are important tools for identification of compounds targeting different GPCR classes, but to determine the functional properties and biological responses of ligands, functional assays are necessary (Zhang and Xie, 2012).

Ligand affinity can also be measured by biophysical techniques such as isothermal titration calorimetry (ITC), surface plasmon resonance (SPR) and fluorescence polarization (FP) (Du et al., 2016). ITC measures heat exchange during the binding process, and provides characteristics such as the affinity, enthalpy and entropy of a reaction. In general, the macromolecule under investigation is placed in a chamber in the calorimeter before the ligand is titrated into the chamber. The heat released, if the reaction is exothermic, or absorbed during the binding is measured and the data is used for calculating binding characteristics (Du et al., 2016). SPR can measure kinetics, affinity and specificity in real time without using labels. The optical-based method measures changes in the refraction index upon binding to proteins immobilized on a sensor surface made up of a thin film of gold on a glass support. As ligands bind to the protein, an increase in the refraction index can be measured and after a desired association time, the solution without ligands is injected to dissociate the ligand binding complexes. This causes an decrease in the refraction index, and the refraction index curves can be used to calculate the rate constants (Du et al., 2016). FP measures kinetics based on the principle that polarized light becomes unpolarized over time, and a decrease in molecular weight caused by disassociation of the ligand-receptor complex causes the emitted light to depolarize (Lea and Simeonov, 2011). The method can also be applied for competition binding assays using fluorescence labeled ligands and unlabeled ligands, where the FP signal can be correlated to the

concentration of the unlabeled ligand necessary to displace the labelled ligands (IC$_{50}$ value) (Du et al., 2016).

Functional assays can be applied to detect activated G-proteins, G-protein mediated events or G-protein independent events (Zhang and Xie, 2012). A GTPγS binding assay can be used to determine if a ligand initiates receptor-G-protein coupling and for identifying intrinsic activity. In addition, the GTPγS assay can be applied independent of which of the four main G-protein families the receptor is interacting with. As activation of a G-protein causes exchange of Gα-bound GDP to GTP, the radioactive GTPγS is added and binds the Gα subunit and radioactivity can be counted (Zhang and Xie, 2012).

The four main families of G-proteins initiate different intracellular responses upon activation and the choice of assay is therefore dependent on which family of G-protein the receptor recruits. Many G-protein dependent assays are based on detecting the second messenger after ligand binding and receptor activation, and thereby require the receptor coupling mechanism to be known. cAMP-based assays are frequently used when the GPCR is coupled with G$_{i/o}$ and/or G$_s$ that causes negative or positive stimulation of adenylyl cyclase and thereby affects the cellular levels of cAMP which can be detected by the assay (Fig. 4). Labeled cAMP can be introduced in the assay to compete with endogenous cAMP, and later be detected by anti-cAMP antibody (Zhang and Xie, 2012). There are multiple variants of the cAMP assay both radiolabeled and radio-free approaches (Zhang and Xie, 2012). Please see the methods section for further description of the cAMP assay applied in this thesis.

GRKs phosphorylate specific intracellular sites of GPCRs and cause recruitment of arrestins that promote receptor internalization (Hilger et al., 2018). This processes can be investigated both by receptor internalization- and β-arrestin recruitment assays. However, receptor internalization can be studied in several ways, but very often specific antibodies binding to an extracellular part of the receptor is used. The antibody is co-internalized with the receptor upon activation and may be detected by a fluorophore-labeled secondary antibody or by tagging the receptor with fluorescent proteins (Zhang and Xie, 2012). β-arrestins are also involved in G-protein independent signaling and can act as scaffolds that interact with various proteins such as the signaling protein Extracellular signal-regulated kinase 1/2 (ERK 1/2), nonreceptor tyrosine kinases like Src, and trafficking proteins (Lefkowitz, 2005). Assays targeting β-arrestins can be used to study biased GPCR signaling (Zhang and Xie, 2012). The first

commercial recruitment assay for studying the effects of β-arrestin recruitment upon receptor activation used β-arrestin tagged with green fluorescence protein (GFP) that emits green fluorescence upon light exposure which is monitored by an imaging system (Zhang and Xie, 2012).

1.3.4 G-Protein coupled receptors as drug targets

Disruption or malfunction of GPCR signaling pathways may lead to a wide range of diseases and disorders, and GPCRs are therefore valuable therapeutic targets. Despite that approximately 35 % of all marketed U.S Food and Drug Administration (FDA) approved drugs target in total 108 unique GPCRs, this number constitutes only a fraction of the GPCRs encoded by the human genome (Hauser et al., 2017; Hu et al., 2017). The non-sensory GPCRs are targets for the majority of GPCR drugs; however, only a minority of them are currently therapeutically exploited. Identification of targets and novel ligands is necessary for treating diseases where the existing marketed drugs are giving insufficient effects or extensive side effects.

Few marketed drugs that act on GPCRs have been developed using structure-based methods, as the number of solved 3D structures of GPCRs until recently was very limited. However, advances in structural biology during the last 20 years have increased the number of known GPCR 3D structures tremendously. An import breakthrough came in year 2000 with the release of the X-ray crystallography structure of bovine rhodopsin (Palczewski et al., 2000), and the development and increase in cryogenic electron microscopy (cryo-EM) structures the past 5 years (Shen, 2018) have given new opportunities within the field. The number of solved GPCR structures has dramatically increased since the release of the bovine rhodopsin structure with currently 321 resolved structures of the 7TM domain (March 2019). In total, 74 of 321 solved receptor complexes are in an active state with an agonist bound. At present, structures of 62 unique GPCRs are present in the Protein Data Bank (PDB) database (Pándy-Szekeres et al., 2018).

In addition, the progress in the discovery and development of allosteric modulators of multiple GPCRs is advancing drug discovery by providing candidates that are more selective than ligands targeting the orthosteric site (Conn et al., 2014). The conserved nature of the orthosteric binding site between GPCRs makes it challenging to obtain ligands with high selectivity compared to allosteric ligands. As consequence, the use of ligands targeting the orthosteric

binding site may lead to side effects and drug tolerance in treatment. Targeting allosteric modulation is an alternative approach to inhibit or potentiate the effect of the receptor upon binding of endogenous ligands. However, development of allosteric modulators is also challenging. The measurable effect of a modulator can differ depending of the orthosteric ligand used, and thereby complicating screening. In addition, the allosteric binding site is not as highly conserved between species as the orthosteric site and specie specific differences may affect testing of potential drug candidates in animal models (Conn et al., 2014). The concept of biased agonism has also contributed to an increased understanding of receptor activation (Hauser et al., 2017) and possibilities for more selective drug candidates (Hauser et al., 2017).

1.4 Class C of G-protein coupled receptors

Class C members are distinguished from other GPCR classes by the large extracellular domain that contains the orthosteric binding site. This domain is called Venus flytrap (VFT) domain due to the resemblance to the carnivorous plant. The extracellular domain is connected to the 7TM by a cysteine rich domain (CRD), which is absent in the GABA$_B$-R (Chun et al., 2012) (Fig. 6). Class C GPCRs are obligate dimers, heterodimers as the GABA$_B$-R, or homodimers as mGluRs (which can also form heterodimers) and the CaSR (Fig. 6) (Chun et al., 2012; Kaupmann et al., 1998). The transmembrane heptahelical domain hosts an allosteric binding site, and different studies have indicated that the allosteric site is located at a site corresponding to the orthosteric site in class A GPCRs (Harpsøe et al., 2016; Pin et al., 2003). The mGluRs are the most studied class C receptors, and the only subclass with a full 3D structure, the cryo-EM structure of mGlu5 (Fig. 7) (Koehl et al., 2019). The mGluRs are therefore the main source for structural knowledge about class C GPCRs and frequently used as references in molecular modelling studies of other class C members.
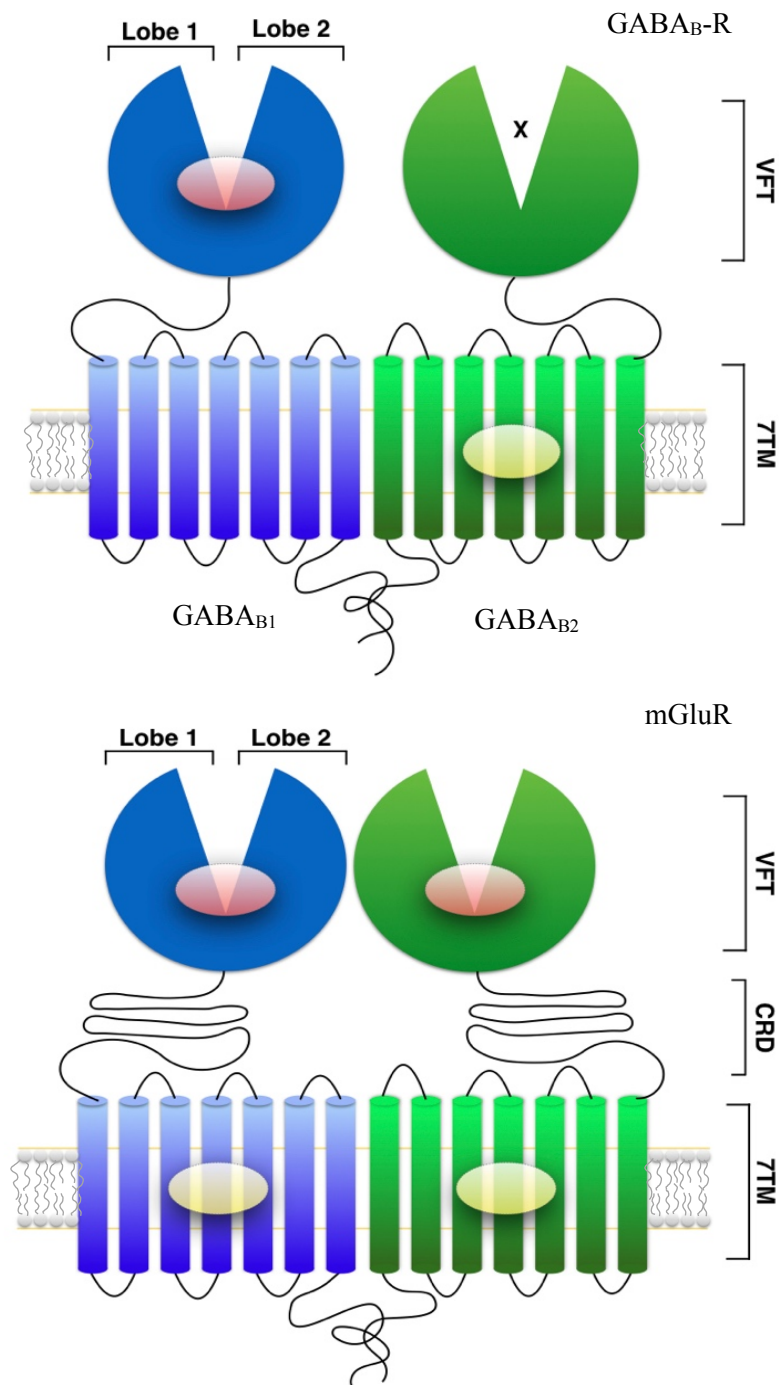
Figure 6 – A schematic illustration of the structural organization of the $GABA_B$-R (above) and of the subclass mGluR (below). $GABA_B$-R is an obligatory heterodimer, whereas mGluR forms a homodimer. Red spheres - orthosteric binding site, yellow sphere - allosteric binding site.

Agonist binding in the VFT induces conformational changes in all domains leading to transduction of signals from the extracellular part to the intracellular site and activation of G-proteins (Chun et al., 2012; Rondard et al., 2011). Full activation of mGluRs requires agonist binding in the orthosteric binding site of both VFTs in the dimer, while for the $GABA_B$-R only the VFT of $GABA_{B1a/b}$ needs to be occupied (Fig. 6) (Grushevskyi et al., 2019; Pin et al., 2004).

Single-molecule Förster resonance energy transfer (smFRET) studies of mGluR2 and mGluR3 have shown that the VFTs oscillate between the open/inactive and the closed/active conformations without ligand present, and that ligand binding shifts the conformational equilibrium depending on the function of the ligand (Grushevskyi et al., 2019; Olofsson et al., 2014). The same mechanism is thought to apply to all class C members, but has still not been confirmed for the GABA$_B$-R. X-ray structures of GABA$_B$-R VFTs, FRET and Bioluminescence resonance energy transfer (BRET) studies have described the open/inactive conformation associated with antagonist binding and closed/active conformation associated with agonist binding, while conformational details about intermediate states are not known (Geng et al., 2013; Lecat-Guillet et al., 2017). These studies have also shown that the extracellular domains of mGluRs are associated with larger conformational changes and VFT rotations than the extracellular domains of the GABA$_B$-R (Geng et al., 2013; Lecat-Guillet et al., 2017).

The VFTs of most class C members are connected to the heptahelical domain through a linker region consisting of approximately 80 residues with 9 completely conserved cysteines, the CRD. The exception is the GABA$_B$-R with a shorter linker region without the conserved cysteines (Chun et al., 2012). The crystal structure of the extracellular region of the mGluR3 receptor showed that the CRD has a length of 40 Å, and thereby physically separates the VFT from the 7TM domain (Muto et al., 2007).

Structural studies of mGluR5 show that activation of the receptor causes a substantial compaction of the dimer, causing the two complementary receptor subunits of the dimer to form interactions (Fig. 7) (Koehl et al., 2019). In the inactive state, only lobe 1 of the dimers are in contact, as for GABA$_B$-R (Geng et al., 2013; Koehl et al., 2019). Activation of the receptor causes reorganization of the VFT dimer interface and closure of the VFTs, leading to conformational changes bringing the two dimer subunits closer together (Koehl et al., 2019). The average atomic distance between Glu527 located centrally in the two CRD domains of the homodimer decreased from 43 Å in the inactive state to 10 Å in the active state (Fig. 7). The distance between the two 7TM domains also decreased, and a rotation of approximately 20° of each of the 7TM domains was observed (Koehl et al., 2019). Activation of the 7TM heterodimer of GABA$_B$-R also causes a rearrangement of the dimer interface where the TM6 of each monomer forms the new interface between GABA$_{B1a/b}$ and GABA$_{B2}$, as opposed to the inactive state where the interface is formed mainly by TM5. However, the structural rearrangements of

GABA$_B$–R 7TM dimer during activation are proposed to be smaller than for mGluRs (Xue et al., 2019).
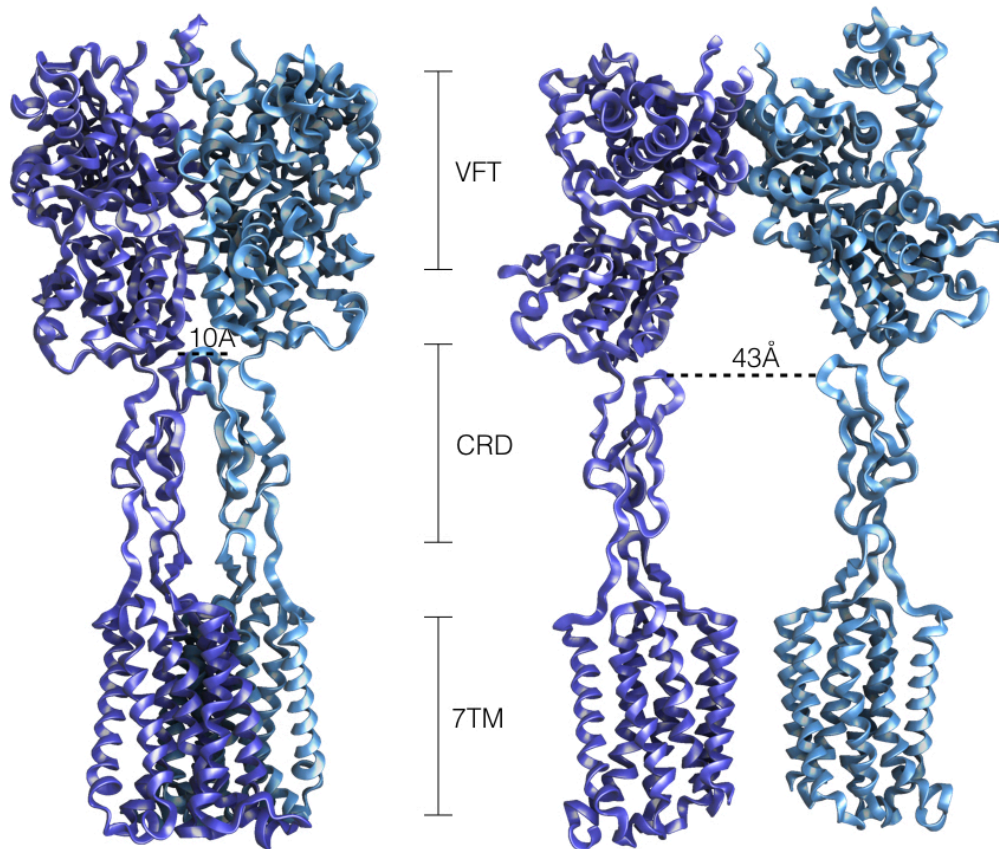

Figure 7 – The structural re-organization of mGluR5 upon receptor activation can be seen when comparing the Cryo-EM crystal structure of the mGluR5 in the active state (left) (PDB ID: 6N51) and the inactive state (right) (PDB ID: 5N52) (seen in the same view). The average atomic distance between Glu527 in the CRD of the heterodimer decreased 33 Å from the inactive (right) to the active state (left) (Koehl et al., 2019).

These results are in consistency to the smaller conformational changes observed in GABA$_B$-R VFT compared to mGluR and indicate that the structural changes of the entire receptor upon activation are more comprehensive in mGluRs than in the GABA$_B$-R (Geng et al., 2013; Koehl et al., 2019; Lecat-Guillet et al., 2017; Xue et al., 2019). The changes upon activation of mGlu5 are likely to enable two previously unexplored dimer interaction interfaces between ECL2 in the 7TM domains and between the CRD domains, giving two rigid attachment points. Mutational studies of residues within these interfaces suggested that these interactions are necessary for a stable transmission of agonist-induced conformational changes from the VFT to the intracellular signaling domain (Koehl et al., 2019).

The intracellular C-terminal domains of class C GPCRs are large, with approximately 250 residues in the CaSR and between 250 and 500 for mGluRs depending on the subtype, while GABA$_{B1b}$ contains 94 and GABA$_{B2}$ contains 190 residues (Calver et al., 2001; Riccardi and Brown, 2010; Willard and Koochekpour, 2013). The C-terminal region has high sequence variations between the receptors, and is thought to play a role in coupling to signaling proteins and scaffolding (Chun et al., 2012). In the case of GABA$_B$-R, the GABA$_{B2}$ is responsible for intracellular trafficking of GABA$_{B1a/b}$ from the endoplasmic reticulum (ER) to the membrane, because GABA$_{B2}$ masks a retention signal by coiled-coil interaction with the C-terminal domain of GABA$_{B1a/b}$ (Burmakina et al., 2014; Gassmann and Bettler, 2012).

1.4.1 Structure and mechanism of the GABA$_B$ VFTs

The GABA$_B$-R is an obligate heterodimer comprised of the GABA$_{B1a/b}$ and GABA$_{B2}$ subunits (Calver et al., 2000; Geng et al., 2013) where each subunit contains an extracellular domain connected to a heptahelical transmembrane domain by a linker region (Fig. 6). GABA$_{B1a}$ and GABA$_{B1b}$ are isoforms encoded by the same gene *GABBR1*, and structurally they only differ in the N-terminal region with the presence of a sushi domain on the GABA$_{B1a}$ subunit (Biermann et al., 2010). The sushi domain is reported to function as an intracellular sorting signal responsible for trafficking this isoform into axons (Biermann et al., 2010) and has not been implicated to affect the pharmacology or kinetics in heterologous cells (Benke, 2012; Gassmann and Bettler, 2012).

Radiolabeled ligand- and site-directed mutagenesis studies, and later X-ray crystal structures have shown that in contrast to the mGluRs, only the VFT of the GABA$_{B1a/b}$ subunit and not the VFT of GABA$_{B2}$ contains a binding site for the endogenous agonist GABA (Geng et al., 2013; Jones et al., 1998; Kniazeff et al., 2002; Urwyler et al., 2005). In addition, sequence analysis show that none of the residues implicated in ligand binding in GABA$_{B1a/b}$ are conserved in GABA$_{B2}$ VFT (Geng et al., 2012). In the active closed state of the GABA$_{B1a}$ VFT, the GABA$_{B2}$ VFT remains in an open inactive state (Geng et al., 2013). Also, binding studies with recombinant receptor mutants showed that the VFT of GABA$_{B1a/b}$ is functional in the absence of the GABA$_{B2}$ VFT, but with reduced agonist affinities (Liu et al., 2004; Nomura et al., 2008). In addition to increasing agonist affinity, the GABA$_{B2}$ VFT is suggested to impact receptor activation by promoting signal transduction from the extracellular side to the intracellular site

contributing to increased agonist efficacy (Liu et al., 2004; Nomura et al., 2008). The sequence identity between $GABA_{B1a/b}$ and $GABA_{B2}$ VFTs is 33% (Frangaj and Fan, 2017).

There are in total nine available X-ray crystal structures of the $GABA_B$-R VFT dimer in the PDB (Geng et al., 2013), but the complete 3D structure that includes all receptor domains has not been solved. The structures show that the VFT heterodimer is formed by non-covalent interactions between the $GABA_{B1a/b}$ and $GABA_{B2}$ (Fig. 8) and each VFT contains two distinct domains, the N-terminal Lobe 1 (LB1) and the C-terminal Lobe 2 (LB2) (Figs. 6 and 8). The $GABA_{B1a/b}$ and $GABA_{B2}$ VFTs are similar in sequence length (approximately 400 residues), and the LB1 and LB2 of $GABA_{B1a/b}$ are structurally similar to the corresponding lobes of $GABA_{B2}$ (Fig. 8) (Geng et al., 2013). The X-ray structures show that the LB1 of $GABA_{B1a/b}$ VFT interacts with the LB1 of $GABA_{B2}$ VFT both in the active and inactive VFT states. The interactions between LB1-LB1 in the VFTs are fully facilitated by non-covalent interactions which involves patches of hydrophobic interactions, hydrogen bonds and a salt bridge (Geng et al., 2013). The hydrophobic interactions are mainly facilitated by three conserved tyrosine residues that form stacking interactions at the LB1-LB1 interface (Fig. 8). Upon receptor activation, large conformational changes causes the LB2 domains of $GABA_{B1a/b}$ and $GABA_{B2}$ to form an additional large non-covalent heterodimer interface (Geng et al., 2013) (Fig. 8). The LB2-LB2 interface is facilitated by a rich hydrogen bond network including the key residues Thr198, Glu201 and Ser225 of $GABA_{B1a/b}$ LB2 and Asp204, Gln206, Asn213 and Ser233 of $GABA_{B2}$ VFT LB2 (Fig. 8). A site-directed mutagenesis study of the interfacial residues observed in the activated VFT dimer, showed that the conserved tyrosine residues were important for agonist dependent G_i-protein activity and GABA-induced GIRK currents (Geng et al., 2012; Rondard et al., 2008). The mutations also decreased the GABA induced stimulation of [^{35}S]GTP-γS binding, but had no effect on the GABA affinity (Geng et al., 2012).
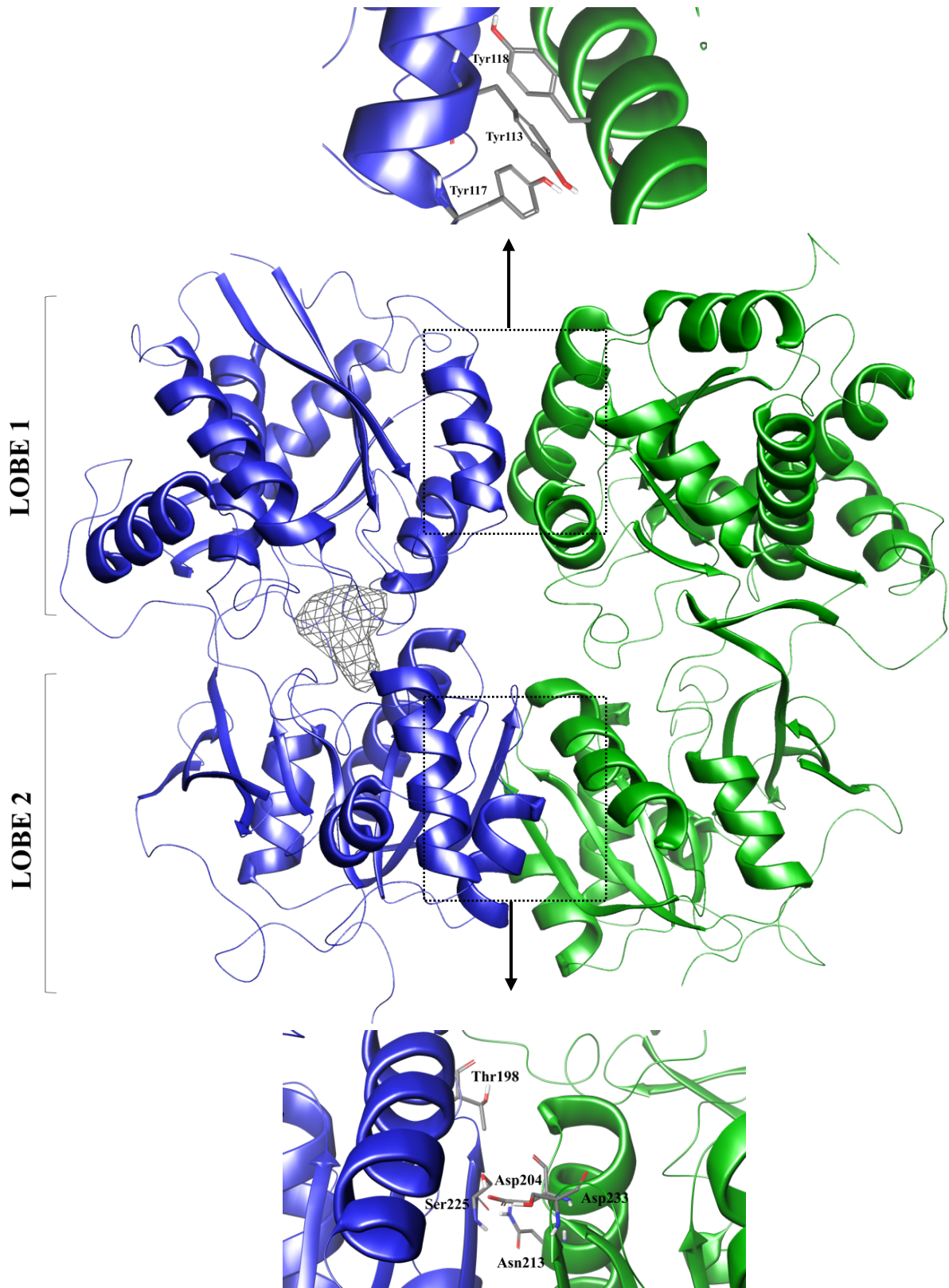
Figure 8 – The heterodimeric extracellular GABA$_B$-R VFTs in the active state with amino acids important for Lobe1-Lobe1 and Lobe2-Lobe2 interactions displayed. Blue – GABA$_{B1a/b}$ VFT, green – GABA$_{B2}$ VFT, gray – illustration of the approximate position of the orthosteric binding site (PDB ID: 4MS4) (Geng et al., 2013).

The linker region between the VFT and 7TM in both of GABA$_B$-R subunits is composed of approximately 40 residues and is not cysteine rich as in other class C GPCRs (Margeta-Mitrovic et al., 2001). The linker has not been shown to be critical for the activation and signal transduction from the VFT to the 7TM domain (Margeta-Mitrovic et al., 2001; Rondard et al., 2011). However, the distance between the C-terminus of the two LB2 subunits decreases from 45 Å to 32 Å upon activation and is thereby likely to contribute to changes in the orientation of the two 7TM domains relative to each other (Geng et al., 2013; Lecat-Guillet et al., 2017). The transmembrane part of GABA$_{B2}$ hosts an allosteric binding site as shown by binding studies of the isolated GABA$_{B2}$ subunits (Binet et al., 2004). It is also well demonstrated by studies manipulating the receptor composition that the GABA$_{B2}$ subunit is responsible for G-protein binding (Galvez, 2001).

1.4.2 GABA$_{B1}$ orthosteric binding site and ligand recognition

Agonists bind in a pocket located in the crevice of LB1 and LB2 of GABA$_{B1a/b}$ (Fig. 6 and Fig. 9), and induce large conformational change into the GABA$_{B1a/b}$ VFT such that the LB1 and LB2 interact and form a stable closed conformation in timescales necessary for full receptor activation (Geng et al., 2013; Møller et al., 2017).

Residues located in LB1 are responsible for anchoring both agonists and antagonists in the binding pocket (Geng et al., 2013). The LB1 residues Trp65, Ser130, Gly151, Ser153, His170, and Glu349 interact with both agonists and antagonists (Fig. 9). Mutational studies followed by radioligand - and [^{35}S]GTPγS - binding assays showed that the mutation of Trp65 to Ala abolished the effects of ligand binding and function of the receptor (Geng et al., 2013). Mutating His170 to Ala prevented antagonist binding, but had less effect on agonist binding (Geng et al., 2013).

Interactions with Tyr250 in LB2 seem to be unique for agonists (Evenseth et al., 2019; Geng et al., 2013), while Trp278 located in the same domain interacts with high affinity but not low affinity antagonists, in addition to agonists (Fig. 9) (Froestl, 2010; Geng et al., 2013). Interactions with residues both in LB1 and LB2 are likely to be a requirement for agonist activation, and causes the agonists to become buried within the closed receptor. This is supported by mutational studies showing that Trp278 and Tyr250 were critical for agonist binding with less effect on binding of antagonists (Galvez et al., 2000; Geng et al., 2013).
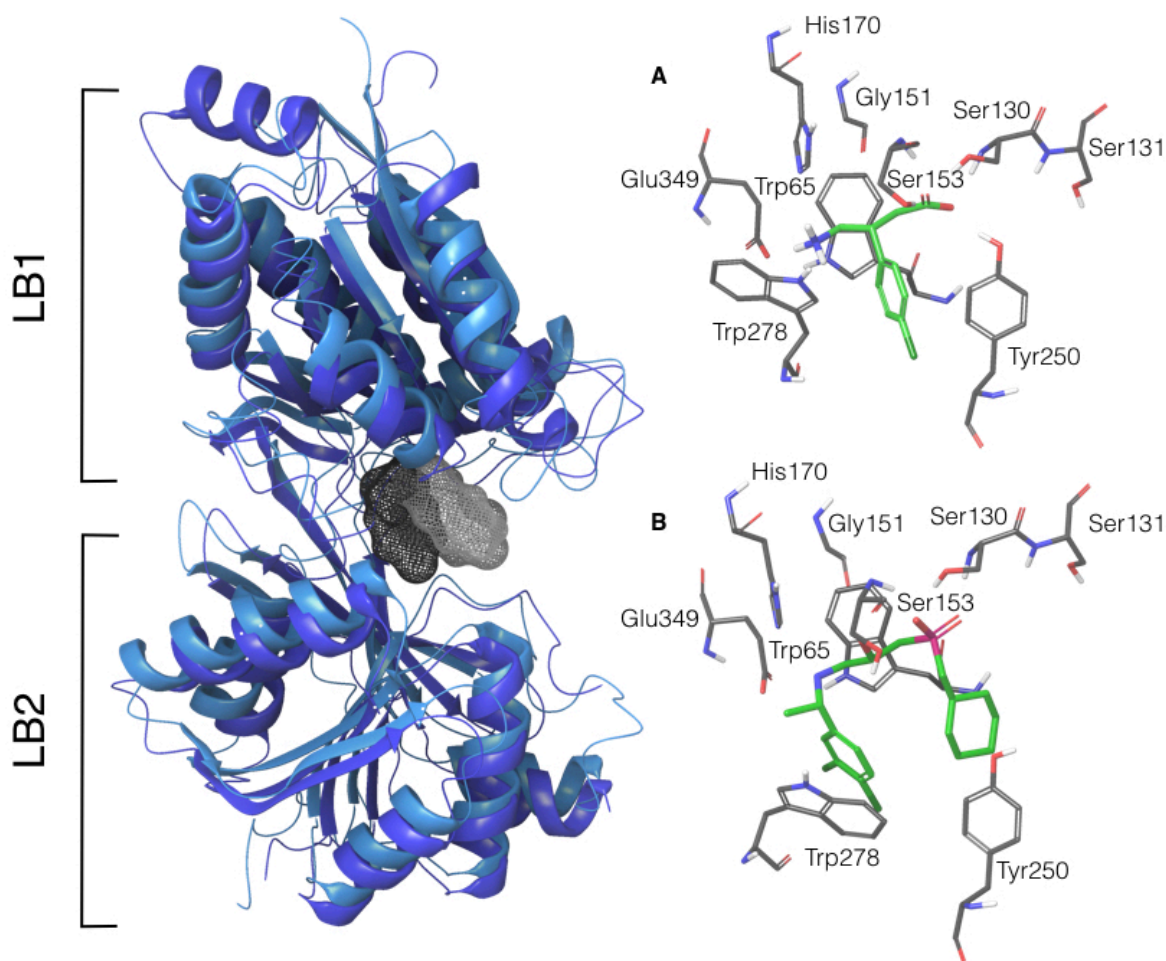
Figure 9 – Superposition of GABA$_{B1}$ VFT in the active state (PDB-ID: 4MS4 - dark blue) and the inactive state (PDB ID: 4MR7 – light blue) with the binding pocket displayed as a mesh (black -active state, gray -inactive state) (left). The agonist baclofen (A) and the antagonist CGP54626 (B) in the active- and inactive orthosteric binding pocket. Ligands are surrounded by the residues important for ligand binding where Tyr250 and Trp278 is located in GABA$_{B1}$ VFT LB2, while the other residues are located in LB1.

All of the GABA$_{B1a/b}$ VFT co-crystalized ligands are GABA derivatives with an α-acid group and an γ-amino group (Geng et al., 2013). These groups participate in hydrogen bonding with the receptor independent of intrinsic activity, where the α-acid group commonly are stabilized by Ser130 and Ser153, while Glu349 and His170 are stabilizing the γ-amino groups orthosteric binding site (Fig. 9). Linking interaction pattern to ligand activity and affinity has though proven to be a difficult task as highly similar compounds show similar receptor interaction patterns despite opposite activities, e.g. baclofen and 2-hydroxysaclofen (Geng et al., 2013). Larger and more bulky antagonists, like CGP54626 and CGP62349, are thought to prohibit formation of a stable closed conformation by forming few and variable interactions with the LB2, most probably as a result of the size compared to agonists (Geng et al., 2013). As

antagonist binding favors the open conformation that corresponds to the resting or inactive state of the receptor, the antagonist remains accessible to the surrounding solvent (Geng et al., 2013)

1.4.3 GABA$_B$ receptor signaling

Activation of both pre- and postsynaptic GABA$_B$-Rs by agonists results in inhibition of adenylyl cyclase (AC) through the G$\alpha_{i/o}$ pathway (Fig. 10) (Gassmann and Bettler, 2012). In the presynaptic terminal, binding of Gα to AC causes decreased levels of cAMP, which prevents vesicle fusion and thereby neurotransmitter release (Gassmann and Bettler, 2012). In addition, the G$\beta\gamma$ subunit of the G protein binds directly to voltage-gated Ca^{2+} channels (VGCC), resulting in inhibition of inward rectifying Ca^{2+} channels necessary for vesicle fusion (Gassmann and Bettler, 2012). The G$\beta\gamma$ subunit can also directly attach to SNAP receptors (SNARE) that are responsible for anchoring vesicles to the synaptic membrane and thereby inhibit presynaptic membrane vesicle fusion (Gassmann and Bettler, 2012). In the postsynaptic membrane, the G$\beta\gamma$ subunit also binds and inhibits the VGCC, but in this case it contributes to a hyperpolarization and inhibits the release of many neurotransmitters including noradrenaline, serotonin and dopamine (Gassmann and Bettler, 2012). Postsynaptic, the cAMP-dependent PKA signaling pathway is affected by the inhibition of AC (Gassmann and Bettler, 2012). This results in inhibition or reduced permeability of ion channels such as the ionotropic glutamate receptor NMDA receptor-mediated Ca^{2+} influx (Skeberdis et al., 2006). In addition, the G$\beta\gamma$ subunit stimulates the G-protein coupled inwardly rectifying K$^+$ channels (GIRK), resulting in inhibition of postsynaptic potential and decreased long-term potentiation (LTP) (Bettler et al., 2004; Misgeld et al., 1995).

The receptors function as auto- or heteroreceptors on both inhibitory and excitatory terminals. When GABA is released from a GABAergic neuron, it is likely that it can inhibit further release by binding to presynaptic autoinhibitory receptors that serve as a negative feedback loop (Kobayashi et al., 2012). These autoreceptors can also be activated by GABA released by a single action potential (Biermann et al., 2010). GABA$_B$-Rs are also found on non-GABAergic neurons where they act as heteroreceptors and inhibit the release of other neurotransmitters such as glutamate from glutamatergic neurons (Biermann et al., 2010). Glutamatergic neurons have GABA$_B$-Rs located both on the axon (GABA$_{B1a}$ isoform) and dendrites (both GABA$_{B1a}$ and GABA$_{B1b}$ isoforms) (Biermann et al., 2010).
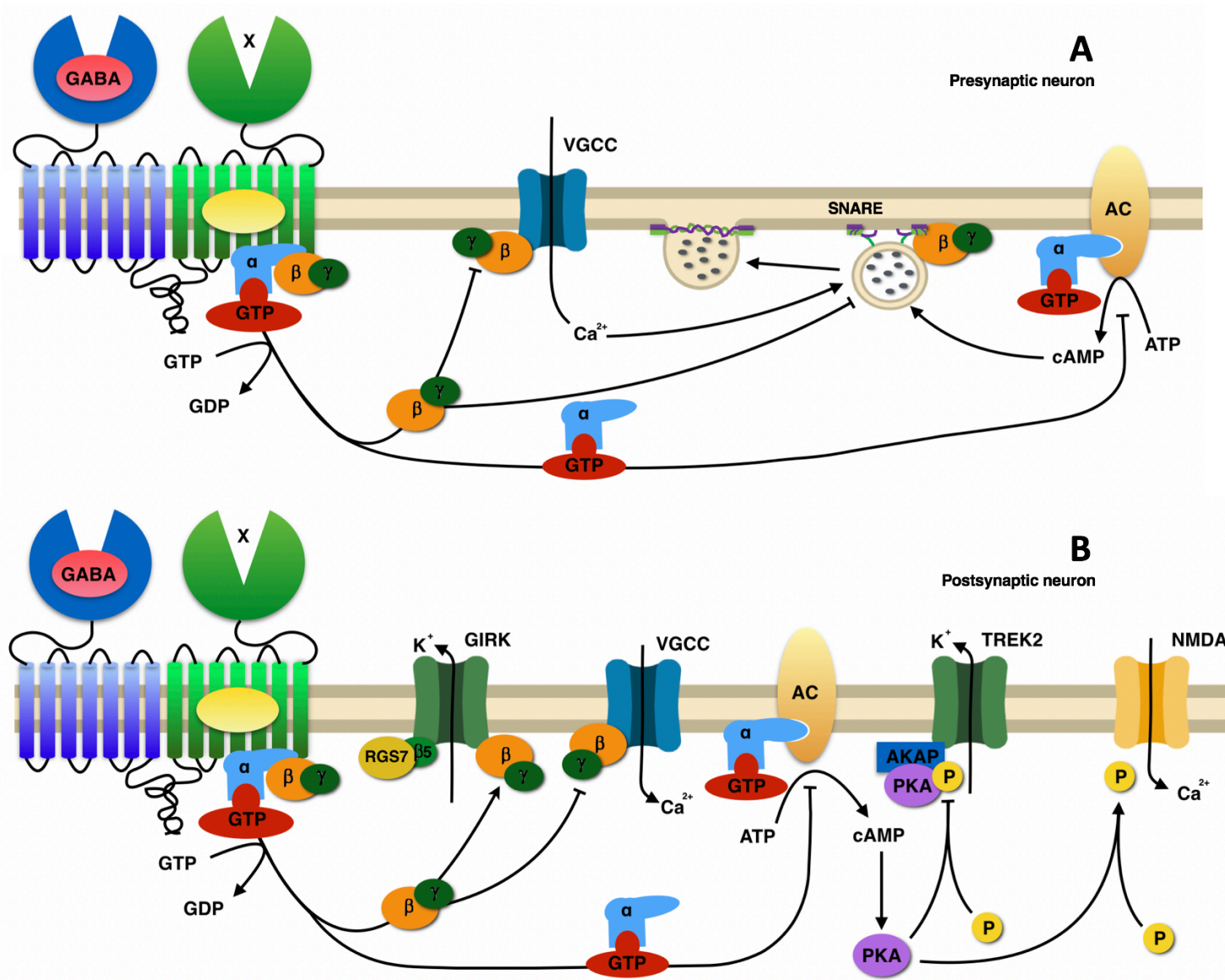
Figure 10 – Activation of the GABA$_B$-R and signaling pathways in A) presynaptic neuron and B) postsynaptic neuron. (figure modified from (Gassmann and Bettler, 2012). AC – Adenylyl Cyclase, GTP – Guanosine Triphosphate, cAMP – Cyclic Adenosine Monophosphate, ATP – Adenosine Triphosphate, VGCC – Voltage-gated Ca^{2+} Channel, GIRK – G-protein Coupled Inwardly Rectifying K$^+$ channel, TREK2 – Twik-related K+ channels, NMDA – N-methyl-D-aspartate, PKA – Protein Kinase A, AKAP – A-kinase anchoring protein, P – Phosphate, SNARE – soluble *N*-ethylmaleimide-sensitive factor attachment protein receptor.

1.4.4 GABA$_B$ receptor desensitization

Prolonged activation of the GABA$_B$-Rs can lead to receptor desensitization (Gassmann and Bettler, 2012). GABA$_B$-R does not necessarily follow classical desensitization mechanisms established for other GPCRs where phosphorylation-dependent uncoupling of G-proteins from the receptor by GRKs causes recruitment of arrestins and receptor internalization (Benke, 2012; Terunuma et al., 2010). There are evidences for that the GABA$_B$-R subunits may not be substrates of GRKs and that the receptor becomes internalized by other mechanisms (Terunuma et al., 2010). Different mechanisms for GABA$_B$-Rs desensitization have been proposed and the specific mechanisms may dependent on the neuronal population (Benke, 2012). A suggested phosphorylation-dependent pathway involves C-terminal association of N-ethylmaleimide (NEM) sensitive fusion proteins that causes recruitment of protein kinase C (PKC) which ensures phosphorylation followed by desensitization (Benke, 2012). An alternative suggested phosphorylation-independent pathway involves direct association between the C-terminal and GRK4 (a member of the G-protein coupled receptor kinase family), where GRK4 plays a central role in agonist-induced desensitization without phosphorylation (Benke, 2012; Terunuma et al., 2010). Phosphorylation of Ser867 in GABA$_{B1a/b}$ by calmodulin-dependent protein kinase II (CaMKII) induces endocytosis and thereby impairments of the receptor function (Gassmann and Bettler, 2012). Phosphorylation of Ser783 in the C-terminal of the GABA$_{B2}$ by AMP-dependent protein kinase (AMPK) is coupled to receptor recycling, whereas dephosphorylation of this residue has been associated with lysosomal degradation (Gassmann and Bettler, 2012). Phosphorylation of other serine residues in the C-terminal part of GABA$_{B2}$, and activity of potassium channel tetramerization domain-containing (KCTD) protein family have also been linked to the processes of surface stability, desensitization, recycling and degradation of the GABA$_B$-R (Benke, 2012; Gassmann and Bettler, 2012).

1.4.5 GABA$_B$ receptor-related pathophysiology

Disruption of GABA$_B$-R signaling pathways are connected to a variety of diseases and neuropsychiatric disorders such as depression, anxiety, schizophrenia, drug abuse and addiction, and gastroesophageal reflux disorder (GERD) (Calver et al., 2000; Fatemi et al., 2017; Heaney and Kinney, 2016; Pilc and Nowak, 2005; Tyacke et al., 2010; Varani et al., 2018). The effectors activated upon pre- and post-synaptic GABA$_B$-R activation are known to regulate expression of a long-lasting increase in signal transmission, which is favorably

associated with learning and memory (Gassmann and Bettler, 2012). The endogenous precursor of GABA, γ-hydroxybutyrate (GHB) is also a weak GABA-R agonist marketed as a therapeutic drug for treatment of narcolepsy, but as the compound also binds other receptors, the connection between the $GABA_B$-R binding and the pharmacological effects is uncertain (Carter et al., 2009; Gassmann and Bettler, 2012).

Recent studies have linked stimulation by baclofen to the reduction of addiction-related behavior towards nicotine, cocaine and alcohol in preclinical animal models (Augier et al., 2017; Varani et al., 2018). Drugs of abuse stimulate the reward system in the brain, called the mesolimbic system, which controls the release of the reward-associated neurotransmitter dopamine (Varani et al., 2018). In 2018, Varani *et. al.* published a comprehensive study on the involvement of the $GABA_B$-Rs on rewarding effects of nicotine by neurochemical, biochemical, molecular alterations and behavioral studies (Varani et al., 2018). Nicotine stimulates nAchRs located on GABAergic, glutamatergic and dopaminergic neurons, causing release of dopamine and rewarding properties (Varani et al., 2018).When the animals were pre-treated with baclofen, the drug activated $GABA_B$-Rs in dopaminergic and GABAergic neurons which significantly reduced the dopamine release by inhibition of the dopaminergic neurons (Varani et al., 2018, 2014).

The $GABA_B$-R agonist baclofen has also been shown to have anxiolytic effects in animal cognition models and has been implied to reverse anxiogenic responses from addiction-related withdrawal (Cryan and Kaupmann, 2005; File, S.E, 1993; Pilc and Nowak, 2005; Pizzo et al., 2017). Antagonists on the other hand have shown to exhibit antidepressant effects in a variety of animal models (Cryan and Kaupmann, 2005; Cryan and Slattery, 2010; Pilc and Nowak, 2005). Abnormal peripheral serum concentrations of GABA and glutamate, in addition to reduced levels of the enzyme GAD in the brain causing reduced levels of GABA, have been found in young adults diagnosed with depression and schizophrenia (Fatemi et al., 2017). Clinical and post-mortem examination of patients with clinical depression has also revealed changes in GABAergic neurons and regional changes in the concentration of the $GABA_B$-R isoforms in CNS ($GABA_{B1a/b}$ / $GABA_{B2}$), which may support the theory of involvement of the GABAergic system in depression (Fatemi et al., 2017; Ghose et al., 2011; Lissemore et al., 2018).

The activation and regulation mechanisms of the receptor can also be affected by binding of NAMs or PAMs to the 7TM allosteric site. There are currently no allosteric modulators

marketed for therapeutic use, though a PAM, ADX771441, is in phase I clinical trial towards alcohol-related behavior (Augier et al., 2017). Another concept that complicates and stresses the need for discovery of new orthosteric ligands to increase the knowledge about physiology and pathophysiology, is the fact that ligands may show functional selectivity by being an agonist for one signaling pathway and an antagonist for other pathways. Biased agonism (functional selectivity) is well described for class A GPCRs and class C mGluRs, but was recently suggested for PAMs of GABA$_B$-R (Emery et al., 2012; Sengmany and Gregory, 2016; Sturchler et al., 2017). The GABA$_B$-R PAMs GS39783 and BHF177 were found to have functional selectivity for intracellular signaling pathways in a various functional assays such as ERK$_{1/2}$ phosphorylation (Sturchler et al., 2017).

1.4.6 Characteristics of ligands targeting the orthosteric binding site of GABA$_B$

Today, the majority of the approximately 55 known GABA$_B$-R agonists and antagonists are GABA analogues (Evenseth et al., 2019; Froestl et al., 1996, 1995a, 1995b). The only FDA approved drug targeting the GABA$_B$-R is the agonist baclofen, which is used as a muscle relaxant and antispastic agent (Herman et al., 1992; Pilc and Nowak, 2005a). Baclofen has multiple pharmacokinetic limitations such as low penetration through the blood-brain barrier (BBB), a short duration of action and patients develop rapid tolerance (Deguchi et al., 1995; Lal et al., 2009). A large effort on development of drugs targeting the GABA$_B$-R has resulted in many structural analogues of GABA, but surprisingly many of these have shown to not bind to the receptor despite the high structural similarity to GABA (Brown et al., 2015). This emphasizes the need and benefit of discovering new GABA$_B$-R ligands and chemotypes different from GABA to study functional selectivity that promote beneficial and block deleterious pathways, in addition to being able to substitute baclofen in clinical applications. This knowledge can enhance our understanding on mechanism of activation, clarification of the role of different signaling pathways and potentially benefit in understanding of therapeutic effects.

The first known GABA derivative was baclofen, which was obtained by adding an halogenated phenyl ring to the β-carbon (Fig. 11) (Enna, 1997). Further, new series of potent GABA$_B$-R agonists was discovered by replacement of the carboxylic acid of GABA for unsubstituted phosphinic- and methylphosphinic acids (Froestl et al., 1995a). A series of antagonists was also derived from GABA and baclofen by replacing the α-acid group with substituted phosphonic-

and sulfonic acid groups (Froestl, 2010; Froestl et al., 1996, 1995b). The baclofen analogues were found to be low affinity antagonists, such as 2-hydroxysaclofen (Fig. 11) that is one of the compounds available in X-ray crystal complexes (PBD ID: 4mqf). Despite that this compound show antagonistic properties, the interaction pattern is more similar with the interaction patterns of agonists including the VFT residues His170, Glu349, Ser130 and Ser 153 (Geng et al., 2013). The GABA phosphinic acids analogues were found to be high affinity antagonists in the lower nanomolar range when benzyl substituents were added (Fig. 11) (Blackburn and Bowery, 2010; Froestl et al., 1995b).
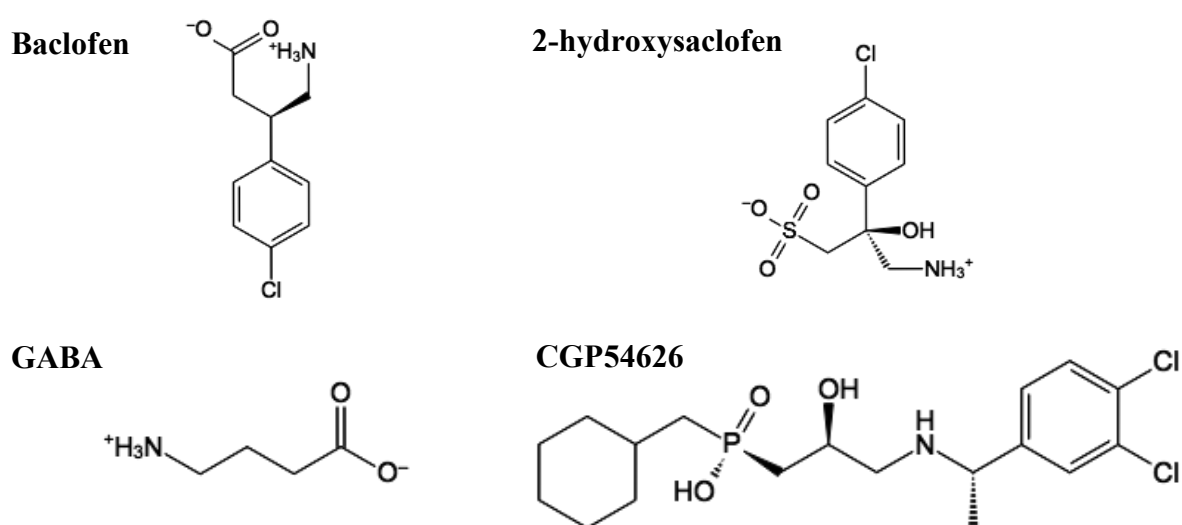
Figure 11 – Structure of the agonists baclofen, the baclofen analogue 2-hydroxysaclofen which is a weak agonist, GABA, and the strong antagonist CGP54626.

1.5 Computer-based methods in structural biology and drug discovery

1.5.1 Conventional drug discovery

Drug discovery is the process of identifying new pharmaceutical ligands for a target. Identification of novel ligands with the ability to modulate the activity of biomolecular targets can contribute to the understanding of pathological and physiological mechanisms and to the development of new drugs (Coudrat et al., 2017; Sliwoski et al., 2014). Taken into consideration the high number of potential drug candidates, high-throughput screening (HTS) is essential for effective identification of novel ligands binding specific targets. HTS is often the first step in the process of identifying potentially new drug candidates, called hits, before the hits are optimized, and the efficacy and selectivity towards the target *in vitro* are determined. The next step in preclinical testing is animals studies to establish pharmacokinetics and toxicological profiling (Mohs and Greig, 2017). The next step is clinical trials, where drug candidates are tested on an increasing number of humans during the course of three phases to establish efficacy in humans and identify putative toxic effects among other properties (Mohs and Greig, 2017). The drug development process from identification of drug targets and potential candidates to marketing normally takes 12-15 years and the costs are estimated to reach billions of dollars (Mohs and Greig, 2017; Rang and Dale, 2012).

Conventional approaches in the field of drug discovery rely mainly on stepwise synthesis and assays for screening large number of compounds to identify potential drug candidates (Sliwoski et al., 2014). During the last decades, efforts have been put into computational molecular modelling strategies for drug design and screening. The use of molecular modelling methods to identify drug candidates towards a target of interest is cost- and time effective compared to sole *in vitro* screening, and combined with *in vitro* methods, computational methods may speed up the screening process (Sliwoski et al., 2014).

1.5.2 Molecular mechanics and force fields

Molecular modelling includes all computer aided approaches that aspires to study characteristics such as chemical and physical properties of molecules and molecular systems, and mimic their behavior (Sansom and Smith, 1998). The first step in molecular modelling studies is often to generate computer models of molecular structures, before applying these

models in different types of calculations of molecular properties. The basis for most of the calculations is a molecular mechanical (MM) description of the molecules. In MM, the potential energy of a molecular system is approximated by treating each atom including the atomic particles as a point, or sphere, which are assigned charges (Leach, 2001). The points are connected by springs (bonds) and the energy within the system is calculated from terms such as bond stretching, angle bending, bond rotations (torsional energy associated with relative orientation of atoms in a dihedral or torsion angle) and non-bonded interactions (Patrick, 2017). Treating each atom with all its particles as a point is based on the Born-Oppenheimer approximation, which expresses that the movements of electrons will follow the movements of the nuclei (Leach, 2001). This assumption makes it possible to calculate the energy of the system as a function of the sphere coordinates (Leach, 2001). A contrast to this approach is quantum mechanics (QM), where the energy of the system is calculated by explicitly following the movement of all atomic particles in the system (Höltje et al., 2008).

In MM, the potential energy of a system is calculated as a function of conformations reflecting the atom coordinates in space with 6N degrees of freedom and force constants (empirical parameters) by using a force field (FF) (Höltje et al., 2008; Leach, 2001). Most FF first assign an atom type to each atom in the system that contains information about the hybridization state (number of single, double or triple bonds a specific atom forms) and in some cases additional information about the local environment (Leach, 2001). The potential energy of a system is calculated as a function of intra- and inter molecular forces between these points with energetic penalties associated with deviation of bond lengths, angels and torsions from reference (i.e. X-ray/NMR structures) or equilibrium values derived experimentally or by *ab initio* QM calculations (Leach, 2001). Assigning atom types is therefore also important because variables such as angle and bond length change depending on the type of bond between the atoms (Leach, 2001). Calculation of the potential energy as a sum of the steric energy in terms of deviations from unrestrained ideal values, and non-bonded terms such as the van der Waals potential and the electrostatic coulomb potential together with force constants make up the FF (Höltje et al., 2008). The total energy of the system is in fact a calculation of the intramolecular strain in relation to the ideal molecule, where all deviations from the "natural" unstrained molecule leads to an increase in the energy (Höltje et al., 2008). The general equation of a force field can be written as equation 1:

$$E_{tot} = (E_{bonds} + E_{angles} + E_{torsion}) + (E_{elec} + E_{vdw}) \quad (1)$$

where the total energy is a function of the covalent and non-covalent bonding terms (Höltje et al., 2008).

More sophisticated force fields such as the MM2, MM3 and MM4 have additional terms, including improper torsions and out-of-plane bending motions (González, 2011; Leach, 2001). These types of force fields are more appropriate for calculations involving "small" molecules as they also have a comprehensive atom typing schemes e.g. differentiate types of carbon atom like those present in a cyclopropane, cyclopropene or a carbonyl (Leach, 2001). In addition, some force fields provide parameters for every single atom within the system (all-atom FFs, e.g. the Schrödinger OPLS3 FF (Harder et al., 2016)), while others exclude the non-polar hydrogens (united-atom FFs, e.g. the GROMOS96 FF (Hu and Jiang, 2009)) or represent molecules as "super atoms" (coarse-grained potential e.g. the Martini FF (Periole and Marrink, 2013)). Hybrid force fields also exists, using both MM and QM to calculate the potential energy where the parts under investigation often are represented by QM, while the less relevant parts are represented by MM (González, 2011; Höltje et al., 2008; Vanommeslaeghe et al., 2014).

A suitable FF describes as many different molecules as possible with a certain accuracy. Several FFs have been developed and the selection of an appropriate FF is dependent on the target under investigation and the goal of the study. The number of terms and the quality of the parameters will affect the potential energy function and thereby the reliability of the function (Höltje et al., 2008). Calculations where high accuracy is necessary, like investigation of ligand interaction with a binding site, would require all atoms of the binding site and the ligand to be explicitly described in order to not loose essential information on interaction.

1.5.3 Structural representation of molecules and energy minimization

In order to perform molecular calculations on proteins or other molecules, a 3D structural representation of the target is necessary. The 3D structure of proteins and other macromolecules can be determined by experimental methods such as X-ray crystallography, nuclear magnetic resonance (NMR) spectroscopy or cryo-EM. If the target does not have a solved experimental structure, theoretical 3D homology models can be constructed if an appropriate template is available (Vyas et al., 2012). This approach takes advantage of the observation that tertiary structure is more conserved than the primary structure of proteins belonging to the same family

(Chothia and Lesk, 1986), and uses the resolved structure of a homologous protein as a template for constructing the theoretical model of the protein target of interest.

The atomic coordinates of experimentally determined 3D structures or homology models must be geometry/energy optimized using MM computational methods as unfavorable bond lengths and angels, and torsions may be present in the structure (Patrick, 2017). Optimization is performed by an energy minimization where the aim is to identify a stable and low-energy conformation of the protein and/or the ligand. There may be a large number of low energy conformations, and on an energy surface the conformation with the lowest energy is called the global energy minimum (Fig. 12) (Leach, 2001). There are multiple available energy minimization algorithms and the choice of algorithm is dependent of various factors such as size of the molecular system in consideration, computational requirements and robustness of the methods. Two of most popular minimization algorithms are the conjugated gradient and steepest decent methods. Sometimes a combination of these two methods is also used. These methods locate a minimum point on an energy surface by gradually changing the coordinates of the system as they move closer to this point based on previous iterations (Leach, 2001).
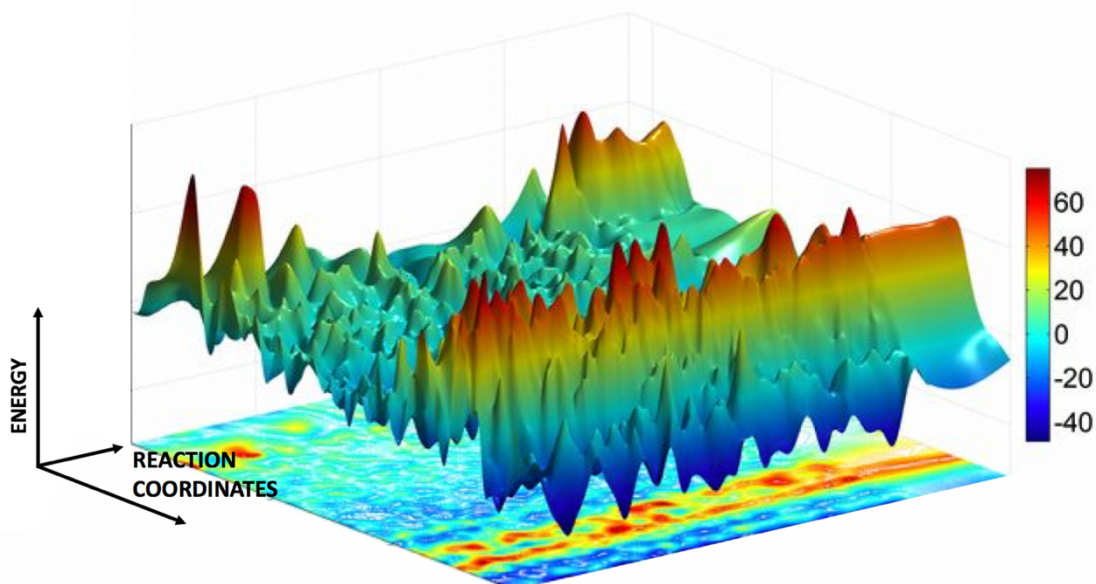
Figure 12 – An illustration of an energy landscape of the folding states of a protein with the reaction coordinates along the x and z axis and the free energy along the y axis. The landscape shows multiple hills (saddle points) indicated with arrows that leads to local minimums (green and yellow colors) and a global minimum (blue color) (modified from Bai et al., 2013).

1.5.4 Conformational dynamics

Structural motions and dynamics are necessary for the interplay between biological molecules. During the process of drug recognition and binding, the drug and the target are adopting to the structure of each other, and the drug binding target conformation is not necessary the lowest energy conformation obtained from experimental studies. Computer simulations can be used to study conformational dynamics and may give insight into dynamic processes that are impossible to study by traditional experimental methods. Several theoretical methods are available for studying conformational dynamics.

1.5.4.1 Molecular dynamics

In a biomolecular system, every single atom has a specific mass, position in space and movement of certain velocity. The time-line of atomic movements has been experimentally studied indicating that the position of an atom change within 1-2 femtoseconds (fs), and this information has been utilized in numerical models for mimicking molecular behavior (Leach, 2001).

Molecular dynamics (MD) is one of the commonly used methods that can be applied for conformational analysis and studies on time-dependent structural motions. MD uses Newton's laws of motion to mimic the evolution of a collection of interacting atoms as a function of time (Höltje et al., 2008). The simulation time is divided into time steps in the fs range in order to include the fastest motions of the system (Leach, 2001). At the beginning of the simulation, the gradient of the potential energy function is used to calculate the forces acting on each atom in the system, while the acceleration and velocities are generated randomly (Leach, 2001). Based on the initial position, new positions and velocities are updated at time t using Newton's laws of motion (Leach, 2001; Patrick, 2017). The results are successively collected in a trajectory that specifies how the position and velocity of particles vary with time.

Newton's second law of motion states that the acceleration of a system is dependent on its mass and the forces acting upon the object and is calculated as:

$$F_i(t) = m_i \, a_i(t) \quad (2)$$

where F_i is the net force on atom i at time t, m_i equals the mass of atom i and a is the acceleration of atom i at time t (Fehske et al., 2008).

As atoms are constantly moving, molecular systems can obtain a broad variety of conformations, where some are high in energy states (saddle points), while other are low energy states (local or global minimums) (Fig. 12). In an MD simulation, there is always a risk that the simulations are not long enough to reach all energetically favorable conformations (Henzler-Wildman and Kern, 2007). This means that the system can be trapped in a local energy minimum without having explored the conformational space to access other local energy minimum or even the global minimum (Fig. 12). In nature, conformational changes of the protein main chain and protein folding occur in microsecond (μs) to second scales (Henzler-Wildman and Kern, 2007), and with timesteps in the fs range, millions to trillions of timesteps are required to simulate in the nano- to millisecond (ns to ms) events. The required amount of computational power and storage space needed to perform such MD simulations on a system of a certain size is the limiting factor even with the current generation of computers where multiple processors can be used in parallel to perform the calculation (parallel computing) (Lindahl, 2015). However, tremendous progress has taken place in the field since the publication of the first MD simulation, the *in vacuo* 9.2 picoseconds (ps) simulation of the 58 amino acid protein bovine pancreatic trypsin inhibitor, in 1977 (McCammon et al., 1977). For instance, the activation mechanism of the β_2-adrenergic receptor (a class A GPCR) has been studied by performing 50 μs MD simulations of the receptor-agonist complex embedded a lipid bilayer and explicit water molecules (Dror et al., 2011). MD simulations have also been successfully applied to other studies like ligand binding/unbinding and protein folding (Zhu et al., 2017).

1.5.4.2   Metadynamics and Path Collective Variables

Sampling of rare events, exploration of reaction coordinates and reconstructing free energy surfaces associated with certain events can be calculated by using biased sampling algorithms like metadynamics (MetaD) (Branduardi et al., 2007). The method rely on a physical pathway describing a movement of interest as a function of a few reaction coordinates (Barducci et al., 2011). These movements of a system are biased by adding a history-dependent bias potential in the form of Gaussians to the appropriately chosen reaction coordinates, called collective variables (CV) (Laio and Gervasio, 2008). These variables must be carefully chosen as they should represent the slow degrees of freedom and represent the states of the system under investigation (Barducci et al., 2011).

Selecting appropriate CVs is highly challenging as macromolecules have large degrees of freedom and topological complexity. The bias potential is deposited as a sum of Gaussian functions along points visited in space and thereby encouraging the system to explore new regions (Barducci et al., 2011). The sum of Gaussians added to the system is then used to reconstruct an estimator of the free energy and at the same time, providing the system with energy to escape local minima and explore higher energy conformations in the phase space that unbiased MD cannot access (Laio and Gervasio, 2008). The principle of the algorithm is often explained by using the example of a person out walking at night who falls into a pool (Laio and Gervasio, 2008). The pool edges are too steep for climbing out, and the darkness makes it difficult to detect the shallowest point. If the person has access to sand, she could deposit this sand in her current position (Gaussians) and by some point she would be able to climb out. By the time she climbs out, larger regions of the pool have been explored and she is likely to climb out from the shallowest point (Laio and Gervasio, 2008). The positions of the deposits could afterwards be used to reconstruct the negative image of the pool (free energy).

Deciding when to terminate a MetaD simulation can be difficult because the energy does not converge to a definite value, but the molecular system rather fluctuates around or starts revisiting previous visited conformational space, and in the worst case is pushed into irrelevant conformational space (Barducci et al., 2008). Well-Tempered MetaD (WT-MetaD) has been developed in the effort to overcome this problem, where the Gaussian height is rescaled and decreased during the course of the simulation (Barducci et al., 2008).

There are multiple CVs that can be applied, including dihedrals, angles, and atomic distances, and in addition a path may also be used as a CV (PCV) (Laio and Gervasio, 2008). PCVs provide an optimal description of the process under investigation, given that the endpoints of the transition are known and an educated guess of the underlying mechanism is made. Specifically, with PCVs, the path joining the endpoints is described by an ensemble of intermediate structures in conformational space ($\mathbf{x}$) which represent the so-called frameset ($i =$ 1, 2, …, N). The frameset is used as a reference when running a simulation of the target of interest, and the simulation is evaluated by following the progression along the path and the distance from the path through the following variables ("CV Documentation," n.d.):

$$S = \frac{\sum_{i=1}^{N} i \exp\left(-\lambda R[\mathbf{x}-\mathbf{x}_i]\right)}{\sum_{i=1}^{N} \exp\left(-\lambda R[\mathbf{x}-\mathbf{x}_i]\right)} \qquad (3)$$

$$Z = -\frac{1}{\lambda} \ln\left(\sum_{i=1}^{N} \exp\left(-\lambda R[\mathbf{x} - \mathbf{x}_i]\right)\right) \tag{4}$$

where i is the index of the frameset ranging from 1 to N (number of frames in the path), the S and X are distance functions from each of the high-dimensional frames R[x-x_i], and λ is a smoothening parameter (Branduardi et al., 2007).

In essence, if the description of the path from endpoints A to B is incorrect, large values of Z representing the distance from the path (often measured in mean square deviation from an optimal alignment) can be observed and the reaction under investigation might be incomplete ("Adaptive variables I," n.d.). A simple visualization of the S(X) and Z(X) variables are showed in figure 13.
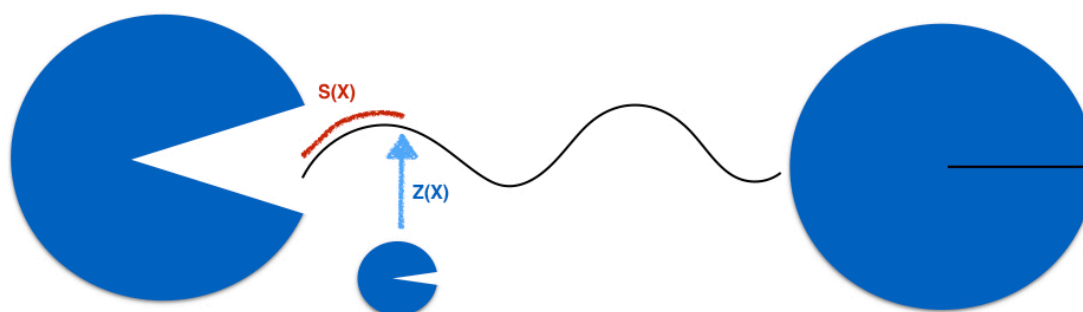
Figure 13 – A schematic illustration of variables calculating the progression along the path (S(X)) between the endpoints and the distance (Z(X)) from the path. The endpoints are illustrated as the inactive (open) and active (closed) VFT conformations.

1.5.4.3 Monte Carlo

Monte Carlo simulation is a stochastic method that generates conformations of a system by random particle sampling (Höltje et al., 2008). After performing a random move, an energy minimization is performed and the new configuration is compared to the previous one. If the new conformation is in a lower stable energy state, the conformation is accepted and used as a starting point for the next iteration (Leach, 2001; Patrick, 2017). The method provides an ensemble of conformations, but does not provide any information about time evolution (Paquet and Viktor, 2015). If the method is run for sufficient amount of time, the whole conformational space should in theory be covered, but with a high risk of resampling already visited conformations (Höltje et al., 2008). The method is not restricted by the size of the system; however, very flexible systems may not converge due to the large conformational space (Höltje et al., 2008).

1.5.5 Water models

Water molecules are the most important and active biomolecules in nature as they are essential in processes such as stabilization of macromolecular structures, dynamics, function and interactions. Ligand binding induces a conformational change in the receptor and displacement of water molecules can increase the binding affinity (Höltje et al., 2008). The water molecules might also bridge protein and ligand interactions (Lemmon and Meiler, 2013). In molecular modelling, water molecules are important components that can be included in a macromolecular system implicitly or explicitly (Leach, 2001).

In implicit water models, there is no actual water molecules present in the system, but a dielectric model is added to the electrostatic interaction term calculated by the FF as the effect of a solvent will dampen theses intermolecular forces (Leach, 2001). In contrast, explicit solvation models specifically encounter solvent interactions with the solute (Leach, 2001). In simple water models such as transferable intermolecular potential 3P (TIP3P) and simple point charge (SPC) model (Mark and Nilsson, 2001), three interaction sites for electrostatic interactions are included in which the two hydrogen atoms are given a slightly positive charge which is balanced by a negative charge on the oxygen atom and only oxygen atoms in interacting water molecules are participating in van der Waals interactions (Leach, 2001).

In exhaustive sampling methods such as MD and MC, explicit water molecules are preferably used in order to make the systems as realistic as possible to increase the accuracy of the calculations. When docking a large database during virtual screening (VS), the inclusion of water molecules becomes much more difficult (Höltje et al., 2008). The ligand binding mode may not be known and the positions of water molecules might not be known, and both position and numbers of water molecules for binding may vary between ligands. If resolved 3D structures of the target are available, this could provide information about the presence of water molecules, but incorporating them into a VS process might be inaccurate and is computationally demanding. The included water molecules are often treated as a part of the protein in a fixed position and ligands should therefore be docked with and without the presence of water to evaluate the effect (Höltje et al., 2008). The consequences of not considering the presence of water molecules might include incorrect binding mode, and studies investigating the accuracy of predicting correct ligand pose by re-docking ligands into their respective 3D structures were significantly improved by the presence of crystallographic water molecules (de Graaf et al.,

2005). However, in such cases compared to using a water model, the results only affect the sampling of ligands and not the scoring (Lemmon and Meiler, 2013).

1.5.6 Virtual Screening

In silico (computer-aided) methods applied in a process that aims to identify active molecules from chemical databases, is called virtual screening (Shoichet, 2004). A VS protocol can be seen as a complementary approach to experimental HTS (Coudrat et al., 2017). There are a wide variety of computational techniques and algorithms that can be used in a VS, and the methods are divided into two major categories; active compounds retrieved based on knowledge of excising ligands (ligand-based methods) or available structure information (structure-based methods) (Aparoy et al., 2012). In 2010, Ripphausen *et al.* reported, after a comprehensive study on published VS procedures, that structure-based methods were much more commonly used than ligand-based methods (322 published studies using structure-based methods as the last step in the VS protocol against 107 studies using ligand-based methods), despite the fact that ligand-based methods on average identified ligands with higher potency (Ripphausen et al., 2010).

Screening libraries containing millions of compounds can be time-consuming and computational exhausting. This is one of the reasons for that a typical work-flow often combines both ligand- and structure based methods, in addition to filtering methods (Sliwoski et al., 2014). Starting a VS campaign with the less time consuming methods such as filtering procedures is beneficial to reduce the large number of compounds to a more manageable size where more comprehensive methods can be applied like docking or extensive energy calculations such as Linear Interaction approximation (LIA) or MD (Sliwoski et al., 2014). The result of the work-flow is a library of ligands theoretically predicted to bind the target, that must be further tested/evaluated experimentally (Fig. 14) (Sliwoski et al., 2014).

There are multiple methods that can be applied for *in vitro* testing and the choice of method depends on factors such as the amount of ligands to test and the target protein in the study. High-throughput methods such as radioligand binding studies are often used as a first step in the screening procedure to remove unlikely binders effectively (Zhang and Xie, 2012). Other high-throughput methods such as cAMP- or calcium assays can be applied for investigation of intracellular signaling pathways, given that the coupling mechanisms are known (Zhang and

Xie, 2012). In later stages of the *in vitro* evaluation, more accurate and time-consuming methods such as the SPR are applied to further characterize the remaining potential candidates.
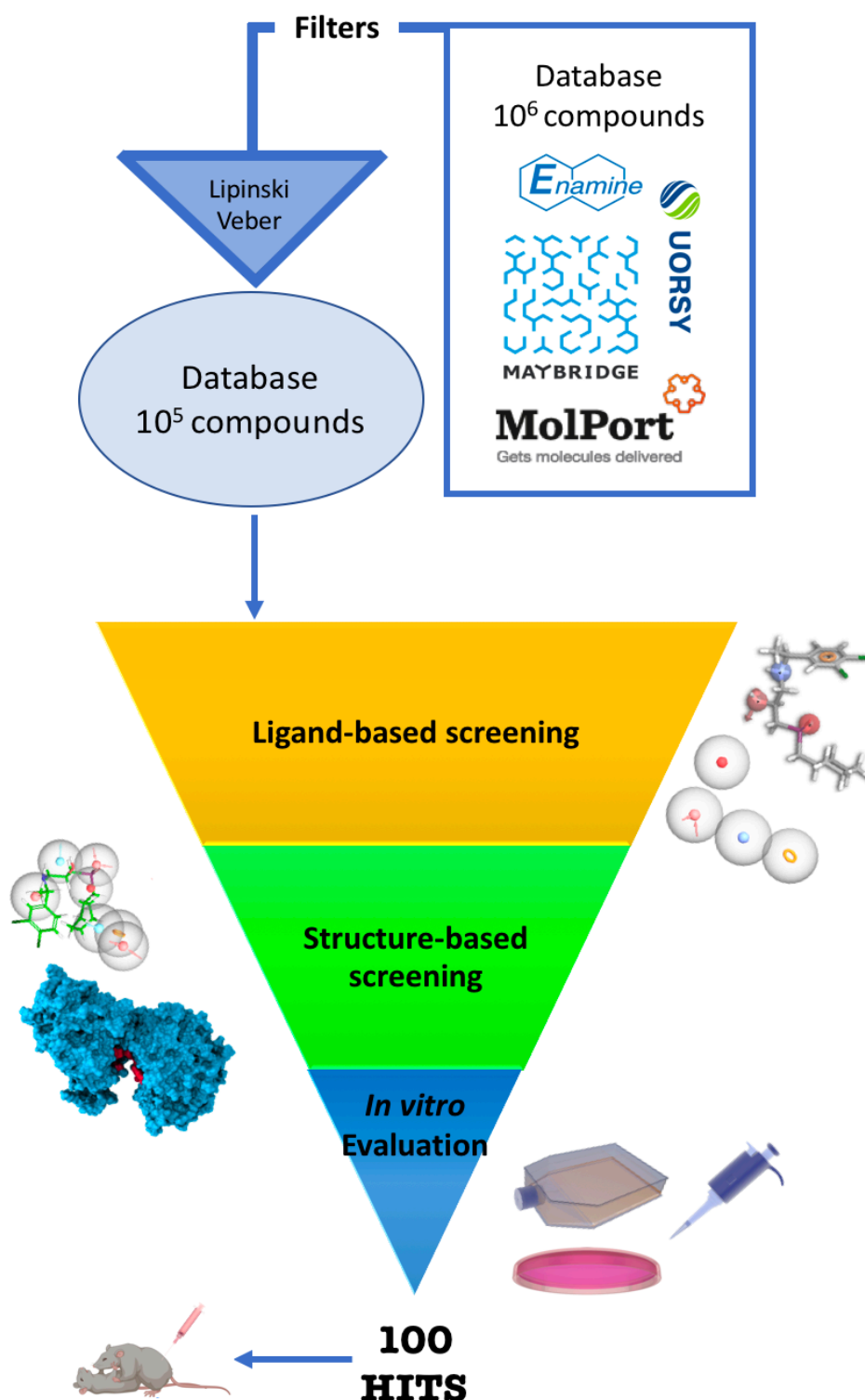
Figure 14 – An illustration of a classical VS work-flow starting from filtering followed by ligand-based and structure-based screening, selection and verification of potential hits.

1.5.6.1 Ligand databases for Virtual Screening

There are multiple commercially available databases of compounds that can be used for *in silico* screening. Typically, these databases contain up to millions of compounds, from natural products to synthetic compounds. The ZINC database is a curated collection of commercially available chemical compounds that in 2016 contained more than 100 million compounds (Irwin and Shoichet, 2016), and will continue to grow as it has been estimated that the number of drug-like molecules that could be synthesized are approximately 10^{33} (Polishchuk et al., 2013). Databases often provide options of different subsets of compounds from unfiltered collections to lead-like collections.

1.5.6.2 Filtering of ligand databases

A compound can be labeled as drug- or lead-like compound based on a set of rules (filters) determined from analysis of approved pharmaceuticals and compounds reaching phase II of clinical trials (Lipinski et al., 2001; Yusof and Segall, 2013). The most commonly applied filters for determining drug-likeness is the Lipinski's "rule of five" (Lipinski et al., 2001) and the Veber's rules (Veber et al., 2002). The "rule of five" describes a set of characteristics that drugs with good bioavailability (high proportions reaching systemic circulation) share, after oral administration (Battista et al., 2015; Lipinski et al., 2001). Lipinski's "rule of five" states that compounds with molecular weight < 500 Da, octanol-water partition coefficient (log P) < 5, the number hydrogen bond acceptors < 10 and the number of hydrogen bond donors < 5, have good oral bioavailability (Lipinski et al., 2001). Lipinski suggested that if a compound breaks two of the rules it is less likely to be absorbed (Lipinski et al., 2001). After testing more than 1100 drugs in rat, Veber *et al.* suggested two additional rules for ensuring bioavailability after oral administration (Veber et al., 2002). They found that ligands with an oral bioavailability of $\geq 20\%$ after oral administration have a polar surface area (PSA) of ≤ 140 Å^2, and a number of rotatable bonds of ≤ 12, and suggested that both molecular flexibility and PSA influence drug absorption (Veber et al., 2002).

Drugs that act in the CNS, e.g. antidepressant and anxiolytic drugs, are required to have more strict characteristics than previously described due to the presence of the BBB. The blood vessels transporting nutrition and waste products in and out of the CNS, have a unique property allowing them to tightly regulate the flow of molecules and serves multiple functions including maintenance of the homeostasis and protection of the CNS. In contrast to endothelial cells blood

vessels elsewhere, the endothelial cells of these vessels are connected by tight junctions, surrounded by a special cell type called astrocytes (a non-neuronal cell in the CNS) in addition to other supportive cell types and together they comprise the blood-brain-barrier (BBB) (Daneman and Prat, 2015). It has been estimated that more than 98 % of the approved drugs do not cross the BBB (Geldenhuys et al., 2015) and multiple studies have investigated the necessary properties of a drug to penetrate the BBB by passive diffusion (Geldenhuys et al., 2015; Konovalov et al., 2007; Yan et al., 2013). Ghose *et al.* (2012) did a comprehensive study that included 943 approved drugs, and suggested following BBB penetrating criterions: PSA < 76 $Å^2$, > one nitrogen atom, < 7 linear chains outside a ring structure, < 3 polar hydrogens, solvent-accessible surface area of 460-580$Å^2$, a volume of 740-970 $Å^3$, and the Schrödinger QikProp CNS value > 0 (Ghose et al., 2012).

The Lipinski, Veber and "BBB" rules have many strengths and weaknesses, and exceptions of the rules exist. A study, investigating the 82 best-selling drugs reported by the American Information Medical Statistics in 2007, found that 11.7 % of the drugs did not follow two or more of the Lipinski rules (Gimenez et al., 2010). Another analysis of data retrieved from the US FDA on small-molecule drugs showed that out of 1204 unique drugs, 885 passed the rule of five but only 70 % of the 885 compounds were administered orally (Overington et al., 2006). Compounds produced by living organisms, called natural products, such as the macrolide class antibiotics (Benet et al., 2016), are also excluded from the "rule of five" because they are substrates for transporters in the body (Lipinski et al., 2001). This show that the rules should be encountered more as guidelines than strict rules. Filtering large databases of millions of compounds is necessary to decrease and remove a substantial amount of unlikely drug candidates. Rejecting potential good candidates is always a risk, especially if rules are too strictly emphasized, and the filtration criteria should therefore be carefully selected. Both Lipinski´s and Veber´s rules are related to oral administration, which is the most preferred route of administrations and other routs of administration such as topical or parenteral have other rules (Yusof and Segall, 2013).

There are also filters that more extensively calculates the physicochemical properties than the The Lipinski, Veber and "BBB" rules. Pharmacokinetic properties such as absorption, distribution, metabolism, elimination and toxicity (ADMET) can be included in the screening process (Ntie-Kang, 2013). ADMET properties are commonly applied in the process where hits from the screening are optimizing to be more favorable for biological activity, called hit-to-lead

optimization and for further optimizing leads (Sliwoski et al., 2014). Calculations of some ADMET-based properties can also be applied earlier in the screening process, to eliminate unlikely candidates (Sliwoski et al., 2014). An ADMET profile can include descriptors such as solvent-accessible surface area including the size of the hydrophobic area, number of likely metabolic interactions, polarizability, binding to serum albumin, number of reactive groups just to mention a few properties (Ntie-Kang, 2013). The Schrödinger (*Schrödinger Release 2019-3*, 2019) software offers calculation of ADMET profiles, where a total of 52 properties are encountered including the previous motioned filters for oral absorption and gives an estimate of the likelihood that a compound will have undesirable properties (Schrödinger, 2019).

1.5.6.3   Ligand-based drug discovery methods

In general, Ligand-based Drug Discovery (LBDD) is a term used for methods that are based on utilizing information about the structure of known active- and inactive ligands and constructing a predicative relationship between their structure and the activity (Höltje et al., 2008). LBDD is based on the very basic assumption that similar ligands have similar biological activity (Martínez-Archundia et al., 2018). The most common and important methods within this category are pharmacophore models, fingerprint methods and quantitative structure activity relationship (QSAR) (Aparoy et al., 2012).

1.5.6.3.1 Fingerprinting

Binary 2D fingerprinting is a widely used ligand-based method applied in drug discovery with the purpose of characterizing and comparing molecules to find structural similarities. Characteristics of molecules are described by using a set of bits (numbers) representing the presence or absence of chemical moieties within ligands and together these bits form a binary fingerprint (Duan et al., 2010). The ligands are fragmented into different sized fragments before the presence or absence of features are displayed as "on" bits by flipping the integer from 0 to 1 in the bit string (Cereto-Massagué et al., 2015). There are multiple different fingerprinting methods that differ in the way they perform molecular fragmenting, atom typing schemes and hashing, but the main objective for all methods is to transform a molecular representation into a bit string (Cereto-Massagué et al., 2015; Duan et al., 2010). Some fingerprinting methods also compare the absence or presence of features in a molecule to pre-defined schemes of substructures before turning on bits if the substructure is found, called substructure key-based fingerprints (Fig. 15) (Cereto-Massagué et al., 2015).
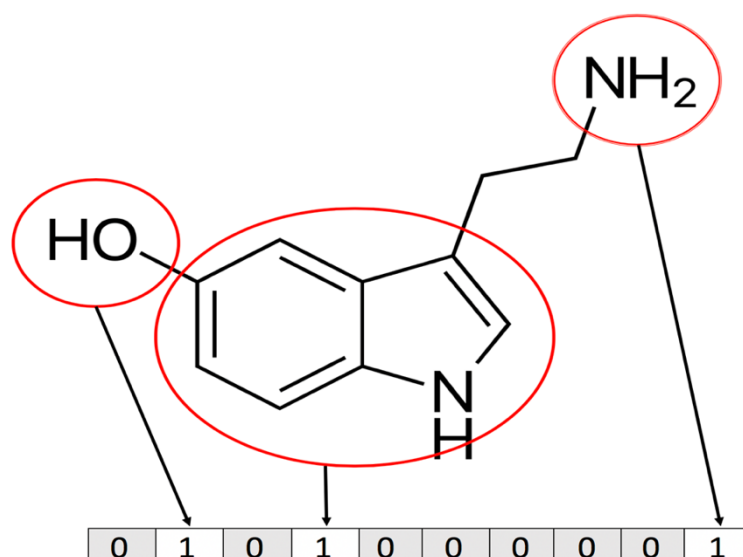
Figure 15 – Representation of a hypothetical 10-bit substructure keys-based fingerprint. Three bits are set (integer 1) because the substructure they represent is present in the molecule.

2D fingerprinting methods are commonly used to screen databases to identify new ligands with similar characteristics using a similarity index (Duan et al., 2010). Tanimoto similarity index is one of the most commonly used similarity metrics methods and computes the similarity between two molecules by calculating the relationship between "on" bits shared by the ligands in relation to "on" bits in the individual molecules according to equation 3 (Cereto-Massagué et al., 2015; Duan et al., 2010).

Tanimoto similarity = c / (a + b - c)   (5)

where a is the number of activated bits in molecule A, b is the number of activated bits in molecule B and c is the number of active bits shared between molecule A and B (Duan et al., 2010).

1.5.6.3.2   Ligand-based pharmacophore modelling

A pharmacophore model is a representation of the 3D arrangement of chemical- and steric features that are in common for active molecules targeting a specific protein (Horvath, 2010). Pharmacophore models should represent the 3D features necessary for activity, and in theory represent the complementarity of the target binding pocket (Höltje et al., 2008). When multiple active ligands are available they can be clustered based on their structures in order to develop multiple pharmacophore models that cover a greater chemical space (Horvath, 2010).

The typical workflow for generating pharmacophore models starts with identification and collection of active ligands before conformational sampling of the ligands. The next step is assigning atom types or classification of atoms according to their chemical environment and potential interaction behavior based on their chemical characteristics (Horvath, 2010). The ligands are then aligned or superimposed in such a way that a maximum numbers of common features overlap in the geometrical space (Fig. 16) (Sliwoski et al., 2014). A common feature map is then generated with features such as aromatic rings, hydrogen bond donors and acceptors, cations and anions and hydrophobic areas (Fig. 16) (Sliwoski et al., 2014). The models are commonly implemented as spheres with a matching-tolerance radius (Sliwoski et al., 2014). After common pharmacophores models are constructed, they are often ranked based on the "matching-rate" with the ligands in the dataset (Güner, 2000). A last evaluation step is often performed to test the selectivity of the models, where the models are testes against inactive ligands (Sliwoski et al., 2014).

The pharmacophore models can be applied for screening a compound database to identify new potential active ligands that can be mapped to the 3D hypothesis (Salam et al., 2009).
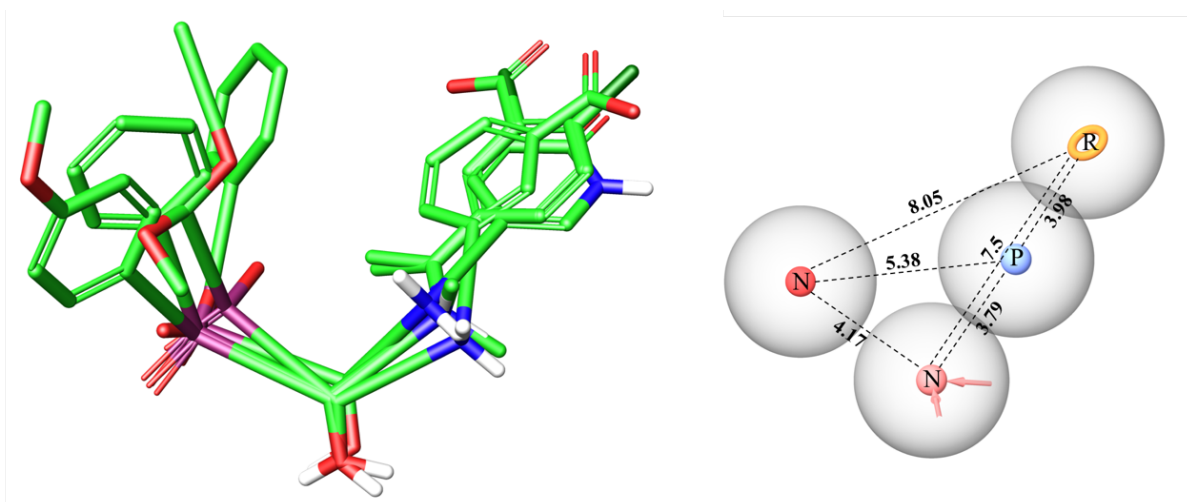
Figure 16 – Ligand-based pharmacophore model with features shown as spheres. Left) Multiple ligands are superimposed to find common pharmacophore features. Right) A pharmacophore model with 4 pharmacophore features and the intersite distance (Å) between the features. Red (N) - Negatively charged, orange (R) – aromatic ring and blue (P) – positively charged.

1.5.6.4 Structure-based drug discovery methods

Structure-based Drug Discovery (SBDD) methods elucidate the structural information of the drug target from either experimentally resolved 3D structures and/or homology models, or implicitly by using pharmacophore models that in theory consists of features complementary to the binding pocket (Höltje et al., 2008). The most common and important method within SBDD is docking and scoring, where ligands are sampled in the binding pocket and scored according to energies associated with specific poses in order to select the best pose and rank the different ligands (Huang and Zou, 2010).

1.5.6.4.1 Docking and scoring

The process of ligand binding to a target was initially described in 1894 by Emil Fischer as "key in a lock" concept where complementary geometric shapes are required for the substrate (key) to fit in the enzyme (lock) (Koshland, 1995). This principle was later modified by Koshland who described the binding of a substrate to an enzyme as a dynamic process where the enzyme underwent conformational changes, a process named induced fit (Koshland, 1995). In molecular modelling, one approach of molecular docking is the process where a ligand is placed within the binding site of a target with the main goal to predict the ligand conformation, orientation and binding affinity (Kitchen et al., 2004; Morris and Lim-Wilby, 2008). A sampling algorithm is used for searching ligand conformations and orientations, and a scoring function is used to estimate the "match", in terms of relative binding affinity, between the ligand and the binding pocket (Kitchen et al., 2004). Ideally, sampling algorithms should reproduce the experimental binding mode and the scoring function should also rank that binding mode highest among all generated conformations.

Both ligands and their macromolecular targets are flexible in nature, but including flexibility in docking is computationally very costly and, hence, different docking procedures have been developed. In a rigid docking process, the ligands only have some degrees of freedom by only allowing rotation and translation while the target is kept rigid, while in a semi-flexible approach the target is kept rigid and the ligand fully flexible by prior generation of multiple conformations (Höltje et al., 2008). There are also methods for including structural flexibility into the amino acids of the receptor binding pocket. The Schrödinger suite of program has a solution called Induced fit docking (IFD) (Sherman et al., 2006). The protocol can be divided in four major steps 1) Initial ligand sampling, 2) Receptor sampling, 3) Ligand resampling and

4) Final scoring (Sherman et al., 2006). The first step is to generate a diverse ensemble of poses of the docked ligand without generating unlikely poses. To reduce steric clash between the ligands and the unmodified binding pocket, side chains that are predicted to be highly flexible are mutated to alanine and the van der Waals radii is scaled (Sherman et al., 2006). The next step includes sampling of the protein structure with considerations to the previous sampled ligand pose, resulting in receptor conformations optimized for the ligand poses. The residues previously replaced with alanine are restored and an energy minimization is performed on residues with at least one atom within 5Å of the ligand, after the conformations of the residues have been predicted (Sherman et al., 2006). This step also includes energy minimization of the generated ligand poses from step 1, before each complex are ranked according to the energy. The ligands are further resampled in the previously optimized receptor structures and the previous softened potentials are set to the original values (Sherman et al., 2006). The final step is ranking the complexes according to score accounting for both estimated the docking score and strain- and solvation terms (Sherman et al., 2006).

Protein flexibility can also be ensured by using a slightly different approach called ensemble docking. The Internal coordinate mechanics (ICM) software offers this methodology where docking into a stack of pre-generated target conformations is performed, called 4D docking (Bottegoni et al., 2009). Ideally, the descriptions used for representing binding pocket conformations are obtained from multiple crystal structures of the target, but this is not always possible due to unavailability or too similar conformation of the crystal structures. A stack or ensemble of conformations can in that case be generated by optimizing side-chains within the ligand binding pocket (Gabrielsen et al., 2012; Kitchen et al., 2004).

The structure of the target and the selected ligands must be structurally prepared before docking by defining features such as ionization, chirality, adding hydrogens, assigning bond orders and energy minimization among other properties. 3D space and characteristics of the binding pocket can be pre-defined and described by a grid energy map that stores the energy information of the binding site and simplify interaction energy calculations (Höltje et al., 2008). Grid maps are used by most docking programs, and usually take into account features such as shape, electrostatic-, van der Waals- and steric properties of the binding pocket (Patrick, 2017). Various fragments or atoms are often used as probes to measure these interactions with residues in the binding site, before the values corresponding to different grid points are stored (Sliwoski

et al., 2014). When ligands are docked, the binding strength can quickly be calculated by identification of ligand atoms interacting with pre-calculated grid points (Patrick, 2017).

It is always a challenge to balance accuracy and efficiency during docking and scoring. The Schrödinger suite contains the Glide package which offers an array of options for accuracy and speed by providing docking and scoring algorithms that can be applied for different purposes, like screening of databases with high throughput virtual screening (HTVS) or docking by standard precision (SP) or extra precision (XP). HTVS and SP docking functions use series of hierarchical filters to search for the optimal ligand pose within the target structure (Friesner et al., 2004; Halgren et al., 2004). This process includes steps such as exhaustive enumeration of ligand torsions, torsional space refinement of the ligand in the grid using a FF in conjugation with a distance-dependent dielectric model, and finally a post-docking minimization with full flexibility of the ligand (Friesner et al., 2004; Halgren et al., 2004). These algorithms are less strict in the way that they identify ligands with reasonable propensities to bind, without strict rejection of poses that may diverge from the ideal complex complementarity in terms of energy, but are fast in terms of time by using on average only 2 second/compound for HTVS and 10 seconds/compound for SP (Friesner et al., 2004). The Glide XP methodology is much more comprehensive than the previously explained HTVS and SP and the procedure is reported to use 2 minutes/compound (Friesner et al., 2006). Various rigid fragments of the ligands are "anchored" within the binding pocket based on complementarity between the ligand and the grid map, before the software "grows" the flexible parts of the ligand step-by-step to achieve better ligand poses (Friesner et al., 2006). Various positions of the anchors are clustered before a representative from each cluster is selected and the side chain is grown from relevant points on the anchor. Candidate poses are selected based on the score of each conformation eliminating structures with steric clash between side chains. In the last step the selected candidate poses are minimized using Glide's energy function and ranked according to MM energy and empirical scoring terms (Friesner et al., 2006). If selected poses have penalties of various types, such as insufficient hydrogen bonding between ligand and target compared to the solvated protein in the unbound state, they are re-grown as an attempt to escape these penalties. The final single pose is selected based on an empirical scoring function composed of ligand–protein energy contributions and penalties to predict the relative binding affinities (Friesner et al., 2006).

A large number of scoring algorithms have been developed to evaluate protein-ligand complementarity and predict the binding free energy. The free energy of a binding process is given by the Gibbs-Helmholtz equation:

$$\Delta G = \Delta H - T\Delta S \quad (6)$$

where ΔG is the free energy, ΔH the enthalpy, T temperature in Kelvin and ΔS the entropy (Höltje et al., 2008).

The binding free energy can further be related to the binding constant K_i by the following equation:

$$\Delta G = - RT \ln K_i \quad (7)$$

where R is the gas constant (Höltje et al., 2008).

The scoring methods vary considerably in accuracy and speed. Methods such as Linear Interaction Energy (LIE) (Åqvist et al., 1994) or Free Energy Perturbations (FEP) (Cournia et al., 2017) can be used for quite accurate predictions, but they are computational expensive because they include features such as larger degrees of conformational freedom and sometimes explicit water models (Höltje et al., 2008). Such methods therefore have limitations in a VS approach. In high-throughput screening, quick methods are preferred to roughly estimate the energy with the aim to optimize the placement of ligands and the rank them (Höltje et al., 2008).

Scoring functions can be categorized into three main groups (1) MM force-field-based scoring functions, (2) Empirical scoring functions, (3) Knowledge-based scoring functions, and in addition consensus scoring is also used for ranking (Huang and Zou, 2010). Force-field-based based scoring functions calculate the ligand binding energy based on the individual interaction terms described in the FF which includes van der Waals- and electrostatic energies, in addition to the torsions, angles and bond stretching (Huang and Zou, 2010). Empirical scoring functions such as Glide score (Friesner et al., 2004), combine energies calculated for the individual components from the FF with experimental binding affinities to calculate a final energy score (Huang and Zou, 2010). Knowledge-based scoring functions use structural information extracted from experimentally determined ligand-protein complexes based on potential of mean force (Höltje et al., 2008). Consensus scoring is not a scoring function, but a technique where multiple different scoring functions are compared to improve the probability of detecting true active ligands.

1.5.6.4.2 MM-GBSA

The Molecular Mechanics Generalized-Born and Surface Area (MM-GBSA) tool is commonly used as a post-processing step in a VS workflow. The method approximates the binding free energy by encountering the MM energies, the surface area energy and differences in solvation energy by encountering the ligand and protein both in the unbound and bound states using an solvation model (Eq. 6) (Knight et al., 2014). The method can provide a more accurate estimation of binding energies compared to methods such as docking where only the bound state is considered, and more efficiently than expensive sampling methods such as free energy perturbation (Knight et al., 2014). The ligands and the poses are ranked according to the estimated MM-GBSA score that is estimated based on the following calculation:

$$G_{bind} = \Delta E_{MM} + \Delta E_{solv} + \Delta E_{SA} \quad (6)$$

ΔE_{MM} is sum of the differences in force field energy (bonded and non-bonded terms) between the bound and unbound states. The ΔE_{solv} is the difference in solvation energy between the bound and unbound states of the ligand and the protein by using an implicit or explicit solvent model, and the ΔE_{SA} is the difference in the surface energy between the two states (Knight et al., 2014).

Sampling of the protein and ligand can be achieved by MD simulations, MC sampling or by minimization. Using MD or MC is more computational demanding than performing a simple minimization, but provides dynamic effects whereas minimization heavily depends on the starting structures (Genheden and Ryde, 2015).

1.5.6.4.3 Structure-based pharmacophore modelling

Structure-based information can be utilized to develop pharmacophore hypotheses from the protein binding pocket. A docking program such as Glide with the XP scoring function (Friesner et al., 2004) can be used to energetically describe ligand-receptor structures as it is a comprehensive algorithm describing energy terms of a complex by encountering hydrophobic sites, π-π and π-cation interactions as previously described. The ligand-receptor energies can be calculated by either docking known active ligands, fragment libraries from vendors or purely based on the structure of the target binding pocket alone, before the pharmacophore sites are generated using the same six chemical features as used for ligand-based pharmacophores: hydrogen bond donating and accepting, negative and positive ionizable, aromatic

and hydrophobic groups (Sliwoski et al., 2014). The ligand-receptor energies calculated from the scoring function after refinement of a ligand pose are energetically mapped onto atoms of the binding pocket, before pharmacophore sites are generated (Salam et al., 2009). The energies of atoms contributing to each pharmacophore site are summarized, ranked and the most favorable sites are selected for the final hypothesis with the possibility to modify the desired number of features in the hypothesis composition (Salam et al., 2009). The pharmacophore hypothesis can then be applied in VS approach to identify ligands complementary to the structure-based pharmacophore features.

1.5.6.5 Linear interaction energy and linear interaction approximation

LIA is a simplification of the linear interaction energy (LIE) method (Åqvist et al., 1994). Both methods are used for prediction of binding affinities of unknown ligands based on the experimental affinity values of known active ligands used as a training set. In LIE, the conformations of ligands in the training set and the target are sampled during MD simulations or Monte Carlo minimizations both in the bound and unbound states (Åqvist et al., 1994; Åqvist and Marelius, 2001). In the LIA, energy minimizations are used for conformational sampling (Liaison Manual 5.8, 2015). The simulation data are analyzed and in combination with the empirically derived affinity data, three scaling factors for the energy terms van der Waals energy (α), electrostatic energy (β) and a cavity term (γ) are generated (Liaison Manual 5.8, 2015). These scaling factors can subsequently be used to predict binding energies for other unknown ligands for the same target using the following equation:

$$\Delta G = \alpha \left(U^b_{vdw} - U^f_{vdw} \right) + \beta \left(U^b_{elec} - U^f_{elec} \right) + \gamma \left(U^b_{cav} - U^f_{cav} \right) \quad (7)$$

where b = bound form of the ligand, f = free form of the ligand, U_{vdw} = van der Waals energy, U_{elec} = electrostatic energy, U_{cav} = cavity energy term in a Surface Generalized Born (SGB) continuum solvent model where the cavity term is proportional to the exposed surface area of the ligand. α, β, and γ are the derived coefficients (Alam and Naik, 2009; Liaison Manual 5.8, 2015).

2 Aim of the study

The involvement of the GABA$_B$-R in the pathophysiology of different diseases and disorders makes it an interesting target for drug intervention. At present, there are few known ligands targeting the orthosteric binding site of GABA$_B$-R and the majority are GABA analogues. The low structural diversity of known GABA$_B$-R ligands may indicate that the conformational space of the orthosteric GABA$_B$-R binding site and of GABA$_B$-R agonists and antagonists are not fully explored. Ligand recognition and binding, activation and signal transduction are dynamic processes requiring conformational changes of both receptor and ligand. Other structurally stable VFT conformations than the closed/active and opened/inactive structures from X-ray crystallography may exist and be favorable for binding of yet unexplored chemical scaffolds of ligands. Understanding the conformational dynamics, and identifying intermediate VFT conformations associated with the oscillation between the open/inactive and the closed/active conformations may therefore be valuable for the identification of new orthosteric GABA$_B$-R ligands.

The aims of this study was to enhance our knowledge about the structural dynamics of the GABA$_B$-R VFT and utilize available structural information about the receptor and known agonists and antagonists to identifying novel orthosteric ligands. First, we aimed to establish a VS workflow as an effort to identify new ligands targeting the orthosteric binding site. Secondly, we aimed study the movement of the VFT to explore conformational energies associated with the transition from active closed VFT state to inactive open VFT state to understand if the receptor oscillates between these states independently of the presence of an agonist.

The goals of the work described in the thesis can be divided into three specific tasks:
- Evaluation of the applicability of commonly used ligand- and structure-based VS methods when the available structural information about ligands is limited to a small selection of structural analogs (paper 1).
- Application of selected ligand- and structure-based methods in a VS workflow to identify new ligands binding to orthosteric binding site (paper 2).
- Study the transitions between active and inactive conformations of the GABA$_{B1}$ VFT and the free energy associated with the transitions to improve our knowledge about the

structural dynamics of receptor and the mechanism associated with receptor activation, in addition to potentially identify other metastable VFT conformations (paper 3).

3 Methods

3.1 Paper 1 and 2

3.1.1 Software

The Schrödinger software package (*Small-Molecule Drug Discovery Suite 2018-4*) was used for all molecular modelling calculations in paper 1 and 2. The available crystal structures of GABA$_B$-R VFT were downloaded from the protein data bank (PDB ID: 4MR7, 4MR8, 4MR9, 4MQE, 4MQF, 4MRM, 4MS1, 4MS3 and 4MS4) and pre-processed in Schrödinger Protein Preparation wizard with default settings (Protein Preparation Wizard, 2017).

Known GABA$_B$-R agonists, antagonists and assumed non-binding ligands (decoys) were prepared using Schrödinger LigPrep with default settings (LigPrep, 2017). Molprint2D (M2D) fingerprints were generated before hierarchical clustering of agonists and antagonists based on Tanimoto similarity with the average cluster linkage method using Schrödinger's Canvas software (Canvas, 2017), as a first step in the ligand-based approach. Schrödinger's Qikprop was used for ADMET filtering of selected databases used for VS. Pharmacophore models for each cluster of agonist, antagonists and outliers were generated using the Phase software which is included in the Schrödinger Small-Molecular Drug Discovery suit (Phase, 2017). The structure-based pharmacophore models were generated based on all available X-ray crystal structure complexes of the GABA$_B$-R VFT by mapping a library of fragments in the binding pockets using the Schrodinger's Phase software (Phase, 2017).

Docking of fragments, GABA$_B$-R agonists and antagonists, decoys and the virtual database was performed by Schrödinger Glide software (Glide, 2017, 2015). SP docking was used for decoys and known agonists and antagonists, while a virtual screen workflow (VSW) tool combining HTVS, SP and XP docking were used for the VS of compound databases. Only 10% of the top scored compounds from HTVS and SP docking were kept, and 100% of the output was kept after XP docking. The false positive decoys identified based on docking score (scoring better than the threshold selected by docking of agonists and antagonists), were applied in a LIA model generated using Schrodinger Liaison software in combination with the strike software (Liaison, 2015; Strike version 2.2, 2015). The output from VSW was post-processed with Prime MM-GBSA to estimate the relative binding affinity (Prime, 2017).

3.1.2 Traditional computer-aided drug discovery methods

A total of 55 ligands were collected from the literature and considered active towards the GABA$_B$-R. M2D fingerprints were calculated for each of the compounds, before they were used to cluster the compounds based on similarity using Tanimoto similarity using the average linkage method, which resulted in six clusters after manual adjustments. As the clustering was able to separated agonists from antagonists, and X-ray crystal structures were available of both active and inactive receptor conformations, we intended to develop screening methods that theoretically also should split between antagonists and agonists. Cluster 1 was generated by merging singletons and doubletons, containing both agonists and antagonists, and considered as a cluster of outliners. An average fingerprint (modal fingerprint) of each cluster was calculated, and the selectivity tested by applying them to screen GABA$_B$-R ligands and decoys from other clusters.

In paper 1, pharmacophore models were generated for each cluster and evaluated by mapping against decoys and known agonists and antagonists in order to identify the numbers of false and true positives and true and false negatives that were used to calculate the Matthews correlation coefficient (MCC) and "Goodness of Hits" (GH) (Matthews, 1975; Seal et al., 2013). One pharmacophore model was selected to represent each cluster, resulting in 4 models for agonists and 1 model for antagonist. An additional model representing agonists and antagonist from cluster 1 was also included to potentially retrieve both agonist and antagonists during VS. These models were applied as the first step in the VS, keeping compounds retrieved from agonist-based and antagonist-based pharmacophore models separate.

The compounds retrieved from ligand-based pharmacophore step were docked into selected X-ray crystal structures. For evaluation of methods in paper 1, one presumed active (from a complex with agonist) and one presumed inactive (from a complex with antagonist) GABA$_B$-R conformation were selected (PDB ID: 4MR7 for antagonist and 4MS4 for agonist) for docking. In paper 2, all available GABA$_B$-R X-ray crystal structures with an agonist or antagonist were used for docking the compounds retrieved form the ligand based pharmacophore VS. The compounds retrieved from the agonist specific pharmacophore models were docked into agonist induced active receptor conformations (PDB IDs: 4MS3 and 4MS4), while potential antagonists were docked into the six antagonist induced receptor conformations (PDB IDs: 4MR7, 4MR8, 4MR9, 4MQF, 4MRM and 4MS1). The compounds retrieved using the pharmacophore model generated from the outliners were docked into grid maps

representing both the active and inactive receptor conformations. In both papers, the binding pockets described by grid maps were defined using the centroid of the co-crystalized ligand. The map size was increased from the default box size of 10 $\mathring{A}^3$ to 15 $\mathring{A}^3$, to ensure docking of ligands with a larger size that the co-crystalized ligands. Only Glide SP docking was applied for the method validation in paper 1. However, in paper 2, we applied all Glide docking algorithms, keeping 10 % of the best scored ligands after HTVS and SP, but 100 % after the XP docking. In addition we generated 3 poses per ligand as required for MM-GBSA postprocessing.

LIA models are linear regression models generated by combining experimental activity data with theoretically calculated descriptors such as van der Waal and electrostatic forces to create a model for predicting or correlate binding energy. In paper 1, the LIA method was evaluated for its applicability in VS. The method not only encounters forces in the complex, but also the ligand and the receptor in an unbound state solvated in an implicit water model. The methods is a simplification of the LIE method originally proposed by Åqvist et al. (Åqvist et al., 1994). We generated one LIA model for affinity prediction of agonists and one for antagonists. The models were generated by selecting approximately 50 % of the agonists and antagonists with known experimental pIC50 values as training sets, before evaluating the models on the remaining known agonists and antagonists. After docking known active ligands and false positive decoys from the ligand based approach, ligands scoring better than threshold values, defined by redocking agonists and antagonists, were applied in the LIA models to evaluate their ability to identify ligands as false positive.

After docking of the compounds from the pharmacophore screening in paper 2, an inhouse script was used to select one pose of each compound based on docking score, remove duplicates (ligands present from more than one vendors), predicted affinity and identify the number of grid maps the ligands were docked into. The compound after removal of duplicates were clustered by Tanimoto similarity matrix based on M2D fingerprints before candidates from the different clusters were selected, visually inspected in the binding pocket, purchased and experimentally tested.

3.1.3 Experimental verification of ligands

A total of 37 hits were purchased and tested in a cAMP assay using Chinese Hamster Ovarian cells stably overexpressing the human $GABA_B$-R receptor and on WT CHO-K1 cells without the receptor. The HitHunter cAMP assay from DiscoverX was applied to investigate the cellular effects of the hits on the receptor activation. The assay uses two β-galactosidase fragments that works as enzyme donors conjugated with cAMP and an enzyme acceptors, in addition to anti-cAMP antibodies and a substrate (DiscoverX, n.d.). When the levels of endogenous cAMP is high, it binds and saturates the cAMP antibody causing the excess levels of donor cAMP to complement with the enzyme acceptor. Combination of these two fragments forms an active enzyme that hydrolyzes the substrate, resulting in a detectable chemiluminescent signal (DiscoverX, n.d.) (Fig. 17).
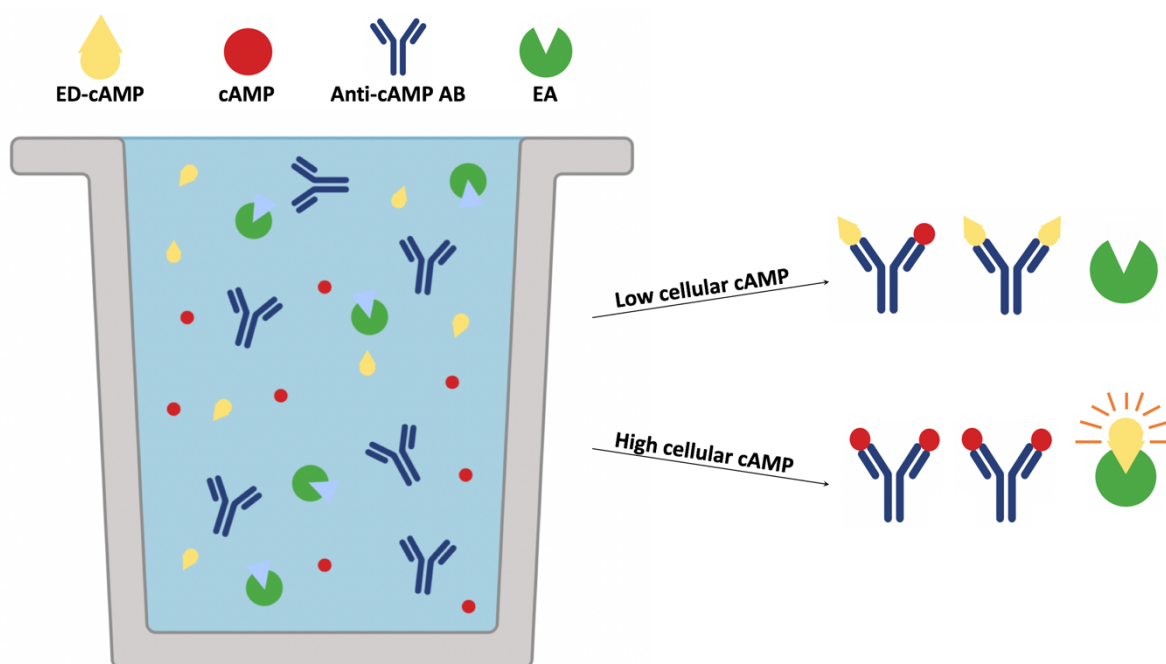
Figure 17 – A simplified illustration of principle behind the HitHunter cAMP assay from DiscoverX. The EA enzyme becomes activated upon ED-cAMP binding which causes hydrolyzation of a substrate causing a detectable light signal. ED – enzyme donor, EA – enzyme acceptor and AB – antibody. (Figure modified from DiscoverX manual (DiscoverX, n.d.))

The compounds were dissolved in 100 % Dimethyl sulfoxide (DMSO), before the solubility was tested in the assay buffer. Three compounds showed low solubility. The 34 remaining compounds were tested in a single concentration (10 μM) together with forskolin (50 μM), a compound that stimulates adenylyl cyclase resulting in cAMP production (Seamon et al., 1981), in the WT cells to evaluate the off-target effects. Testing on the CHO-K1 GABA$_B$-R cells were performed using a single concentration (10 μM) of the test compound, together with forskolin (30 μM) and GABA (EC$_{20}$ and EC$_{80}$ concentration, respectively). The selected concentrations of GABA, EC$_{20}$ and EC$_{80}$, were used to investigate the possibility of the compounds to also functioning as PAMs or NAMs (Klein et al., 2013). The cells were harvested washed and resuspended in Hank´s Balanced Salt Solution (HBSS), followed by 2 hour pre-incubation at 25°C. After adding compound mixture, the reaction proceeded for 24 minutes at 25°C before the cAMP reagents were added and incubated without light in additional 14-16 hours at room temperature. The cAMP signals were measured on a ClarioStar® plate reader (BMG LABTECH) for the luminescence readout.

3.2 Paper 3

3.2.1 Molecular dynamics simulation and metadynamics

The MD simulations were performed with GROMACS using the AMBER99SB-ILDN force field, before the conformations of the resulting trajectories were clustered using a GROMACS clustering tool (Berendsen et al., 1995). The freely available climber tool was used to connect the trajectory clusters (Weiss and Levitt, 2009), before the PLUMED *driver* utility (Tribello et al., 2014) was used to calculate the progress of the morphed path along the reaction coordinates of the unbiased MD using the path as a PATHMSD collective variable. The visual molecular dynamics (VMD) program was used for visualization and RMSD calculation to analyze the obtain path (Humphrey et al., 1996). GROMACS patched with Plumed was used to perform a Well-Tempered Metadynamics (WT-MetaD) using the path as a CV.

Six 1 μs MD simulations without ligand present were performed. One simulation was started from the X-ray crystal structure of the $GABA_B$-R apo form (PDB id: 4MQE), two were started from an open agonist induced conformation (PDB IDs: 4MS3 and 4MS4) after removal of agonist, while three were started from an antagonist induced (PDB IDs: 4MQF, 4MR7 and 4MR8) after removal of the antagonist. The six molecular systems were equilibrated by a 100 ps simulations using the NVT ensemble (constant number of atoms (N), volume (V) and temperature (T)) followed by a 5 ns NPT (constant number of atoms (N), pressure (P) and temperature (T)) equilibration. Production runs of 1 μs were performed as an extension of the previously NPT ensemble with coordinate sampling every 10 ps. RMSD analysis showed overlapping conformational space indicating that the reaction coordinates for the transition between closed/active conformation to the open inactive conformation were explored during the simulation. The trajectories were merged before performing a cluster analysis on the aggregated trajectory. Cluster centroids were selected and connected using by the climber tool. An in-house script was used to extract equispaced frames that were applied as a path collective variable in a WT-metaD.

4 Summary of results

4.1 Paper 1

In Silico Methods for the Discovery of Orthosteric GABA$_B$ Receptor Compounds, Linn M. Evenseth, Dawid Warszycki, Andrzej J. Bojarski, Mari Gabrielsen and Ingebrigt Sylte, *Molecules, 2019, DOI 10.3390/molecules24050934*

The relative low number of known agonists and antagonists for the GABA$_B$-R complicates the use of computer aided drug-discovery methods for identifying new orthosteric ligands. At the moment 13 antagonists and 42 agonists are known, and the majority are of them are GABA analogues. The low number of ligands that cover a relatively small conformational space reduces the quality of ligand-guided studies and complicates the validation of structure-based methods. Classical ligand-based methods such as fingerprinting and pharmacophore mapping and structure based-methods like structure-based pharmacophores, docking and LIA were tested for their applicability to identify new orthosteric GABA$_B$-R. All methods were evaluated by their ability to separate 55 known agonist and antagonists from decoys, generated in a ratio 1:50 per active compound. The results showed that modal fingerprints generated from fingerprints of clustered ligands and structure-based pharmacophores could not discriminate between active ligands and decoys. However, the results from the structure-based pharmacophores based on docking of fragments gave a good insight into the properties of the binding pocket. Based on the result, we could conclude that that combining ligand-based methods with different structure-based methods, despite low accuracy on individual methods, can identify active ligands in front of assumed inactive ligands and confirmed inactive ligands and reduce the number of false positives during VS.

4.2 Paper 2

Identification of orthosteric GABA$_B$ receptor compounds by virtual screening,

Linn S. M. Evenseth, Imin Wushur, Dawid Warszycki, Andrzej J. Bojarski, Mari Gabrielsen and Ingebrigt Sylte, *Manuscript, 2019*

A VS workflow was employed to screen a collection of databases including Vitas M, Chembridge, Chemdiv, Maybridge, UORSY, Specs and Enamine. The methods used in the workflow was selected based on the results from paper 1 in order to identify new ligands targeting the orthosteric binding site of the GABA$_B$-R. A combination of ligand-based and structure-based approaches optimized to be selective for agonists or antagonists was applied to screen a library of 8.2 million compounds. The library was filtered with to a small selection of ADMET properties, reducing the number of compounds to approximately 5.3 million. The 6 cluster-based pharmacophore models generated in paper 1 were applied for screening of the remaining library, reducing the number of compounds to ~ 686.000. There are in total 8 available X-ray crystal structures of the GABA$_B$-R VFT co-crystalized with agonists or antagonist and they represent small differences of the binding pocket. In the structure-based part of the VS protocol, compounds retained by agonist based pharmacophore models were docked into two X-ray crystal structures representing closed/active conformations, while compounds retained by antagonist based pharmacophore models were docked into 6 X-ray crystal structures representing open/inactive conformations. A Glide docking workflow was used for the docking, consisting of HTVS, SP and XP docking. The retained compounds were post-processed by MM-GBSA calculation, which resulted in 2761 potential agonists and 71960 antagonists. The compounds were structurally clustered and compounds from each cluster were selected for *in vitro* testing based on visual inspection of complexes, XP gscore, relative binding affinity from the MM-GBSA calculation and the number of grid maps the compound could dock into. Based on the VS screening, 37 ligands were ordered, but only 34 were soluble and thereby tested in a functional cAMP assay using Chinese hamster ovary cells stably overexpressing the human GABA$_B$-R (CHO-K1 cells) and on WT CHO-K1 cells. The results indicate that two out of the eight currently tested compounds, have antagonistic properties.

4.3 Paper 3

Exploring the conformational dynamics of the extracellular Venus flytrap domain of the GABA$_B$ receptor: a path-metadynamics study,
Linn S. M. Evenseth, Riccardo Ocello, Mari Gabrielsen, Matteo Masetti, Ingebrigt Sylte, and Andrea Cavalli, *Manuscript, 2019*

In this study, we aimed to investigate the structural dynamics of the GABA$_{B1}$ VFT and describe the natural behavior of this domain in absence of ligands. A total of six molecular dynamic (MD) simulations of one microsecond were run, from both the inactive/open and closed/active states, to possibly explore the conformational transitions state of the GABA$_{B1b}$ VFT. The six trajectories were merged and based on cluster analysis of the trajectory, centroids were extracted and linked in order to describe the structural movements between the two states in an optimized path. The optimized path further used as a path-CV in a WT-MetaD to fully characterize the transition between the two states and reconstruct the Free Energy Surface (FES) associated with the transition. The results show that the pool of trajectories could be used to derive a suitable reaction coordinate for describing the full transition between the open and closed states. However, the individual six simulations did not show a full transition. The results from the metadynamics showed two local minimum on the FES corresponding to the closed/active and the open/inactive conformations. The two local minimums were iso-energetic, but the energy barriers separating these conformations was of 20 kcal/mol. This results indicate that the transition is not likely to occur in the absence of an agonist. Other metastable intermediate states were also observed, and these states might play an important role in the receptor transition. Analysis of selected metastable states showed that most of the investigated residues located in the binding pocket where stable during the simulation. However, conformational changes were observed for two residues located in lobe 2 of the VFT.

5 Discussion

The GABA$_B$-R plays an important role in neurotransmission by binding the main inhibitory neurotransmitter GABA and is involved in the regulation of cellular inhibition and excitation (Bettler et al., 2004). Dysregulation of the receptor has not surprisingly been linked to a broad variety of diseases and disorders (Bittiger et al., 1996; Tyacke et al., 2010). The receptor was linked to major depressive disorder already in the beginning of the 1980´s and since then the receptor has frequently been targeted in different drug discovery efforts against affective disorders (Lloyd et al., 1985; Lloyd and Pilc, 1984; Pilc and Nowak, 2005). Despite all the efforts to develop GABA$_B$-R drugs, there is currently only one drug on the market targeting the GABA$_B$-R, the agonist baclofen (Froestl et al., 1995b, 1995a). New orthosteric ligands are important for elucidating the structure and activity of the receptor and increase the understanding of signaling and pathophysiology.

5.1 Application and evaluation of computer-aided methods in a virtual screening workflow

Combining ligand-based and structure-based methods in VS workflows can be more effective and accurate than applying either of the approaches alone. The choice of methods often depends on the available information about the target of interest. For ligand-based approaches it is necessary with available data about active- and preferably inactive ligands, while structure-based methods requires one or multiple 3D models of the target (Sliwoski et al., 2014). The size and chemical diversity of the ligand dataset affects the accuracy and thereby the functionality of a method. This was demonstrated in paper 1 when evaluating ligand-based methods for their application in a screening protocol against GABA$_B$-R (Evenseth et al., 2019). The dataset of active orthosteric ligands was quite small, containing only 55 highly similar ligands as most of them are GABA analogues. After hierarchical clustering of the ligands based on similarity between the M2D fingerprints with mol2 atom-typing scheme, modal fingerprints were generated for each cluster. The modal fingerprints were evaluated by their ability to retrieve actives and decoys. The results showed that the method was not selective for active ligands within the cluster from which the modal FPs were generated and retrieved multiple decoys. Decoys are assumed non-binders generated from the active ligands to match the physical chemistry of these, but topological dissimilar, to decrease the possibility of them being

actual binders (Mysinger et al., 2012). However, as long as the decoys are not verified experimentally, it is impossible to rule out that they are actual inactive compounds.

The pharmacophore models also suffered from the structurally narrow selection of ligands and the default inter-site distance had to be modified from 2 Å to 1.5 Å for two of the clusters, creating stricter hypothesis. Changing this constraint allows pharmacophore features to be in a closer proximity and thereby increased the number features and diversity between the generated models. In addition, only one pharmacophore model for each of the 6 clusters of agonists and antagonists was evaluated to have an acceptable quality for further application. Larger datasets comprised of chemical diverse ligands generates more diverse pharmacophore models as seen in comprehensive pharmacophore studies on targets such as the serotonin 5-HT$_{1A}$ receptor with > 3.500 known active ligands (Warszycki et al., 2013). Application of the selected pharmacophore models from paper 1 in the VS protocol (paper 2), showed that the less accurate models retrieved up to approximately 75.000 compounds compared to approximately 11.000 compounds in one of the better performing models (Fig. 18). We also included a nonspecific pharmacophore model generated based on mapping compounds from a cluster consisting of a mixture of agonists and antagonists in the VS, and this model retrieved approximately 500.000 compounds. The aim of applying this pharmacophore model in the VS was to potentially identify new structural chemotypes. We did not consider the high number of theoretically false positive hits as negative, since we had the option to apply more robust methods in the following steps. If that was not an option, the process of selecting candidates for experimental verification would be more difficult as the number of candidates would be very high.
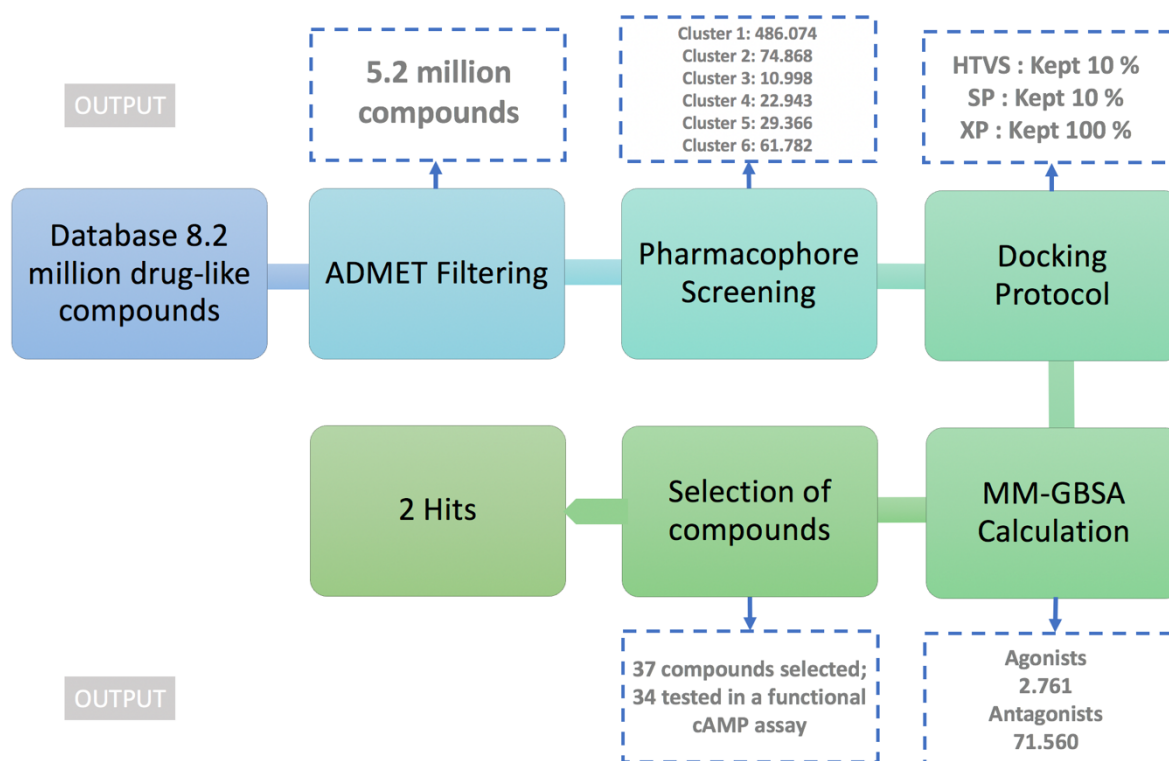
Figure 18 – A summary of the workflow from VS screening to experimental testing with corresponding results (presented in paper 1 and 2). HTVS: high throughput virtual screening, SP: standard precision, XP: extra precision, MM-GBSA: Molecular Mechanics-Generalized Born Surface Area.

Structure-based methods are in general preferred when structural data of high quality are available because the ligands can be customized according to the properties of the binding pocket. However, Ripphausen *et al.* reported in 2010 that despite higher success rates of structure-based screening, hits from ligand-based approaches have a considerably higher potency (Ripphausen et al., 2010). A balance between accuracy and computational costs is important when planning a VS approach, but essentially the choice depends on the available data.

Only two out of the nine available GABA$_B$-R VFT X-ray crystal structures were used in paper 1 to save calculation time. The choice supported by the low RMSD between the structures showing that they were highly similar. Also, in this paper we did not aim to evaluate the selectivity of the available X-ray structures. The two X-ray crystal structures with the highest resolutions were selected to represent the agonist-bound active conformation, and the antagonist-bound inactive conformation. Fragments were docked into the selected structures before e-Pharmacophores were generated using the default maximum numbers of features. A quantitative evaluation of these models was impossible as the required matching level was set to 3 due to the size of the ligands, resulting in retrieval of multiple decoys that in addition was

ranked higher than any of the active ligands. As pointed out in paper 1, generating e-Pharmacophores by docking fragment libraries can in our case be expedient for the purpose of describing binding pocket properties in lead-optimization purposes.

Receptors and ligands are structurally flexible molecules and ligand recognition and binding induces conformational changes in the ligand binding site. The changes can be a movement of a simple side chain to backbone movement or larger rearrangement of a domain (B-Rao et al., 2009). Incorporating structural flexibility in docking studies is very important for prediction of the ability of a ligand to bind, and for predicting the correct pose. However, incorporating structural flexibility in a docking algorithm is difficult due to the large number of degrees of freedom in a macromolecular complex, and the complex interactions between the target and the ligands, which both increase the calculation time considerably (B-Rao et al., 2009). Despite that the available X-ray structures were similar as calculated by RMSD in paper 1, there were small variations in the binding pocket such as a flip of approximately 170° of the Trp278 located in lobe 2 of agonist-bound receptor conformations. We applied all the nine available crystal structures in the actual VS campaign presented in paper 2, and performed multiple docking studies. Incorporation of ligand flexibility was handled by using the full Glide VSW docking protocol, that uses three different docking algorithms; HTVS, SP and XP (Friesner et al., 2004).

The extensive VSW protocol was only applied in the actual screening protocol (Paper 2) and not when evaluating the methods (Paper 1). The main goal of using the VSW protocol was to remove unlikely drug candidates from the library, and due to the large amount of hits from the pharmacophore screening we had to apply a stricter docking protocol than initially thought.

5.2 Linear Interaction Approximation

The LIA methodology is a simplified version of the original LIE method where sampling is performed by minimization, MD or Monte Carlo using an implicit water model (Åqvist et al., 1994). The results from evaluation of this method was acceptable, despite that the coefficients α and β made non intuitive sense. The value of both α and β should be positive when the bound state is favored over the free unbound ligand. Other studies have also reported similar observations, where the α and β coefficients favor the unbounded state (Alam and Naik, 2009). As discussed in paper 1, there might be various reasons for this results including insufficient sampling and handling of water molecules. This method was removed from the Schrödinger software in 2015, and was therefore not be applied in the evaluation hits from the VS work-

flow. The MM-GBSA methodology was instead applied as this method also calculates the ligand binding energy considering the ligand and the receptor in a bound and unbound states solvated in an implicit water model.

5.3 In vitro evaluation of hits from VS

Hits from the VS protocol were evaluated based on the Glide XP score (gscore) and MM-GBSA score, before the compounds were clustered. Cluster centroids were selected and visually investigated, before 37 candidates were purchased (paper 2).

Functional cAMP assay is a high-throughput method that can easily be applied to investigate ligands effect on production of cAMP upon GPCR activation. The assay requires pre-knowledge of the coupling mechanism of the GPCR since cAMP levels most commonly are affected through activation of $G\alpha_s$ and $G\alpha_{i/o}$ pathways. Our candidates are currently being evaluated by their ability to effect the cAMP levels in a CHO-K1 cell line stably expressing the human $GABA_{B(1b,2)}$-R that couples to $G\alpha_{i/o}$.

Before applying the candidates to the recombinant cells, they were tested in WT CHO-K1 cells to evaluate if the compounds bound to other targets than the $GABA_B$-R. In total, 20 of them showed activity in WT cells and were therefore not be further evaluated in the cells overexpressing the $GABA_B$-R. Out of the remaining 14, only 8 have been tested in the cAMP assay using CHO cells expressing the $GABA_B$-R.

The obtained results show that a single concentration of the test compounds in the assay without GABA, did not reduce the levels of cAMP and thereby ruled out that the compounds could be agonists. Applying the EC_{20} concentration of GABA without results also ruled out that the compounds could be PAMs, as a PAM theoretically should have increased the potency and reduce the cAMP formation. Two of the compounds was able to increase the cAMP formation indicating antagonist or NAM activity. These two compounds were further evaluated in a GABA dose-response studies with fixed concentration of each compound (30 µM). Compound 23 showed an increase in cAMP formation at high GABA concentrations, while compound 28 increased the cAMP concentration at low GABA concentrations in addition. These results indicate that compound 23 and 28 might have weak antagonistic properties. However, we cannot confirm that the compounds actually bound to the orthosteric binding pocket as they also could be NAMs with intrinsic activity, and further testing is therefore required. Application

of a radioligand binding assay would determine more certain the site of binding and binding affinity.

As the cAMP assay is based on detecting activation of a specific pathway, compounds that might exhibit functional selectivity are likely to be reject. In the case of our studies, we cannot rule out that 6 of the tested compounds might have functional selectivity for other G-protein independent or independent pathways. β-arrestin recruitment assay is a high-throughput method that could be applied to investigate functional selectivity towards a G-protein independent pathway (Zhang and Xie, 2012). Also, performing additional G-protein dependent assays for potentially detecting other cellular effects of ligand activation should be considered because of the ability for the compounds to act as an agonist (or PAM) for one pathway and antagonist (or NAM) for others. The $GABA_B$-R can also affects the intracellular calcium levels by different mechanisms such as regulating the NMDA receptor or by activating PLC in a synergy with mGluRs coupled to $G\alpha_q$, causing increased calcium levels (Gassmann and Bettler, 2012). A calcium mobilization assay using a chimeric G-protein could therefore be considered to investigate alternative functions or pathways. Sturchler *et al.* recently published a study highlighting the benefit of using multiple assays to investigate and characterize the function of ligands by performing multiple experiments including cAMP assay, calcium mobilization assay and measuring ERK activation (Sturchler et al., 2017). The study investigated 3 $GABA_B$-R allosteric modulators with similar pharmacokinetic properties. The results showed that all compounds increased the GABA potency in the cAMP assay, indicating that they were PAMs. Two of the compounds had no effect on calcium mobilization, while one of the compounds decreased the GABA potency and thereby executed NAM activity. Only one of the compounds showed increased ERK activation, while the others had no effects (Sturchler et al., 2017). The results of this study clearly highlights the complexity of intracellular signaling and emphasizes the importance of combining multiple experimental procedures if possible.

The two compounds were retrieved by pharmacophore models originally generated based on agonists and they were therefore docked into the closed/active receptor conformation. This result, together with the results from docking of the known antagonists (Paper 1) show that antagonists can also fit in the closed receptor conformation as described for mGluRs (Muto et al., 2007). However, the docking score was poorer than of the agonist, and we still believe that in a natural environment with full flexibility of the protein and the ligand, the antagonist would not be able to stabilize a closed conformation of the VFT. The calculated Tanimoto similarity

matrix showed that compound 23 was similar to some of the antagonists. Compound 28 represents a completely new chemotype that is highly similar to already approved drugs targeting other receptors (results not disclosed).

5.4 Molecular dynamics and metadynamics to study Venus flytrap dynamics

Molecular dynamics simulations can provide a great understanding of the atomic motions as function of time. In order to properly include the fastest motions of a system such as bond bending and stretching and correctly integrate the equation of motion, sampling in the fs range is necessary (Leach, 2001). Sampling of the movement of every atom in a system at such a timescale, makes this an accurate method that fully describes protein dynamics (Henzler-Wildman and Kern, 2007). However, many interesting biological events such as large domain changes upon ligand binding or protein-protein interaction occurs in μs to second timescales, which would result in the need of 10^9 to 10^{15} MD steps to explore the motions (Barducci et al., 2011). In addition, solvent and maybe the cellular membrane need to be added, resulting in extremely expensive calculations in terms of memory and time consumption, where only 100 ns can take multiple days to run depending on the hardware and the number of atoms in the system (Henzler-Wildman and Kern, 2007; Laio and Gervasio, 2008). This implies that MD are used to study local flexibility or so called "fast motions" rather than larger domain motions which is slower and requires crossing energy barriers, thereby referred to as rare events in terms of unbiased MD (Laio and Gervasio, 2008) (Fig 19).
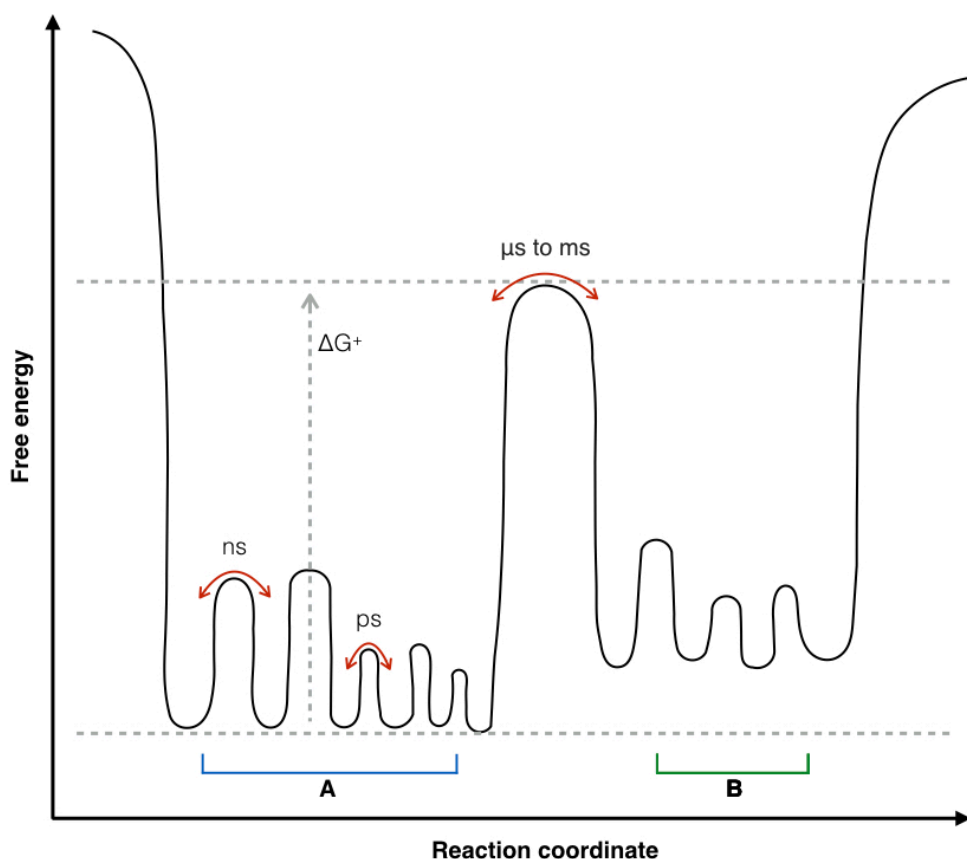
Figure 19 – A simplified illustration of protein dynamics and energy barriers in a one-dimensional free energy landscape. The ΔG^+ illustrates the energy required for the protein to cross the barrier and transition from state A to state B. Such large domain motions often occur in the μs to ms scale, while smaller motions such as side chain rotations often follow in the ps to ns scale due to smaller energy barriers. (Illustration modified from (Henzler-Wildman and Kern, 2007).

Metadynamics is one of several enhanced sampling methods that is capable of overcoming the timescale problem, cross high energy barriers and explore rare events inaccessible through unbiased MD (Henzler-Wildman and Kern, 2007). The method may also discover new reaction pathways because it naturally passes the lowest saddle point of a FES into a new minimum (Barducci et al., 2011). Metadynamics facilitate sampling by adding a force (bias potential) to selected degrees of freedom that represent the process under investigation (Barducci et al., 2011). In paper 3, we used a path representing the transition from the closed state to a wide open state. To our knowledge, there is only very limited number of studies applying path-metadynamics to study conformational transition in molecules of this size. The reaction coordinates for this transition were observed during the unbiased MD when the separate simulations were merged, and was used to construct this path. The wide-open state of the VFT explored by the MD has not been described for any other member of class C and may be a result

of the missing stabilization forces from the $GABA_{B2}$ VFT or it can be a conformation that is seldom explored.

The obtained path was used as a CV in a 2 μs metadynamics run. The result from our study showed that progression along the path proceeded with low Z values, indicating that our path was a good prediction and no alternative transition pathways was discovered. Also, multiple metastable states were detected along the transition, but they were separated by high energy barriers. Only important residues of the binding pocket were analyzed and we found that the majority remained stable during the simulation. The $GABA_{B2}$ VFT has been shown to increase the agonist affinity and stabilize the closed conformation of $GABA_{B1}$ VFT during activation (Geng et al., 2013; Liu et al., 2004; Nomura et al., 2008). However, as the $GABA_{B2}$ VFT is believed to be stably present in an inactive/open state, it might not affect the transitions in other ways than stabilizing the endpoint of $GABA_{B1}$ VFT activation (closed VFT). Our results suggest that the $GABA_{B1}$ VFT requires a ligand to cross these barriers and is capable of closing in the absence of $GABA_{B2}$ VFT.

There are multiple challenges and considerations that need to be accounted for successfully running Metadynamics. The biggest challenge is selection of CVs to describe the process under investigation. There are multiple criteria for selection of an appropriate CV such as it must be able to describe all slow modes of the system and completely distinguish between the initial and final state (Barducci et al., 2011). Another challenge in a standard metadynamics is to decide when the system has converged. The point of convergence can be hard to detect because the free energy fluctuates around the filled FES in addition to the risk of overfilling the FES. This problem can be solved by using a WT-MetaD, where a bias factor is used to rescale the Gaussian height in such a way that when the system is in a local minimum the Gaussians accumulate and the height is reduced. When the system crosses the lowest saddle point and starts exploring a new local minimum, the height becomes restored (Barducci et al., 2011, 2008). As the Gaussians become smaller during the simulation, the convergence becomes smoother on the FES (Barducci et al., 2008). Thus, decreasing Gaussian height should be accompanied by observation of the system revisiting regions in the CV space to ensure convergence. However, deciding the correct value of both the bias factor and the Gaussian height without knowing anything about the energy barriers between the conformations, can be difficult and often requires some trials. If the bias factor is set too

low, the Gaussian height decreases faster and may not provide the system enough potential to escape the local minimum.

5.5 Structural dynamics of the Venus flytrap

The extracellular part of GABA$_B$-R has major structural differences from the mGluRs, which suggest that the receptor mechanisms might be different. The mGluRs can form both homo- and heterodimers, where binding of ligands in both the VFT orthosteric sites is necessary for full receptor activation (Møller et al., 2017). The VFTs of mGluRs is in an equilibrium between the open/active and closed/inactive states and interactions is stabilized by disulfide bonds between the VFTs (Møller et al., 2017). A cysteine rich domain is responsible for linking the VFTs to the 7TM domain, and mutational studies of this region showed impairment of activation (Huang et al., 2011). The GABA$_B$-R is a obligate heterodimer, and only the VFT of GABA$_{B1}$ is capable of binding ligands and GABA$_{B2}$ is necessary for G-protein coupling (Geng et al., 2012; Møller et al., 2017). The GABA$_B$-R linker connecting the VFT to the 7TM, does not possess the conserved cysteine residues. Also, mutational studies of the linker have implicated that changing the sequence has no impact on the activation of the receptor (Margeta-Mitrovic et al., 2001). The structural rearrangement of GABA$_B$-R and mGluRs VFT(s) upon activation is transmitted to the 7TM domains causing a rearrangement of these domains as well, which is necessary for full receptor activation (Møller et al., 2017). The presented studies only focus on the orthosteric binding site in the VFT, and structural mechanisms of the 7TM domain or signal transduction will therefore not be discussed in great detail.

Investigation of the conformational dynamics of mGluR1 by FRET studies using saturating concentrations of agonist show that closure of the VFT occurs in the sub-millisecond velocity (Grushevskyi et al., 2019; Olofsson et al., 2014). The closure of the VFT is directly linked to the repositioning of the 7TM, where the conformational changes occur significantly slower (~ 20 ms) (Grushevskyi et al., 2019). The VFT of mGluR2 was suggested to shift between inactive open and active closed states independent of the ligand, while agonist binding was suggested to shift the equilibrium from a rapid transition between open and closed conformation towards an active closed conformational state (Olofsson et al., 2014). However, Vafabakhsh *et al.,* studied group 2 mGluRs using FRET and found that the VFT interconverts, not only between open and closed states, but also has a short lived intermediate state. FRET studies of GABA$_B$-

R VFT dynamics, could not show the same behavior of the GABA$_B$-R VFT. In fact, it was not found any FRET modulation upon receptor stimulation when labeling the N-terminal domains of the dimer (Lecat-Guillet et al., 2017). Lecat-Guillet *et al.* suggested that the reason for this discrepancy with the suggested VFT mechanism of mGluR, was due to lower structural reorganization upon activation or formation of stable oligomers (Lecat-Guillet et al., 2017). Koehl *et al.* recently showed that activation of the mGluR5 VFTs caused a substantial rearrangement of the extracellular domains causing a compaction propagated to the 7TMs (Koehl et al., 2019). This rearrangement caused the 7TMs to move closer together, in addition to creating a reorientation by a 20° rotation (Koehl et al., 2019). Structural analysis of available resolved X-ray structures of the GABA$_B$-R supports that the conformational rearrangement upon VFT activation is smaller for GABA$_B$-R than for mGluRs (Geng et al., 2013; Koehl et al., 2019). These results together with our results presented in paper 3, strengthens the suggestion that the activation mechanism of mGluRs is not directly transferable to GABA$_B$-R. We have suggested that the open/inactive and closed/active conformations GABA$_B$-R VFT do not alternate naturally between the two states like the mGluRs. Rather, they represent two energetically equal and low energy conformations, separated by sizeable energy barriers of about 20 kcal/mol.

Mutational studies show the importance of specific ligand-protein interactions, where removal of residues can change the activity for ligands. As for the GABA$_B$-R VFT, Trp65 and Ser131 among other residues, were found to disrupt ligand binding and receptor activity (Galvez et al., 1999; Geng et al., 2013). The interaction pattern in a protein-ligand complex may affect the receptor conformation as studies initially investigating allosteric modulation and biased signaling of mGluRs and GABA$_B$-R suggested that the receptor conformation is dependent on the ligand and thereby causing conformational specific pathway activation (Lecat-Guillet et al., 2017; Olofsson et al., 2014). Emery *et al.*, studied ligand bias of mGluR1a and discovered that pathway-activation could be linked to the ligand interaction pattern in the orthosteric binding pocket (Emery et al., 2012). Further, mutational studies of mGluR1a showed that agonists initially capable of activating both the G-protein dependent pathway and arrestins, became pathway biased when certain interactions were eliminated (Emery et al., 2012). These discoveries suggest that ligands can induce different receptor conformations based on interactions with the binding pocket and that even small differences can have major impact on signal transduction to the intracellular side.

In the case of GABA$_B$-R, this could explain why the low affinity antagonists used in paper 1, phaclofen and saclofen (GABA analogues) execute the opposite extracellular function of GABA and baclofen (Froestl et al., 1996, 1995a). The presented study (paper 1) and previous X-ray crystal structures show that the binding of these ligands are mainly facilitated by LB1 and that there are fewer stabilizing interactions for phaclofen and saclofen than for GABA (Geng et al., 2013). This results in less stabilization of these antagonists in the binding pocket and distort VFT closing, causing the receptor to arrange into another conformation associated with a different signaling pathway.

6. Conclusion and future perspectives

The GABA$_B$-R is an important drug target as it binds to the main inhibitory neurotransmitter in the CNS and is associated with a broad variety of diseases. Almost 40 years have passed since the GABA was associated with affective disorders for the first time, and despite all efforts, only a small number of ligands are found to target the receptor. GABA$_B$-R is a very special target, different from other class C GPCRs members by being an obligate heterodimer, missing the cysteine rich domain and by not following the classical desensitization mechanism involving GRKs. Understanding the concept of receptor dynamics, how ligands effect receptor conformation and the coupling to intracellular signaling pathways, is important for the understanding of drug mechanisms and for identification of conformational states that can be targeted by new drugs. The results presented in this study is an effort to enhance the understanding concerning the mechanism and identify new ligand scaffolds.

Ligand-based and structure-based methods were evaluated and applied in a VS protocol to identify, so far, two potential new GABA$_B$-R ligands targeting the orthosteric binding (paper 2). The compounds will be further evaluated in a radioligand binding assay using a tritium-labeled potent antagonist. The successful candidates will be further used to create scaffolds representing structural distinct compound from those already known. The generated e-Pharmacophore models turned out to be useless in a screening procedure due to low selectivity (paper 1), but we will use them to facilitate this work by indicating where the compounds can be modified by adding specific chemical groups to optimize ligand-receptor interactions. In the next round of selecting and purchasing hits, we will use the obtained trajectories (paper 3) to analyze conformational movements and select conformations to be used in a docking procedure representing new receptor conformations.

7. References

Adaptive variables I [WWW Document], n.d. . Plumed. URL https://www.plumed.org/doc-v2.5/user-doc/html/belfast-2.html

Alam, Md.A., Naik, P.K., 2009. Applying linear interaction energy method for binding affinity calculations of podophyllotoxin analogues with tubulin using continuum solvent model and prediction of cytotoxic activity. J. Mol. Graph. Model. 27, 930–943. https://doi.org/10.1016/j.jmgm.2009.02.003

Alberts, B. (Ed.), 2008. Molecular biology of the cell, 5th ed. ed. Garland Science, New York.

Aparoy, P., Kumar Reddy, K., Reddanna, P., 2012. Structure and Ligand Based Drug Design Strategies in the Development of Novel 5- LOX Inhibitors. Curr. Med. Chem. 19, 3763–3778. https://doi.org/10.2174/092986712801661112

Åqvist, J., Marelius, J., 2001. The Linear Interaction Energy Method for Predicting Ligand Binding Free Energies. Comb. Chem. High Throughput Screen. 4, 613–626. https://doi.org/10.2174/1386207013330661

Åqvist, J., Medina, C., Samuelsson, J.E., 1994. A new method for predicting binding affinity in computer-aided drug design. Protein Eng. 7, 385–391.

Augier, E., Dulman, R.S., Damadzic, R., Pilling, A., Hamilton, J.P., Heilig, M., 2017. The GABAB Positive Allosteric Modulator ADX71441 Attenuates Alcohol Self-Administration and Relapse to Alcohol Seeking in Rats. Neuropsychopharmacology 42, 1789–1799. https://doi.org/10.1038/npp.2017.53

Bai, F., Xu, Y., Chen, J., Liu, Q., Gu, J., Wang, X., Ma, J., Li, H., Onuchic, J.N., Jiang, H., 2013. Free energy landscape for the binding process of Huperzine A to acetylcholinesterase. Proc. Natl. Acad. Sci. 110, 4273–4278. https://doi.org/10.1073/pnas.1301814110

Barducci, A., Bonomi, M., Parrinello, M., 2011. Metadynamics. Wiley Interdiscip. Rev. Comput. Mol. Sci. 1, 826–843. https://doi.org/10.1002/wcms.31

Barducci, A., Bussi, G., Parrinello, M., 2008. Well-Tempered Metadynamics: A Smoothly Converging and Tunable Free-Energy Method. Phys. Rev. Lett. 100. https://doi.org/10.1103/PhysRevLett.100.020603

Barrett, K.E., Ganong, W.F. (Eds.), 2010. Ganong's review of medical physiology, 23rd ed. ed, A LANGE medical book. McGraw-Hill Medical, New York.

Basith, S., Cui, M., Macalino, S.J.Y., Park, J., Clavio, N.A.B., Kang, S., Choi, S., 2018. Exploring G Protein-Coupled Receptors (GPCRs) Ligand Space via Cheminformatics Approaches: Impact on Rational Drug Design. Front. Pharmacol. 9. https://doi.org/10.3389/fphar.2018.00128

Battista, E., Page, C.P., Horton-Szar, D., 2015. Pharmacology.

Benet, L.Z., Hosey, C.M., Ursu, O., Oprea, T.I., 2016. BDDCS, the Rule of 5 and drugability. Adv. Drug Deliv. Rev. 101, 89–98. https://doi.org/10.1016/j.addr.2016.05.007

Benke, D., 2012. Modulation of cell surface GABA B receptors by desensitization, trafficking and regulated degradation. World J. Biol. Chem. 3, 61. https://doi.org/10.4331/wjbc.v3.i4.61

Berendsen, H.J.C., van der Spoel, D., van Drunen, R., 1995. GROMACS: A message-passing parallel molecular dynamics implementation. Comput. Phys. Commun. 91, 43–56. https://doi.org/10.1016/0010-4655(95)00042-E

Bettler, B., Kaupmann, K., Mosbacher, J., Gassmann, M., 2004. Molecular Structure and Physiological Functions of GABAB Receptors. Physiol. Rev. 84, 835–867. https://doi.org/10.1152/physrev.00036.2003

Biermann, B., Ivankova-Susankova, K., Bradaia, A., Abdel Aziz, S., Besseyrias, V., Kapfhammer, J.P., Missler, M., Gassmann, M., Bettler, B., 2010. The Sushi Domains of GABAB Receptors Function as Axonal Targeting Signals. J. Neurosci. 30, 1385–1394. https://doi.org/10.1523/JNEUROSCI.3172-09.2010

Binet, V., Brajon, C., Le Corre, L., Acher, F., Pin, J.-P., Prézeau, L., 2004. The Heptahelical Domain of GABA B2 Is Activated Directly by CGP7930, a Positive Allosteric Modulator of the GABA B Receptor. J. Biol. Chem. 279, 29085–29091. https://doi.org/10.1074/jbc.M400930200

Bittiger, H., Froestl, W., Gentsch, C., Jaekel, J., Mickel, S.J., Mondadori, C., Olpe, H.R., Schmutz, M., 1996. GABAB Receptor Antagonists: Potential Therapeutic Applications, in: Tanaka, C., Bowery, N.G. (Eds.), GABA: Receptors, Transporters and Metabolism. Birkhäuser Basel, Basel, pp. 297–305. https://doi.org/10.1007/978-3-0348-8990-2_33

Blackburn, T.P., Bowery, N. (Eds.), 2010. GABA B receptor pharmacology: a tribute to Norman Bowery, Advances in pharmacology. Elsevier, Acad. Press, Amsterdam.

Bottegoni, G., Kufareva, I., Totrov, M., Abagyan, R., 2009. Four-Dimensional Docking: A Fast and Accurate Account of Discrete Receptor Flexibility in Ligand Docking. J. Med. Chem. 52, 397–406. https://doi.org/10.1021/jm8009958

Branduardi, D., Gervasio, F.L., Parrinello, M., 2007. From A to B in free energy space. J. Chem. Phys. 126, 054103. https://doi.org/10.1063/1.2432340

B-Rao, C., Subramanian, J., Sharma, S.D., 2009. Managing protein flexibility in docking and its applications. Drug Discov. Today 14, 394–400. https://doi.org/10.1016/j.drudis.2009.01.003

Brown, K.M., Roy, K.K., Hockerman, G.H., Doerksen, R.J., Colby, D.A., 2015. Activation of the γ-Aminobutyric Acid Type B (GABAB) Receptor by Agonists and Positive Allosteric Modulators: Miniperspective. J. Med. Chem. 58, 6336–6347. https://doi.org/10.1021/jm5018913

Burford, N.T., Clark, M.J., Wehrman, T.S., Gerritz, S.W., Banks, M., O'Connell, J., Traynor, J.R., Alt, A., 2013. Discovery of positive allosteric modulators and silent allosteric modulators of the -opioid receptor. Proc. Natl. Acad. Sci. 110, 10830–10835. https://doi.org/10.1073/pnas.1300393110

Burmakina, S., Geng, Y., Chen, Y., Fan, Q.R., 2014. Heterodimeric coiled-coil interactions of human GABAB receptor. Proc. Natl. Acad. Sci. 111, 6958–6963. https://doi.org/10.1073/pnas.1400081111

Calver, A.R., Medhurst, A.D., Robbins, M.J., Charles, K.J., Evans, M.L., Harrison, D.C., Stammers, M., Hughes, S.A., Hervieu, G., Couve, A., Moss, S.J., Middlemiss, D.N., Pangalos, M.N., 2000. The expression of GABAB1 and GABAB2 receptor subunits in the cNS differs from that in peripheral tissues. Neuroscience 100, 155–170. https://doi.org/10.1016/S0306-4522(00)00262-1

Calver, A.R., Robbins, M.J., Cosio, C., Rice, S.Q.J., Babbs, A.J., Hirst, W.D., Boyfield, I., Wood, M.D., Russell, R.B., Price, G.W., Couve, A., Moss, S.J., Pangalos, M.N., 2001. The C-Terminal Domains of the GABA B Receptor Subunits Mediate Intracellular Trafficking But Are Not Required for Receptor Signaling. J. Neurosci. 21, 1203–1210. https://doi.org/10.1523/JNEUROSCI.21-04-01203.2001

Canvas, 2017. Schrödinger Release 2017-4. Schrödinger, LLC, New York, NY.

Carter, L.P., Koek, W., France, C.P., 2009. Behavioral analyses of GHB: Receptor mechanisms. Pharmacol. Ther. 121, 100–114. https://doi.org/10.1016/j.pharmthera.2008.10.003

Cereto-Massagué, A., Ojeda, M.J., Valls, C., Mulero, M., Garcia-Vallvé, S., Pujadas, G., 2015. Molecular fingerprint similarity search in virtual screening. Methods 71, 58–63. https://doi.org/10.1016/j.ymeth.2014.08.005

Chang, E., Ghosh, N., Yanni, D., Lee, S., Alexandru, D., Mozaffar, T., 2013. A Review of Spasticity Treatments: Pharmacological and Interventional Approaches. Crit. Rev. Phys. Rehabil. Med. 25, 11–22. https://doi.org/10.1615/CritRevPhysRehabilMed.2013007945

Chebib, M., Johnston, G.A., 1999. The "ABC" of GABA receptors: a brief review. Clin. Exp. Pharmacol. Physiol. 26, 937–940.

Chothia, C., Lesk, A.M., 1986. The relation between the divergence of sequence and structure in proteins. EMBO J. 5, 823–826.

Chun, L., Zhang, W., Liu, J., 2012. Structure and ligand recognition of class C GPCRs. Acta Pharmacol. Sin. 33, 312–323. https://doi.org/10.1038/aps.2011.186

Conn, P.J., Lindsley, C.W., Meiler, J., Niswender, C.M., 2014. Opportunities and challenges in the discovery of allosteric modulators of GPCRs for treating CNS disorders. Nat. Rev. Drug Discov. 13, 692–708. https://doi.org/10.1038/nrd4308

Costanzo, L.S., 2010. Physiology. Saunders/Elsevier, Philadelphia, PA.

Coudrat, T., Simms, J., Christopoulos, A., Wootten, D., Sexton, P.M., 2017. Improving virtual screening of G protein-coupled receptors via ligand-directed modeling. PLOS Comput. Biol. 13, e1005819. https://doi.org/10.1371/journal.pcbi.1005819

Cournia, Z., Allen, B., Sherman, W., 2017. Relative Binding Free Energy Calculations in Drug Discovery: Recent Advances and Practical Considerations. J. Chem. Inf. Model. 57, 2911–2937. https://doi.org/10.1021/acs.jcim.7b00564

Cryan, J.F., Kaupmann, K., 2005. Don't worry 'B' happy!: a role for GABAB receptors in anxiety and depression. Trends Pharmacol. Sci. 26, 36–43. https://doi.org/10.1016/j.tips.2004.11.004

Cryan, J.F., Slattery, D.A., 2010. GABAB Receptors and Depression: Current Status, in: Advances in Pharmacology. Elsevier, pp. 427–451. https://doi.org/10.1016/S1054-3589(10)58016-5

CV Documentation [WWW Document], n.d. . Plumed. URL https://www.plumed.org/doc-v2.5/user-doc/html/_p_a_t_h.html

Daneman, R., Prat, A., 2015. The blood-brain barrier. Cold Spring Harb. Perspect. Biol. 7, a020412. https://doi.org/10.1101/cshperspect.a020412

Davies, M., E. Gloriam, D., Secker, A., A. Freitas, A., Timmis, J., R. Flower, D., 2011. Present Perspectives on the Automated Classification of the G-Protein Coupled Receptors (GPCRs) at the Protein Sequence Level. Curr. Top. Med. Chem. 11, 1994–2009. https://doi.org/10.2174/156802611796391221

de Graaf, C., Pospisil, P., Pos, W., Folkers, G., Vermeulen, N.P.E., 2005. Binding Mode Prediction of Cytochrome P450 and Thymidine Kinase Protein−Ligand Complexes by Consideration of Water and Rescoring in Automated Docking. J. Med. Chem. 48, 2308–2318. https://doi.org/10.1021/jm049650u

Deguchi, Y., Inabe, K., Tomiyasu, K., Nozawa, K., Yamada, S., Kimura, R., 1995. Study on brain interstitial fluid distribution and blood-brain barrier transport of baclofen in rats by microdialysis. Pharm. Res. 12, 1838–1844. https://doi.org/10.1023/a:1016263032765

DiscoverX, n.d. User Manual HitHunter® cAMP Assay for Small Molecules, For Chemiluminescent Detection of cAMP and GPCR Activity.

Dror, R.O., Arlow, D.H., Maragakis, P., Mildorf, T.J., Pan, A.C., Xu, H., Borhani, D.W., Shaw, D.E., 2011. Activation mechanism of the 2-adrenergic receptor. Proc. Natl. Acad. Sci. 108, 18684–18689. https://doi.org/10.1073/pnas.1110499108

Du, X., Li, Y., Xia, Y.-L., Ai, S.-M., Liang, J., Sang, P., Ji, X.-L., Liu, S.-Q., 2016. Insights into Protein–Ligand Interactions: Mechanisms, Models, and Methods. Int. J. Mol. Sci. 17, 144. https://doi.org/10.3390/ijms17020144

Duan, J., Dixon, S.L., Lowrie, J.F., Sherman, W., 2010. Analysis and comparison of 2D fingerprints: Insights into database screening performance using eight fingerprint methods. J. Mol. Graph. Model. 29, 157–170. https://doi.org/10.1016/j.jmgm.2010.05.008

Emery, A.C., DiRaddo, J.O., Miller, E., Hathaway, H.A., Pshenichkin, S., Takoudjou, G.R., Grajkowska, E., Yasuda, R.P., Wolfe, B.B., Wroblewski, J.T., 2012. Ligand Bias at Metabotropic Glutamate 1a Receptors: Molecular Determinants That Distinguish -Arrestin-Mediated from G Protein-Mediated Signaling. Mol. Pharmacol. 82, 291–301. https://doi.org/10.1124/mol.112.078444

Enna, S., 1997. GABAB receptor agonists and antagonists: pharmacological properties and therapeutic possibilities. Expert Opin. Investig. Drugs 6, 1319–1325. https://doi.org/10.1517/13543784.6.10.1319

Erlandson, S.C., McMahon, C., Kruse, A.C., 2018. Structural Basis for G Protein–Coupled Receptor Signaling. Annu. Rev. Biophys. 47, 1–18. https://doi.org/10.1146/annurev-biophys-070317-032931

Evenseth, L., Warszycki, D., Bojarski, A., Gabrielsen, M., Sylte, I., 2019. In Silico Methods for the

Discovery of Orthosteric GABAB Receptor Compounds. Molecules 24, 935.
https://doi.org/10.3390/molecules24050935

Fatemi, S.H., Folsom, T.D., Thuras, P.D., 2017. GABA A and GABA B receptor dysregulation in superior frontal cortex of subjects with schizophrenia and bipolar disorder. Synapse 71, e21973. https://doi.org/10.1002/syn.21973

Fehske, H., Schneider, R., Weiße, A. (Eds.), 2008. Computational Many-Particle Physics, Lecture Notes in Physics. Springer Berlin Heidelberg, Berlin, Heidelberg. https://doi.org/10.1007/978-3-540-74686-7

File, S.E, A., N., 1993. Handling history of rats modifies behavioural effects of drugs in the elevated plus-maze test of anxiety. Eur J Pharmacol 235, 109–112.

Foster, D.J., Conn, P.J., 2017. Allosteric Modulation of GPCRs: New Insights and Potential Utility for Treatment of Schizophrenia and Other CNS Disorders. Neuron 94, 431–446. https://doi.org/10.1016/j.neuron.2017.03.016

Frangaj, A., Fan, Q.R., 2017. Structural biology of GABA B receptor. Neuropharmacology. https://doi.org/10.1016/j.neuropharm.2017.10.011

Fredriksson, R., 2003. The G-Protein-Coupled Receptors in the Human Genome Form Five Main Families. Phylogenetic Analysis, Paralogon Groups, and Fingerprints. Mol. Pharmacol. 63, 1256–1272. https://doi.org/10.1124/mol.63.6.1256

Friesner, R.A., Banks, J.L., Murphy, R.B., Halgren, T.A., Klicic, J.J., Mainz, D.T., Repasky, M.P., Knoll, E.H., Shelley, M., Perry, J.K., Shaw, D.E., Francis, P., Shenkin, P.S., 2004. Glide: A New Approach for Rapid, Accurate Docking and Scoring. 1. Method and Assessment of Docking Accuracy. J. Med. Chem. 47, 1739–1749. https://doi.org/10.1021/jm0306430

Friesner, R.A., Murphy, R.B., Repasky, M.P., Frye, L.L., Greenwood, J.R., Halgren, T.A., Sanschagrin, P.C., Mainz, D.T., 2006. Extra Precision Glide: Docking and Scoring Incorporating a Model of Hydrophobic Enclosure for Protein−Ligand Complexes. J. Med. Chem. 49, 6177–6196. https://doi.org/10.1021/jm051256o

Froestl, W., 2010. Chemistry and Pharmacology of GABAB Receptor Ligands, in: Advances in Pharmacology. Elsevier, pp. 19–62. https://doi.org/10.1016/S1054-3589(10)58002-5

Froestl, W., Mickel, S.J., Hall, R.G., von Sprecher, G., Strub, D., Baumann, P.A., Brugger, F., Gentsch, C., Jaekel, J., 1995a. Phosphinic Acid Analogs of GABA. 1. New Potent and Selective GABAB Agonists. J. Med. Chem. 38, 3297–3312. https://doi.org/10.1021/jm00017a015

Froestl, W., Mickel, S.J., Schmutz, M., Bittiger, H., 1996. Potent, Orally active GABA(B) Receptor Antagonist. Pharmacol. Rev. Commun. 8, 127–133.

Froestl, W., Mickel, S.J., von Sprecher, G., Diel, P.J., Hall, R.G., Maier, L., Strub, D., Melillo, V., Baumann, P.A., 1995b. Phosphinic Acid Analogs of GABA. 2. Selective, Orally Active GABAB Antagonists. J. Med. Chem. 38, 3313–3331. https://doi.org/10.1021/jm00017a016

Gabrielsen, M., Kurczab, R., Ravna, A.W., Kufareva, I., Abagyan, R., Chilmonczyk, Z., Bojarski, A.J., Sylte, I., 2012. Molecular mechanism of serotonin transporter inhibition elucidated by a new flexible docking protocol. Eur. J. Med. Chem. 47, 24–37. https://doi.org/10.1016/j.ejmech.2011.09.056

Galvez, T., 2001. Allosteric interactions between GB1 andGB2 subunits are required for optimalGABAB receptor function. EMBO J. 20, 2152–2159. https://doi.org/10.1093/emboj/20.9.2152

Galvez, T., Parmentier, M.-L., Joly, C., Malitschek, B., Kaupmann, K., Kuhn, R., Bittiger, H., Froestl, W., Bettler, B., Pin, J.-P., 1999. Mutagenesis and Modeling of the GABA B Receptor Extracellular Domain Support a Venus Flytrap Mechanism for Ligand Binding. J. Biol. Chem. 274, 13362–13369. https://doi.org/10.1074/jbc.274.19.13362

Galvez, T., Prézeau, L., Milioti, G., Franek, M., Joly, C., Froestl, W., Bettler, B., Bertrand, H.-O., Blahos, J., Pin, J.-P., 2000. Mapping the Agonist-binding Site of GABA B Type 1 Subunit Sheds Light on the Activation Process of GABA B Receptors. J. Biol. Chem. 275, 41166–41174. https://doi.org/10.1074/jbc.M007848200

Gassmann, M., Bettler, B., 2012. Regulation of neuronal GABAB receptor functions by subunit composition. Nat. Rev. Neurosci. 13, 380–394. https://doi.org/10.1038/nrn3249

Geldenhuys, W.J., Mohammad, A.S., Adkins, C.E., Lockman, P.R., 2015. Molecular determinants of blood–brain barrier permeation. Ther. Deliv. 6, 961–971. https://doi.org/10.4155/tde.15.32

Geng, Y., Bush, M., Mosyak, L., Wang, F., Fan, Q.R., 2013. Structural mechanism of ligand activation in human GABAB receptor. Nature 504, 254–259. https://doi.org/10.1038/nature12725

Geng, Y., Xiong, D., Mosyak, L., Malito, D.L., Kniazeff, J., Chen, Y., Burmakina, S., Quick, M., Bush, M., Javitch, J.A., Pin, J.-P., Fan, Q.R., 2012. Structure and functional interaction of the extracellular domain of human GABA(B) receptor GBR2. Nat. Neurosci. 15, 970–978. https://doi.org/10.1038/nn.3133

Genheden, S., Ryde, U., 2015. The MM/PBSA and MM/GBSA methods to estimate ligand-binding affinities. Expert Opin. Drug Discov. 10, 449–461. https://doi.org/10.1517/17460441.2015.1032936

Ghose, A.K., Herbertz, T., Hudkins, R.L., Dorsey, B.D., Mallamo, J.P., 2012. Knowledge-Based, Central Nervous System (CNS) Lead Selection and Lead Optimization for CNS Drug Discovery. ACS Chem. Neurosci. 3, 50–68. https://doi.org/10.1021/cn200100h

Ghose, S., Winter, M.K., McCarson, K.E., Tamminga, C.A., Enna, S.J., 2011. The GABAB receptor as a target for antidepressant drug action: GABAB receptor expression and depression. Br. J. Pharmacol. 162, 1–17. https://doi.org/10.1111/j.1476-5381.2010.01004.x

Gilchrist, A. (Ed.), 2010. GPCR Molecular Pharmacology and Drug Targeting: Shifting Paradigms and New Directions. John Wiley & Sons, Inc., Hoboken, NJ, USA. https://doi.org/10.1002/9780470627327

Gimenez, B.G., Santos, M.S., Fernandes, J.P.S., et al., 2010. Evaluation of blockbuster drugs under

the Rule-of-five. Pharmazie 148–152. https://doi.org/10.1691/ph.2010.9733

Glide, 2017. Schrödinger Release 2017-4. Schrödinger, LLC, New York, NY.

Glide, 2015. Schrödinger Release 2015-3. Schrödinger, LLC, New York, NY.

González, M.A., 2011. Force fields and molecular dynamics simulations. Éc. Thématique Société Fr. Neutron. 12, 169–200. https://doi.org/10.1051/sfn/201112009

Grushevskyi, E.O., Kukaj, T., Schmauder, R., Bock, A., Zabel, U., Schwabe, T., Benndorf, K., Lohse, M.J., 2019. Stepwise activation of a class C GPCR begins with millisecond dimer rearrangement. Proc. Natl. Acad. Sci. 201900261. https://doi.org/10.1073/pnas.1900261116

Güner, O.F. (Ed.), 2000. Pharmacophore perception, development, and use in drug design, IUL biotechnology series. International University Line, LaJolla, CA.

Halgren, T.A., Murphy, R.B., Friesner, R.A., Beard, H.S., Frye, L.L., Pollard, W.T., Banks, J.L., 2004. Glide: A New Approach for Rapid, Accurate Docking and Scoring. 2. Enrichment Factors in Database Screening. J. Med. Chem. 47, 1750–1759. https://doi.org/10.1021/jm030644s

Harder, E., Damm, W., Maple, J., Wu, C., Reboul, M., Xiang, J.Y., Wang, L., Lupyan, D., Dahlgren, M.K., Knight, J.L., Kaus, J.W., Cerutti, D.S., Krilov, G., Jorgensen, W.L., Abel, R., Friesner, R.A., 2016. OPLS3: A Force Field Providing Broad Coverage of Drug-like Small Molecules and Proteins. J. Chem. Theory Comput. 12, 281–296. https://doi.org/10.1021/acs.jctc.5b00864

Harpsøe, K., Boesgaard, M.W., Munk, C., Bräuner-Osborne, H., Gloriam, D.E., 2016. Structural insight to mutation effects uncover a common allosteric site in class C GPCRs. Bioinformatics btw784. https://doi.org/10.1093/bioinformatics/btw784

Hauser, A.S., Attwood, M.M., Rask-Andersen, M., Schiöth, H.B., Gloriam, D.E., 2017. Trends in GPCR drug discovery: new agents, targets and indications. Nat. Rev. Drug Discov. 16, 829.

Heaney, C.F., Kinney, J.W., 2016. Role of GABAB receptors in learning and memory and neurological disorders. Neurosci. Biobehav. Rev. 63, 1–28. https://doi.org/10.1016/j.neubiorev.2016.01.007

Henzler-Wildman, K., Kern, D., 2007. Dynamic personalities of proteins. Nature 450, 964–972. https://doi.org/10.1038/nature06522

Hilger, D., Masureel, M., Kobilka, B.K., 2018. Structure and dynamics of GPCR signaling complexes. Nat. Struct. Mol. Biol. 25, 4–12. https://doi.org/10.1038/s41594-017-0011-7

Hollenstein, K., de Graaf, C., Bortolato, A., Wang, M.-W., Marshall, F.H., Stevens, R.C., 2014. Insights into the structure of class B GPCRs. Trends Pharmacol. Sci. 35, 12–22. https://doi.org/10.1016/j.tips.2013.11.001

Höltje, H.-D., Folkers, G., Mannhold, R., Kubinyi, H., Timmerman, H., 2008. Molecular Modeling Basic Principles and Applications. Wiley-VCH, Weinheim.

Horvath, D., 2010. Pharmacophore-Based Virtual Screening, in: Bajorath, J. (Ed.), Chemoinformatics and Computational Chemical Biology. Humana Press, Totowa, NJ, pp. 261–298. https://doi.org/10.1007/978-1-60761-839-3_11

Hu, G.-M., Mai, T.-L., Chen, C.-M., 2017. Visualizing the GPCR Network: Classification and Evolution. Sci. Rep. 7, 15495. https://doi.org/10.1038/s41598-017-15707-9

Hu, Z., Jiang, J., 2009. Assessment of biomolecular force fields for molecular dynamics simulations in a protein crystal. J. Comput. Chem. NA-NA. https://doi.org/10.1002/jcc.21330

Huang, S., Cao, J., Jiang, M., Labesse, G., Liu, J., Pin, J.-P., Rondard, P., 2011. Interdomain movements in metabotropic glutamate receptor activation. Proc. Natl. Acad. Sci. 108, 15480–15485. https://doi.org/10.1073/pnas.1107775108

Huang, S.-Y., Zou, X., 2010. Advances and Challenges in Protein-Ligand Docking. Int. J. Mol. Sci. 11, 3016–3034. https://doi.org/10.3390/ijms11083016

Hulme, E.C., Trevethick, M.A., 2010. Ligand binding assays at equilibrium: validation and interpretation: Equilibrium binding assays. Br. J. Pharmacol. 161, 1219–1237. https://doi.org/10.1111/j.1476-5381.2009.00604.x

Humphrey, W., Dalke, A., Schulten, K., 1996. VMD: visual molecular dynamics. J. Mol. Graph. 14, 33–38, 27–28.

Irwin, J.J., Shoichet, B.K., 2016. Docking Screens for Novel Ligands Conferring New Biology: Miniperspective. J. Med. Chem. 59, 4103–4120. https://doi.org/10.1021/acs.jmedchem.5b02008

Jones, K.A., Borowsky, B., Tamm, J.A., Craig, D.A., Durkin, M.M., Dai, M., Yao, W.-J., Johnson, M., Gunwaldsen, C., Huang, L.-Y., Tang, C., Shen, Q., Salon, J.A., Morse, K., Laz, T., Smith, K.E., Nagarathnam, D., Noble, S.A., Branchek, T.A., Gerald, C., 1998. GABAB receptors function as a heteromeric assembly of the subunits GABABR1 and GABABR2. Nature 396, 674–679. https://doi.org/10.1038/25348

Katritch, V., Cherezov, V., Stevens, R.C., 2013. Structure-function of the G protein-coupled receptor superfamily. Annu. Rev. Pharmacol. Toxicol. 53, 531–556. https://doi.org/10.1146/annurev-pharmtox-032112-135923

Kaupmann, K., Malitschek, B., Schuler, V., Heid, J., Froestl, W., Beck, P., Mosbacher, J., Bischoff, S., Kulik, A., Shigemoto, R., Karschin, A., Bettler, B., 1998. GABAB-receptor subtypes assemble into functional heteromeric complexes. Nature 396, 683–687. https://doi.org/10.1038/25360

Kitchen, D.B., Decornez, H., Furr, J.R., Bajorath, J., 2004. Docking and scoring in virtual screening for drug discovery: methods and applications. Nat. Rev. Drug Discov. 3, 935–949. https://doi.org/10.1038/nrd1549

Klein, M.T., Vinson, P.N., Niswender, C.M., 2013. Approaches for Probing Allosteric Interactions at 7 Transmembrane Spanning Receptors, in: Progress in Molecular Biology and Translational Science. Elsevier, pp. 1–59. https://doi.org/10.1016/B978-0-12-394587-7.00001-4

Kniazeff, J., Galvez, T., Labesse, G., Pin, J.-P., 2002. No Ligand Binding in the GB2 Subunit of the GABA B Receptor Is Required for Activation and Allosteric Interaction between the Subunits. J. Neurosci. 22, 7352–7361. https://doi.org/10.1523/JNEUROSCI.22-17-07352.2002

Knight, J.L., Krilov, G., Borrelli, K.W., Williams, J., Gunn, J.R., Clowes, A., Cheng, L., Friesner, R.A., Abel, R., 2014. Leveraging Data Fusion Strategies in Multireceptor Lead Optimization MM/GBSA End-Point Methods. J. Chem. Theory Comput. 10, 3207–3220. https://doi.org/10.1021/ct500189s

Kobayashi, M., Takei, H., Yamamoto, K., Hatanaka, H., Koshikawa, N., 2012. Kinetics of GABA B autoreceptor-mediated suppression of GABA release in rat insular cortex. J. Neurophysiol. 107, 1431–1442. https://doi.org/10.1152/jn.00813.2011

Kobilka, B.K., 2007. G protein coupled receptor structure and activation. Biochim. Biophys. Acta BBA - Biomembr. 1768, 794–807. https://doi.org/10.1016/j.bbamem.2006.10.021

Koehl, A., Hu, H., Feng, D., Sun, B., Zhang, Y., Robertson, M.J., Chu, M., Kobilka, T.S., Laermans, T., Steyaert, J., Tarrasch, J., Dutta, S., Fonseca, R., Weis, W.I., Mathiesen, J.M., Skiniotis, G., Kobilka, B.K., 2019. Structural insights into the activation of metabotropic glutamate receptors. Nature. https://doi.org/10.1038/s41586-019-0881-4

Kolakowski, L.F., 1994. GCRDb: a G-protein-coupled receptor database. Receptors Channels 2, 1–7.

Konovalov, D.A., Coomans, D., Deconinck, E., Vander Heyden, Y., 2007. Benchmarking of QSAR Models for Blood-Brain Barrier Permeation. J. Chem. Inf. Model. 47, 1648–1656. https://doi.org/10.1021/ci700100f

Koshland, D.E., 1995. The Key–Lock Theory and the Induced Fit Theory. Angew. Chem. Int. Ed. Engl. 33, 2375–2378. https://doi.org/10.1002/anie.199423751

Kozasa, T., Hajicek, N., Chow, C.R., Suzuki, N., 2011. Signalling mechanisms of RhoGTPase regulation by the heterotrimeric G proteins G12 and G13. J. Biochem. (Tokyo) 150, 357–369. https://doi.org/10.1093/jb/mvr105

Laio, A., Gervasio, F.L., 2008. Metadynamics: a method to simulate rare events and reconstruct the free energy in biophysics, chemistry and material science. Rep. Prog. Phys. 71, 126601. https://doi.org/10.1088/0034-4885/71/12/126601

Lal, R., Sukbuntherng, J., Tai, E.H.L., Upadhyay, S., Yao, F., Warren, M.S., Luo, W., Bu, L., Nguyen, S., Zamora, J., Peng, G., Dias, T., Bao, Y., Ludwikow, M., Phan, T., Scheuerman, R.A., Yan, H., Gao, M., Wu, Q.Q., Annamalai, T., Raillard, S.P., Koller, K., Gallop, M.A., Cundy, K.C., 2009. Arbaclofen Placarbil, a Novel *R*-Baclofen Prodrug: Improved Absorption, Distribution, Metabolism, and Elimination Properties Compared with *R*-Baclofen. J. Pharmacol. Exp. Ther. 330, 911–921. https://doi.org/10.1124/jpet.108.149773

Lea, W.A., Simeonov, A., 2011. Fluorescence polarization assays in small molecule screening. Expert Opin. Drug Discov. 6, 17–32. https://doi.org/10.1517/17460441.2011.537322

Leach, A.R., 2001. Molecular modelling: principles and applications, 2nd ed. ed. Prentice Hall, Harlow, England ; New York.

Lecat-Guillet, N., Monnier, C., Rovira, X., Kniazeff, J., Lamarque, L., Zwier, J.M., Trinquet, E., Pin, J.-P., Rondard, P., 2017. FRET-Based Sensors Unravel Activation and Allosteric Modulation of the GABA B Receptor. Cell Chem. Biol. 24, 360–370. https://doi.org/10.1016/j.chembiol.2017.02.011

Lee, S.-M., Booe, J.M., Pioszak, A.A., 2015. Structural insights into ligand recognition and selectivity for classes A, B, and C GPCRs. Eur. J. Pharmacol. 763, 196–205. https://doi.org/10.1016/j.ejphar.2015.05.013

Lefkowitz, R.J., 2005. Transduction of Receptor Signals by -Arrestins. Science 308, 512–517. https://doi.org/10.1126/science.1109237

Lemmon, G., Meiler, J., 2013. Towards Ligand Docking Including Explicit Interface Water Molecules. PLoS ONE 8, e67536. https://doi.org/10.1371/journal.pone.0067536

Liaison, 2015. Schrödinger Release 2015-3. Schrödinger, LLC, New York, NY.

Liaison Manual 5.8, 2015. Schrödinger Release 2015-3. Schrödinger, LLC, New York, NY.

LigPrep, 2017. Schrödinger Release 2017-4. Schrödinger, LLC, New York, NY.

Lindahl, E., 2015. Molecular Dynamics Simulations, in: Kukol, A. (Ed.), Molecular Modeling of Proteins. Springer New York, New York, NY, pp. 3–26. https://doi.org/10.1007/978-1-4939-1465-4_1

Lipinski, C.A., Lombardo, F., Dominy, B.W., Feeney, P.J., 2001. Experimental and computational approaches to estimate solubility and permeability in drug discovery and development settings. Adv. Drug Deliv. Rev. 46, 3–26.

Lissemore, J.I., Bhandari, A., Mulsant, B.H., Lenze, E.J., Reynolds, C.F., Karp, J.F., Rajji, T.K., Noda, Y., Zomorrodi, R., Sibille, E., Daskalakis, Z.J., Blumberger, D.M., 2018. Reduced GABAergic cortical inhibition in aging and depression. Neuropsychopharmacology 43, 2277–2284. https://doi.org/10.1038/s41386-018-0093-x

Liu, J., Maurel, D., Etzol, S., Brabet, I., Ansanay, H., Pin, J.-P., Rondard, P., 2004. Molecular Determinants Involved in the Allosteric Control of Agonist Affinity in the GABA B Receptor by the GABA B2 Subunit. J. Biol. Chem. 279, 15824–15830. https://doi.org/10.1074/jbc.M313639200

Lloyd, K.G., Pilc, A., 1984. Chronic antidepressants and GABA synapses. Neuropharmacology 23, 841–842. https://doi.org/10.1016/0028-3908(84)90274-0

Lloyd, K.G., Thuret, F., Pilc, A., 1985. Upregulation of gamma-aminobutyric acid (GABA) B binding sites in rat frontal cortex: a common action of repeated administration of different classes of antidepressants and electroshock. J. Pharmacol. Exp. Ther. 235, 191–199.

Lodish, H.F. (Ed.), 2000. Molecular cell biology, 4th ed. ed. W.H. Freeman, New York.

Luckey, M., 2014. Membrane structural biology: with biochemical and biophysical foundations,

Second edition. ed. Cambridge University Press, Cambridge ; New York.

Margeta-Mitrovic, M., Jan, Y.N., Jan, L.Y., 2001. Ligand-induced signal transduction within heterodimeric GABAB receptor. Proc. Natl. Acad. Sci. 98, 14643–14648. https://doi.org/10.1073/pnas.251554798

Mark, P., Nilsson, L., 2001. Structure and Dynamics of the TIP3P, SPC, and SPC/E Water Models at 298 K. J. Phys. Chem. A 105, 9954–9960. https://doi.org/10.1021/jp003020w

Martínez-Archundia, M., Bello, M., Correa-Basurto, J., 2018. Design of Drugs by Filtering Through ADMET, Physicochemical and Ligand-Target Flexibility Properties, in: Mavromoustakos, T., Kellici, T.F. (Eds.), Rational Drug Design. Springer New York, New York, NY, pp. 403–416. https://doi.org/10.1007/978-1-4939-8630-9_24

Matthews, B.W., 1975. Comparison of the predicted and observed secondary structure of T4 phage lysozyme. Biochim. Biophys. Acta 405, 442–451.

McCammon, J.A., Gelin, B.R., Karplus, M., 1977. Dynamics of folded proteins. Nature 267, 585–590. https://doi.org/10.1038/267585a0

Misgeld, U., Bijak, M., Jarolimek, W., 1995. A physiological role for GABAB receptors and the effects of baclofen in the mammalian central nervous system. Prog. Neurobiol. 46, 423–462. https://doi.org/10.1016/0301-0082(95)00012-K

Miyano, K., Sudo, Y., Yokoyama, A., Hisaoka-Nakashima, K., Morioka, N., Takebayashi, M., Nakata, Y., Higami, Y., Uezono, Y., 2014. History of the G Protein–Coupled Receptor (GPCR) Assays From Traditional to a State-of-the-Art Biosensor Assay. J. Pharmacol. Sci. 126, 302–309. https://doi.org/10.1254/jphs.14R13CP

Mohs, R.C., Greig, N.H., 2017. Drug discovery and development: Role of basic biological research. Alzheimers Dement. Transl. Res. Clin. Interv. 3, 651–657. https://doi.org/10.1016/j.trci.2017.10.005

Møller, T.C., Moreno-Delgado, D., Pin, J.-P., Kniazeff, J., 2017. Class C G protein-coupled receptors: reviving old couples with new partners. Biophys. Rep. 3, 57–63. https://doi.org/10.1007/s41048-017-0036-9

Morris, G.M., Lim-Wilby, M., 2008. Molecular Docking, in: Kukol, A. (Ed.), Molecular Modeling of Proteins. Humana Press, Totowa, NJ, pp. 365–382. https://doi.org/10.1007/978-1-59745-177-2_19

Munk, C., Isberg, V., Mordalski, S., Harpsøe, K., Rataj, K., Hauser, A.S., Kolb, P., Bojarski, A.J., Vriend, G., Gloriam, D.E., 2016. GPCRdb: the G protein-coupled receptor database - an introduction: GPCRdb: the GPCR database. Br. J. Pharmacol. 173, 2195–2207. https://doi.org/10.1111/bph.13509

Muto, T., Tsuchiya, D., Morikawa, K., Jingami, H., 2007. Structures of the extracellular regions of the group II/III metabotropic glutamate receptors. Proc. Natl. Acad. Sci. 104, 3759–3764. https://doi.org/10.1073/pnas.0611577104

Mysinger, M.M., Carchia, M., Irwin, John.J., Shoichet, B.K., 2012. Directory of Useful Decoys, Enhanced (DUD-E): Better Ligands and Decoys for Better Benchmarking. J. Med. Chem. 55, 6582–

6594. https://doi.org/10.1021/jm300687e

Neves, S.R., 2002. G Protein Pathways. Science 296, 1636–1639.
https://doi.org/10.1126/science.1071550

Niciu, M.J., Kelmendi, B., Sanacora, G., 2012. Overview of glutamatergic neurotransmission in the
nervous system. Pharmacol. Biochem. Behav. 100, 656–664.
https://doi.org/10.1016/j.pbb.2011.08.008

Niswender, C.M., Conn, P.J., 2010. Metabotropic Glutamate Receptors: Physiology, Pharmacology,
and Disease. Annu. Rev. Pharmacol. Toxicol. 50, 295–322.
https://doi.org/10.1146/annurev.pharmtox.011008.145533

Nomura, R., Suzuki, Y., Kakizuka, A., Jingami, H., 2008. Direct Detection of the Interaction between
Recombinant Soluble Extracellular Regions in the Heterodimeric Metabotropic γ-Aminobutyric Acid
Receptor. J. Biol. Chem. 283, 4665–4673. https://doi.org/10.1074/jbc.M705202200

Ntie-Kang, F., 2013. An in silico evaluation of the ADMET profile of the StreptomeDB database.
SpringerPlus 2. https://doi.org/10.1186/2193-1801-2-353

Olofsson, L., Felekyan, S., Doumazane, E., Scholler, P., Fabre, L., Zwier, J.M., Rondard, P., Seidel,
C.A.M., Pin, J.-P., Margeat, E., 2014. Fine tuning of sub-millisecond conformational dynamics
controls metabotropic glutamate receptors agonist efficacy. Nat. Commun. 5.
https://doi.org/10.1038/ncomms6206

Overington, J.P., Al-Lazikani, B., Hopkins, A.L., 2006. How many drug targets are there? Nat. Rev.
Drug Discov. 5, 993–996. https://doi.org/10.1038/nrd2199

Paavola, K.J., Hall, R.A., 2012. Adhesion G Protein-Coupled Receptors: Signaling, Pharmacology,
and Mechanisms of Activation. Mol. Pharmacol. 82, 777–783.
https://doi.org/10.1124/mol.112.080309

Palczewski, K., Kumasaka, T., Hori, T., Behnke, C.A., Motoshima, H., Fox, B.A., Le Trong, I., Teller,
D.C., Okada, T., Stenkamp, R.E., Yamamoto, M., Miyano, M., 2000. Crystal structure of rhodopsin: A
G protein-coupled receptor. Science 289, 739–745.

Pándy-Szekeres, G., Munk, C., Tsonkov, T.M., Mordalski, S., Harpsøe, K., Hauser, A.S., Bojarski,
A.J., Gloriam, D.E., 2018. GPCRdb in 2018: adding GPCR structure models and ligands. Nucleic
Acids Res. 46, D440–D446. https://doi.org/10.1093/nar/gkx1109

Paquet, E., Viktor, H.L., 2015. Molecular Dynamics, Monte Carlo Simulations, and Langevin
Dynamics: A Computational Review. BioMed Res. Int. 2015, 1–18.
https://doi.org/10.1155/2015/183918

Patrick, G., 2017. An introduction to medicinal chemistry 6e. Oxford University Press, New York,
NY.

Pereda, A.E., 2014. Electrical synapses and their functional interactions with chemical synapses. Nat.
Rev. Neurosci. 15, 250–263. https://doi.org/10.1038/nrn3708

Periole, X., Marrink, S.-J., 2013. The Martini Coarse-Grained Force Field, in: Monticelli, L., Salonen, E. (Eds.), Biomolecular Simulations. Humana Press, Totowa, NJ, pp. 533–565. https://doi.org/10.1007/978-1-62703-017-5_20

Phase, 2017. Schrödinger Release 2017-4. Schrödinger, LLC, New York, NY.

Pilc, A., Nowak, G., 2005. GABA-ergic hypotheses of anxiety and depression: Focus on GABA-B receptor. Drugs Today 41, 755. https://doi.org/10.1358/dot.2005.41.11.904728

Pin, J.-P., Galvez, T., Prézeau, L., 2003. Evolution, structure, and activation mechanism of family 3/C G-protein-coupled receptors. Pharmacol. Ther. 98, 325–354. https://doi.org/10.1016/S0163-7258(03)00038-X

Pin, J.-P., Kniazeff, J., Binet, V., Liu, J., Maurel, D., Galvez, T., Duthey, B., Havlickova, M., Blahos, J., Prézeau, L., Rondard, P., 2004. Activation mechanism of the heterodimeric GABAB receptor. Biochem. Pharmacol. 68, 1565–1572. https://doi.org/10.1016/j.bcp.2004.06.035

Pizzo, R., O'Leary, O.F., Cryan, J.F., 2017. Elucidation of the neural circuits activated by a GABA B receptor positive modulator: Relevance to anxiety. Neuropharmacology. https://doi.org/10.1016/j.neuropharm.2017.07.021

Polishchuk, P.G., Madzhidov, T.I., Varnek, A., 2013. Estimation of the size of drug-like chemical space based on GDB-17 data. J. Comput. Aided Mol. Des. 27, 675–679. https://doi.org/10.1007/s10822-013-9672-4

Prime, 2017. Schrödinger Release 2017-4. Schrödinger, LLC, New York, NY.

Protein Preparation Wizard, 2017. Schrödinger Release 2017-4. Schrödinger, LLC, New York, NY.

Rang, H.P., Dale, M.M. (Eds.), 2012. Rang and Dale's pharmacology: additional online content: [student consult, activate at studentconsult.com, searchable full text online], 7. ed. ed, Student consult. Elsevier, Churchill Livingstone, Edinburgh.

Riccardi, D., Brown, E.M., 2010. Physiology and pathophysiology of the calcium-sensing receptor in the kidney. Am. J. Physiol.-Ren. Physiol. 298, F485–F499. https://doi.org/10.1152/ajprenal.00608.2009

Ripphausen, P., Nisius, B., Peltason, L., Bajorath, J., 2010. Quo Vadis, Virtual Screening? A Comprehensive Survey of Prospective Applications. J. Med. Chem. 53, 8461–8467. https://doi.org/10.1021/jm101020z

Rondard, P., Goudet, C., Kniazeff, J., Pin, J.-P., Prézeau, L., 2011. The complexity of their activation mechanism opens new possibilities for the modulation of mGlu and GABAB class C G protein-coupled receptors. Neuropharmacology 60, 82–92. https://doi.org/10.1016/j.neuropharm.2010.08.009

Rondard, P., Huang, S., Monnier, C., Tu, H., Blanchard, B., Oueslati, N., Malhaire, F., Li, Y., Trinquet, E., Labesse, G., Pin, J.-P., Liu, J., 2008. Functioning of the dimeric GABAB receptor extracellular domain revealed by glycan wedge scanning. EMBO J. 27, 1321–1332. https://doi.org/10.1038/emboj.2008.64

Salahudeen, M.S., Nishtala, P.S., 2017. An overview of pharmacodynamic modelling, ligand-binding approach and its application in clinical practice. Saudi Pharm. J. 25, 165–175. https://doi.org/10.1016/j.jsps.2016.07.002

Salam, N.K., Nuti, R., Sherman, W., 2009. Novel Method for Generating Structure-Based Pharmacophores Using Energetic Analysis. J. Chem. Inf. Model. 49, 2356–2368. https://doi.org/10.1021/ci900212v

Sansom, C.E., Smith, C.A., 1998. Computer applications in the biomolecular sciences. Part 1: molecular modelling. Biochem. Educ. 26, 103–110. https://doi.org/10.1016/S0307-4412(97)00155-6

Schrödinger, 2019. Qikprop User Manual (online) [WWW Document]. schrodinger.com.

Schrödinger Release 2019-3, 2019. . Schrödinger, LLC, New York, NY.

Seal, A., Yogeeswari, P., Sriram, D., Consortium, O., Wild, D.J., 2013. Enhanced ranking of PknB Inhibitors using data fusion methods. J. Cheminformatics 5, 2. https://doi.org/10.1186/1758-2946-5-2

Seamon, K.B., Padgett, W., Daly, J.W., 1981. Forskolin: unique diterpene activator of adenylate cyclase in membranes and in intact cells. Proc. Natl. Acad. Sci. 78, 3363–3367. https://doi.org/10.1073/pnas.78.6.3363

Sengmany, K., Gregory, K.J., 2016. Metabotropic glutamate receptor subtype 5: molecular pharmacology, allosteric modulation and stimulus bias: Molecular pharmacology of mGlu5. Br. J. Pharmacol. 173, 3001–3017. https://doi.org/10.1111/bph.13281

Shen, P.S., 2018. The 2017 Nobel Prize in Chemistry: cryo-EM comes of age. Anal. Bioanal. Chem. 410, 2053–2057. https://doi.org/10.1007/s00216-018-0899-8

Sherman, W., Day, T., Jacobson, M.P., Friesner, R.A., Farid, R., 2006. Novel Procedure for Modeling Ligand/Receptor Induced Fit Effects. J. Med. Chem. 49, 534–553. https://doi.org/10.1021/jm050540c

Shoichet, B.K., 2004. Virtual screening of chemical libraries. Nature 432, 862–865. https://doi.org/10.1038/nature03197

Skeberdis, V.A., Chevaleyre, V., Lau, C.G., Goldberg, J.H., Pettit, D.L., Suadicani, S.O., Lin, Y., Bennett, M.V.L., Yuste, R., Castillo, P.E., Zukin, R.S., 2006. Protein kinase A regulates calcium permeability of NMDA receptors. Nat. Neurosci. 9, 501–510. https://doi.org/10.1038/nn1664

Sliwoski, G., Kothiwale, S., Meiler, J., Lowe, E.W., 2014. Computational methods in drug discovery. Pharmacol. Rev. 66, 334–395. https://doi.org/10.1124/pr.112.007336

Small-Molecule Drug Discovery Suite 2018-4, n.d. . Schrödinger, LLC: New York, NY.

Smith, J.S., Lefkowitz, R.J., Rajagopal, S., 2018. Biased signalling: from simple switches to allosteric microprocessors. Nat. Rev. Drug Discov. 17, 243–260. https://doi.org/10.1038/nrd.2017.229

Strike version 2.2, 2015. Schrödinger Release 2015-3. Schrödinger, LLC, New York, NY.

Sturchler, E., Li, X., de Lourdes Ladino, M., Kaczanowska, K., Cameron, M., Griffin, P.R., Finn, M.G., Markou, A., McDonald, P., 2017. GABAB receptor allosteric modulators exhibit pathway-dependent and species-selective activity. Pharmacol. Res. Perspect. 5, e00288. https://doi.org/10.1002/prp2.288

Suzuki, N., Hajicek, N., Kozasa, T., 2009. Regulation and Physiological Functions of G12/13-Mediated Signaling Pathways. Neurosignals 17, 55–70. https://doi.org/10.1159/000186690

Sykes, D.A., Stoddart, L.A., Kilpatrick, L.E., Hill, S.J., 2019. Binding kinetics of ligands acting at GPCRs. Mol. Cell. Endocrinol. 485, 9–19. https://doi.org/10.1016/j.mce.2019.01.018

Syrovatkina, V., Alegre, K.O., Dey, R., Huang, X.-Y., 2016. Regulation, Signaling, and Physiological Functions of G-Proteins. J. Mol. Biol. 428, 3850–3868. https://doi.org/10.1016/j.jmb.2016.08.002

Terunuma, M., Pangalos, M.N., Moss, S.J., 2010. Functional modulation of GABAB receptors by protein kinases and receptor trafficking. Adv. Pharmacol. San Diego Calif 58, 113–122. https://doi.org/10.1016/S1054-3589(10)58005-0

Tribello, G.A., Bonomi, M., Branduardi, D., Camilloni, C., Bussi, G., 2014. PLUMED 2: New feathers for an old bird. Comput. Phys. Commun. 185, 604–613. https://doi.org/10.1016/j.cpc.2013.09.018

Tyacke, R.J., Lingford-Hughes, A., Reed, L.J., Nutt, D.J., 2010. GABAB Receptors in Addiction and Its Treatment, in: Advances in Pharmacology. Elsevier, pp. 373–396. https://doi.org/10.1016/S1054-3589(10)58014-1

Urwyler, S., Gjoni, T., Koljatic, J., Dupuis, D., 2005. Mechanisms of allosteric modulation at GABA receptors by CGP7930 and GS39783: effects on affinities and efficacies of orthosteric ligands with distinct intrinsic properties. Neuropharmacology 48, 343–353. https://doi.org/10.1016/j.neuropharm.2004.10.013

Vanommeslaeghe, K., Guvench, O., MacKerell, A.D., 2014. Molecular mechanics. Curr. Pharm. Des. 20, 3281–3292.

Varani, A.P., Aso, E., Moutinho, L.M., Maldonado, R., Balerio, G.N., 2014. Attenuation by baclofen of nicotine rewarding properties and nicotine withdrawal manifestations. Psychopharmacology (Berl.) 231, 3031–3040. https://doi.org/10.1007/s00213-014-3469-6

Varani, A.P., Pedrón, V.T., Aon, A.J., Höcht, C., Acosta, G.B., Bettler, B., Balerio, G.N., 2018. Nicotine-induced molecular alterations are modulated by GABAB receptor activity: GABAB receptors and nicotine. Addict. Biol. 23, 230–246. https://doi.org/10.1111/adb.12506

Veber, D.F., Johnson, S.R., Cheng, H.-Y., Smith, B.R., Ward, K.W., Kopple, K.D., 2002. Molecular properties that influence the oral bioavailability of drug candidates. J. Med. Chem. 45, 2615–2623.

Vernall, A.J., Hill, S.J., Kellam, B., 2014. The evolving small-molecule fluorescent-conjugate toolbox for Class A GPCRs: Fluorescent ligands for GPCRs. Br. J. Pharmacol. 171, 1073–1084. https://doi.org/10.1111/bph.12265

Vyas, V., Ukawala, R., Chintha, C., Ghate, M., 2012. Homology modeling a fast tool for drug discovery: Current perspectives. Indian J. Pharm. Sci. 74, 1. https://doi.org/10.4103/0250-474X.102537

Warszycki, D., Mordalski, S., Kristiansen, K., Kafel, R., Sylte, I., Chilmonczyk, Z., Bojarski, A.J., 2013. A linear combination of pharmacophore hypotheses as a new tool in search of new active compounds--an application for 5-HT1A receptor ligands. PloS One 8, e84510. https://doi.org/10.1371/journal.pone.0084510

Watson, H., 2015. Biological membranes. Essays Biochem. 59, 43–69. https://doi.org/10.1042/bse0590043

Weiss, D.R., Levitt, M., 2009. Can Morphing Methods Predict Intermediate Structures? J. Mol. Biol. 385, 665–674. https://doi.org/10.1016/j.jmb.2008.10.064

Wierońska, J.M., Pilc, A., 2019. Depression and schizophrenia viewed from the perspective of amino acidergic neurotransmission: Antipodes of psychiatric disorders. Pharmacol. Ther. 193, 75–82. https://doi.org/10.1016/j.pharmthera.2018.08.010

Willard, S.S., Koochekpour, S., 2013. Glutamate, Glutamate Receptors, and Downstream Signaling Pathways. Int. J. Biol. Sci. 9, 948–959. https://doi.org/10.7150/ijbs.6426

Wootten, D., Christopoulos, A., Marti-Solano, M., Babu, M.M., Sexton, P.M., 2018. Mechanisms of signalling and biased agonism in G protein-coupled receptors. Nat. Rev. Mol. Cell Biol. 19, 638–653. https://doi.org/10.1038/s41580-018-0049-3

Xue, L., Sun, Q., Zhao, H., Rovira, X., Gai, S., He, Q., Pin, J.-P., Liu, J., Rondard, P., 2019. Rearrangement of the transmembrane domain interfaces associated with the activation of a GPCR hetero-oligomer. Nat. Commun. 10. https://doi.org/10.1038/s41467-019-10834-5

Yan, A., Liang, H., Chong, Y., Nie, X., Yu, C., 2013. In-silico prediction of blood–brain barrier permeability. SAR QSAR Environ. Res. 24, 61–74. https://doi.org/10.1080/1062936X.2012.729224

Yusof, I., Segall, M.D., 2013. Considering the impact drug-like properties have on the chance of success. Drug Discov. Today 18, 659–666. https://doi.org/10.1016/j.drudis.2013.02.008

Zhang, R., Xie, X., 2012. Tools for GPCR drug discovery. Acta Pharmacol. Sin. 33, 372–384. https://doi.org/10.1038/aps.2011.173

Zhu, J., Lv, Y., Han, X., Xu, D., Han, W., 2017. Understanding the differences of the ligand binding/unbinding pathways between phosphorylated and non-phosphorylated ARH1 using molecular dynamics simulations. Sci. Rep. 7. https://doi.org/10.1038/s41598-017-12031-0

Paper I

In Silico Methods for the Discovery of Orthosteric GABAB Receptor Compounds

Linn M. Evenseth [1], Dawid Warszycki [2] , Andrzej J. Bojarski [2] , Mari Gabrielsen [1] and Ingebrigt Sylte [1,*]

[1] Molecular Pharmacology and Toxicology, Department of Medical Biology, Faculty of Health Sciences, UiT —The Arctic University of Norway, NO-9037 Tromsø, Norway; linn.evenseth@uit.no (L.M.E.); mari.gabrielsen@uit.no (M.G.)

[2] Department of Medicinal Chemistry, Institute of Pharmacology, Polish Academy of Science, Smetna 12, 31-343 Kraków, Poland; warszyc@if-pan.krakow.pl (D.W.); bojarski@if-pan.krakow.pl (A.J.B.)

[*] Correspondence: ingebrigt.sylte@uit.no; Tel.: +47-77-64-4705

Abstract: The GABAB receptor (GABAB-R) is a heterodimeric class C G protein-coupled receptor comprised of the GABA$_{B1a/b}$ and GABA$_{B2}$ subunits. The endogenous orthosteric agonist γ-amino-butyric acid (GABA) binds within the extracellular Venus flytrap (VFT) domain of the GABA$_{B1a/b}$ subunit. The receptor is associated with numerous neurological and neuropsychiatric disorders including learning and memory deficits, depression and anxiety, addiction and epilepsy, and is an interesting target for new drug development. Ligand- and structure-based virtual screening (VS) are used to identify hits in preclinical drug discovery. In the present study, we have evaluated classical ligand-based in silico methods, fingerprinting and pharmacophore mapping and structure-based in silico methods, structure-based pharmacophores, docking and scoring, and linear interaction approximation (LIA) for their aptitude to identify orthosteric GABAB-R compounds. Our results show that the limited number of active compounds and their high structural similarity complicate the use of ligand-based methods. However, by combining ligand-based methods with different structure-based methods active compounds were identified in front of DUDE-E decoys and the number of false positives was reduced, indicating that novel orthosteric GABAB-R compounds may be identified by a combination of ligand-based and structure-based in silico methods.

Keywords: GABAB receptor; orthosteric binding site; virtual screening; ligand-based screening; structure-based screening

1. Introduction

Virtual screening (VS) is the application of knowledge-based computational methods to identify novel compounds [1]. VS methods are divided into two major categories: ligand-based drug discovery (LBDD) methods and structure-based drug discovery (SBDD) methods [2]. The LBDD methods use information about known ligands (e.g., structure, target affinity/activity and physico-chemical properties) to search for new compounds, while the SBDD methods use structural information about the drug target and ligand-target complexes. LBDD and SBDD are time- and cost-effective methods that either alone or in combination have led to the discovery of novel compounds towards assorted targets, including the α1a adrenergic receptor, the serotonin transporter and the 5-HT$_7$ receptor [3–6].

γ-Aminobutyric acid (GABA) is the main inhibitory neurotransmitter in the mammalian central nervous system (CNS). GABA exerts its physiological effects by binding to the ionotropic GABA$_A$ and GABA$_C$ receptors and the metabotropic GABAB receptor (GABAB-R) [7]. The GABAB-R is an obligate heterodimeric assembly, comprised of the GABA$_{B1a/b}$ and GABA$_{B2}$ subunits, that belongs to

class C of G-protein coupled receptors (GPCRs) [8,9]. Each subunit contains an extracellular domain called the "Venus flytrap" (VFT) domain, and a heptahelical transmembrane (7TM) domain. The VFTs have a bi-lobular architecture with two distinct domains, Lobe 1 (LB1) and Lobe 2 (LB2), which come into close contact upon agonist binding, hence the name VFT [9]. The GABA$_{B1a/b}$ is responsible for the ligand binding through the orthosteric site located in the VFT. The GABA$_{B2}$ VFT does not bind to any known ligands, as shown by radiolabelled ligand binding and mutagenesis studies, but is important for the activation as the ectodomain interacts with the GABA$_{B1a/b}$ ectodomain to enhance agonist affinity [10,11]. The transmembrane part of the GABA$_{B2}$ subunit hosts an allosteric binding site and is responsible for G-protein coupling [12–14]. The three-dimensional (3D) structure of the entire GABA$_B$-R is not known, however, eight X-ray crystal structures of the VFTs co-crystalized with different agonists or antagonists and one of the VFT apo-form have been published [9].

The GABA$_B$-R is linked to a variety of neurological and neuropsychiatric disorders including memory and learning deficits, addiction, epilepsy, anxiety and depression, and is an interesting target for drug intervention [15–18]. However, at present, the agonist baclofen (β-(4-chloro-phenyl)GABA) is the only marketed drug targeting the GABA$_B$-R. Baclofen is used as a muscle relaxant and antispastic agent to treat muscle spasticity and other muscle symptoms caused by e.g., multiple sclerosis [19,20]. A major drawback with baclofen is the side effects which include dizziness, nausea, insomnia, and hallucinations caused by abrupt withdrawal [21]. Animal models have also linked baclofen and other GABA$_B$-R agonists to anti-addictive effects towards nicotine, cocaine and alcohol, however, clinical studies of baclofen in alcohol abuse have shown conflicting results [22–25]. Animal cognition models such as the swim-test and plus-maze test, have indicated that baclofen also has anxiolytic effects [18,26,27]. GABA$_B$-R antagonists show antidepressant effects in different variants of the swim test [18,28], while baclofen show worsening of depression symptoms [29,30]. The newly discovered concept of ligand bias (ligand functional selectivity) emphasises the benefit of discovering new compounds that promote beneficial signalling pathways, while at the same time blocking potential deleterious GABA$_B$-R pathways. New orthosteric compounds may expand the knowledge about the physiological importance and the activation mechanism of the receptor [31,32], and be interesting as drug or probe candidates, either alone or in combination with allosteric modulators.

At present, fewer than 15 antagonists and approximately 40 agonists are classified as active GABA$_B$-R compounds [33]. Most of them are analogues of GABA or baclofen. Their low structural diversity may indicate that the conformational space of orthosteric GABA$_B$-R compounds is not fully explored. In the present study, we have evaluated the classical LBDD methods, chemical fingerprinting and pharmacophore modelling, and the SBDD methods docking and scoring, structure-based pharmacophores (e-Pharmacophores) and linear interaction approximation (LIA) models for their predicative ability in VS. The aim was to identify a practical VS workflow for identification of orthosteric GABA$_B$-R compounds. Our results suggested that large structural similarities between known compounds limits the feasibility of ligand-based in silico methods, but by combining ligand-based methods with structure-based in silico methods, novel orthosteric GABA$_B$-R compounds may be identified, and the number of false positives may be reduced.

2. Results

2.1. Compound Datasets

All ChEMBL (version 24_1, EMBL-EBI, Hinxton, Cambridgeshire, United Kingdom) compounds tested for GABA$_B$-R activity were downloaded and used to generate two datasets, one with high affinity/activity compounds hereafter called active compounds, and one with low affinity/activity and inactive compounds, hereafter called inactive compounds. Threshold values for being including in the set of active compounds were: IC$_{50}$ < 4100 nM, K$_i$ < 1500 nM, EC$_{50}$ < 25 μM, or fold changes/inhibition indicating higher activity than GABA, and that the compound has been tested in assays of cloned or native human or rat GABA$_B$-R. The IC$_{50}$ value is defined as the half maximum inhibitory concentration,

while the EC$_{50}$ value is the concentration of a compound needed to produce half maximal response [34]. In total, 217 entities were downloaded, but after removal of duplicates the dataset of active compounds contained 55 compounds (13 antagonists and 42 agonists) (Supplementary Material, Table S1), while the inactive contained 97 compounds (Supplementary Material, Table S2).

The active compounds were structurally clustered into four clusters of agonists (cluster 2: 12 compounds, cluster 4: nine compounds, cluster 5: four compounds and cluster 6: 13 compounds), and one of antagonists (cluster 3: 11 compounds). In addition, two antagonists and four agonists not fitting into other clusters were grouped together in cluster 1. In the following, these compounds are termed outliers. A dataset of DUD-E decoys (assumed non-binders) were generated from the structure of the active compounds. Fifty DUD-E decoys were generated per compound, giving a total of 300 DUD-E decoys for the cluster of outliers (cluster 1), 1900 DUD-E decoys for agonists (cluster 2: 600, cluster 4: 450, cluster 5: 200 and cluster 6: 650) and 550 DUD-E decoys for antagonists (cluster 3).

2.2. Fingerprinting

For each cluster of active, molprint2D (M2D) chemical fingerprints were used to generate modal (average) fingerprints that were used to search the active/DUD-E decoy datasets. The Tanimoto similarity metric method was used to evaluate the results. The evaluation showed that the fingerprinting approach was not able to rank active compounds in front of DUD-E decoys (results not shown).

2.3. Development and Evaluation of Ligand-Based Pharmacophore Models

Pharmacophore models were evaluated by mapping the compound datasets of active, inactive and DUD-E decoys to the hypotheses. One pharmacophore model per cluster was selected based on the Matthews correlation coefficient (MCC) and the "Goodness of Hits" score (GH). All pharmacophore hypotheses contained three to five features (Table 1, Figure 1). The statistical evaluation displayed variation in the quality of the generated pharmacophores with a range of the MCC and GH values from 0.20 to 0.95 (Table 1). The model giving lowest GH and MCC scores was generated from the structural cluster containing outliers. In total, 23 of 650 DUD-E decoys generated for GABA$_B$-R antagonists and 115 of 2100 DUD-E decoys generated for agonists were found to be false positives by the pharmacophore mapping. Mapping all 55 actives to the agonist-based models showed that the models not only recognized agonists, but also some of the antagonists. In addition, all agonist based models identified agonists in other clusters. The more general models with few features, like those of cluster 4 and 6, identified most compounds (Table 1). The antagonist-based model identified only antagonists. Mapping of the 97 inactive compounds showed that the pharmacophore models recognized 61 of the compounds in the inactive dataset.

Table 1. The pharmacophore hypotheses with the number of active compounds (#Actives) in the cluster, the number of true positives (TP), false negatives (FN), false positives (FP) and true negatives (TN) obtained after mapping actives and DUD-E decoys to the pharmacophore model. These values were used to calculate the Matthews correlation coefficient (MC) and Goodness of Hit (GH). AR: number of actives retrieved after mapping all active compounds to the models. Abbreviations; Ant: antagonists, Ago: agonists. Feature abbreviations; hydrophobic feature: H, hydrogen bond acceptor feature: A, hydrogen bond donor feature: D, aromatic feature: R, positively charged feature: P, and negatively charged feature: N.

Cluster	Hypothesis	#Actives	Actives		Decoys		MCC	GH	AR	
			TP	FN	FP	TN			Ant	Ago
1	AHHHR *	6	3	3	21	279	0.22	0.20	1	2
2	ADN	12	7	5	30	270	0.31	0.27	11	11
3	ANPR	11	9	2	2	548	0.82	0.82	9	0
4	NPR	9	9	0	2	448	0.90	0.95	12	13
5	DDDHR	4	4	0	55	145	0.22	0.22	3	11
6	DDDN	13	13	0	9	641	0.76	0.68	7	40

*: Outliers (both agonists and antagonists).

Cluster 1

	H1	H2	H3	R
A	3.26	3.36	4.68	3.98
H1		2.14	5.3	4.1
H2			5.13	5.13
H3				8.23

Cluster 2

	D	N
A	3.9	3.12
D		3.23

Cluster 3

	N	P	R
A	4.38	2.92	4.68
N		4.53	5.3
P			3.83

Cluster 4

	P6	R7
N5	5.12	4.47
P6		4.04

Cluster 5

	D2	D3	H	R
D1	1.64	1.64	7.34	4.80
D2		1.64	5.80	3.32
D3			7.14	4.42
H				3.12

Cluster 6

	D2	D3	N
D1	3.26	3.36	4.68
D2		1.64	5.88
D3			6.04
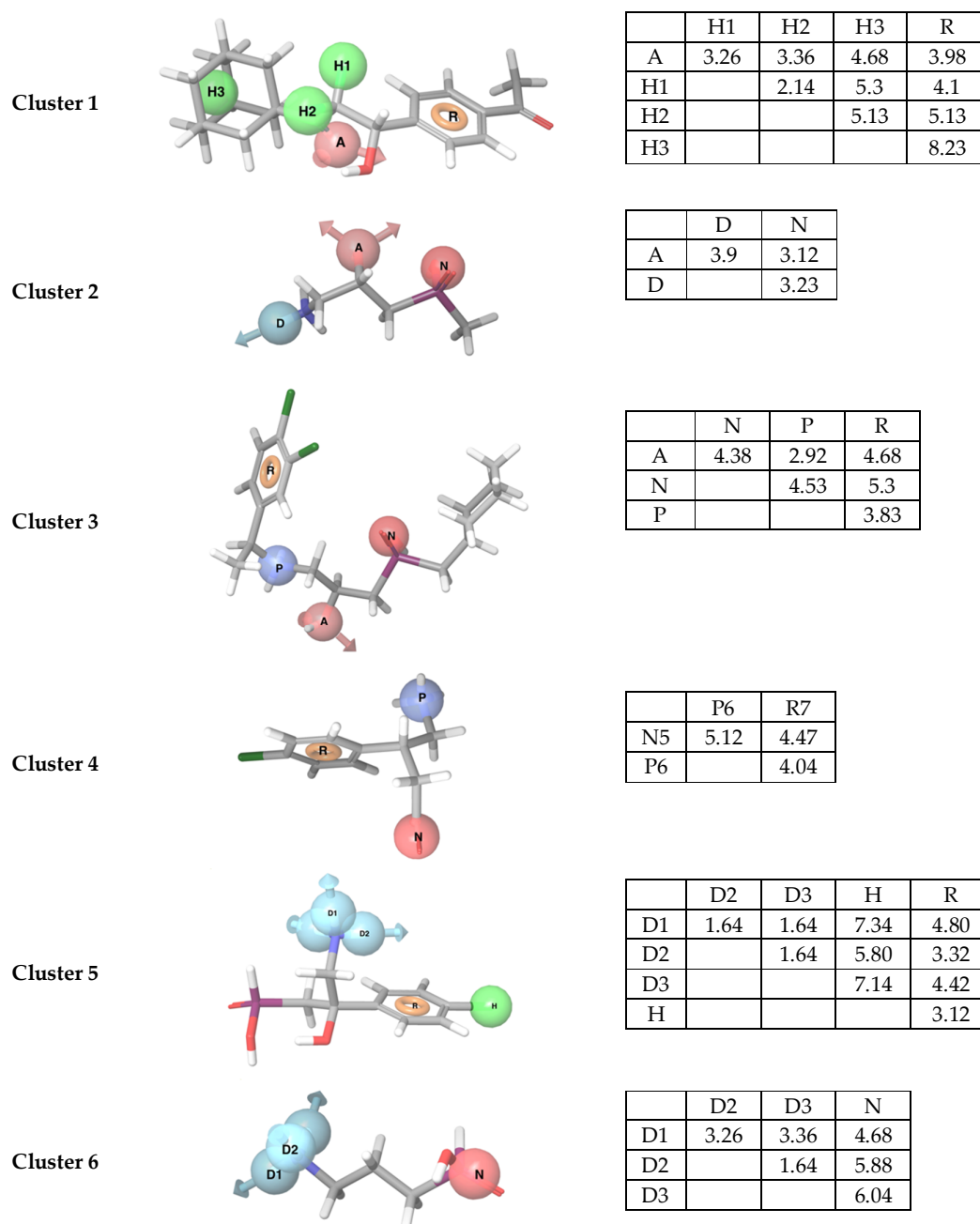
Figure 1. Pharmacophore models obtained from each cluster with the matrix of distances (Å) between features. The best mapped compound for cluster 1–6, CHEMBL2322934, CHEMBL113348, CGP54626, baclofen, 27 and CHEMBL112203, respectively, are displayed. Feature abbreviations; hydrophobic feature: H, hydrogen bond acceptor feature: A, hydrogen bond donor feature: D, aromatic feature: R, positively charged feature; P, and negatively charged feature: N.

2.4. Development and Evaluation of Structure-Based e-Pharmacophore Models

Structure-based pharmacophore models (e-Pharmacophores) for an agonist-induced VFT conformation (Figure 2A) and antagonist-induced VFT conformation (Figure 2B) were generated using the Phase program [35]. A library of 441 unique fragments were mapped to the binding pocket of the antagonist-induced (inactive) VFT conformation (PDB ID: 4MR7) and the agonist-induced (active) VFT conformation (PDB ID: 4MS4).

Mapping the fragment library in the inactive VFT conformation identified an aromatic feature in LB2 close to hydrophobic- and aromatic residues (Tyr250 and Trp278), together with a hydrogen

bond donor and a hydrogen bond acceptor feature (Figures 2B and 3). In LB1, one hydrogen bond donor, one hydrogen bond acceptor and one negative charged feature were identified. These features were connected to Cys129 and the serine residues located in position 130, 131, 152, 153 and 154. Some of these serine residues were involved in both agonist and antagonist binding (Figures 2 and 3) as described by Geng et al. [9].

The e-Pharmacophore features in the agonist-induced VFT were clustered closer together than those of the antagonist-induced, with shorter distances between features (Figure 2). An aromatic group was located close to the Tyr279 and Trp278 in LB2 and Tyr250 in LB2. A hydrophobic feature was located in LB2 in close proximity to the hydrophobic part with aromatic residues almost buried inside the VFT. A hydrogen bond donor was also located in the cleft between LB1 and LB2, almost at the opening of the VFT. Another aromatic ring was located between LB1 and LB2 in close proximity to Trp278, Trp65 and His170. One hydrogen bond donor and one acceptor were in LB1 close to the Ser152 and Ser153 as for the inactive VFT conformation (Figures 2 and 3).

Mapping the datasets of active compounds and DUD-E decoys to the e-Pharmacophore models showed that the e-Pharmacophore features were not selective for active compounds. In the antagonist-induced conformation four of total 13 unique antagonists and 602 DUD-E decoys were mapped, while in the agonist-induced conformation only nine out 42 agonists and 1000 DUD-E decoys (the maximum number) were mapped.
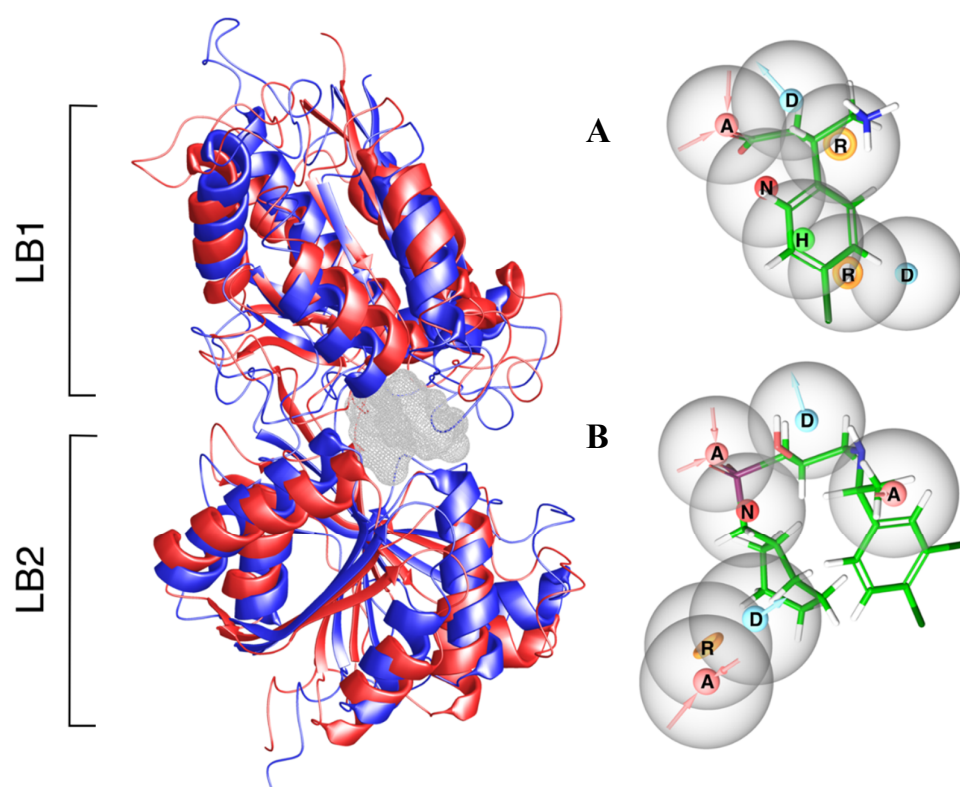
Figure 2. The X-ray crystal structure of the GABA_B-R VFT superimposed in the active (blue) and inactive (red) conformation with the binding pocket cavity showed in grey mesh. (**A**) The e-Pharmacophore of the agonist-induced active VFT conformation displayed with baclofen (**B**) The e-Pharmacophore of the inactive antagonist-induced VFT conformation with the antagonist CGP54626. Both e-Pharmacophores are shown in the same view corresponding to their orientation in the binding pocket cavity (left) with LB1 up and LB2 down. Feature abbreviations; hydrophobic feature: H, hydrogen bond acceptor feature: A, hydrogen bond donor feature: D, aromatic feature: R, positively charged feature: P, and negatively charged feature: N.

2.5. Analysis of the Docking Results

2.5.1. Docking of Active GABA$_B$-R Compounds

The dataset of 55 GABA$_B$-R active compounds were docked in both agonist (PDB ID: 4MS4) and antagonist (PDB ID: 4MR7) induced VFT conformation. The Cα Root Mean Square deviation (RMSD) between these conformations was 7.0 Å, with largest differences in loop regions. The overall RMSD of residues within 5 Å of the co-crystalized ligands was 2.1 Å. Superimposition showed that the active conformation had a more closed VFT than the inactive conformation (Figure 2).

The average docking score of the 42 agonists in the agonist-induced conformation was −8.3 kcal/mol. The best score was −11.2 kcal/mol, while the poorest was −5.7 kcal/mol. Docking antagonists into the agonist-induced VFT gave an average docking score of −5.9 kcal/mol, and with poses inconsistent with X-ray structure complexes. The average docking score for the 13 antagonists in the antagonist-induced VFT was −7.1 kcal/mol, where the best score was −8 kcal/mol and the poorest −5.6 kcal/mol. Docking of the agonists into the antagonist-induced VFT gave an average docking score of −6.4 kcal/mol.

Ser130 and Ser153 interacted with all 55 active compounds, independent of intrinsic activity. The agonists were fully buried within the receptor interior, inaccessible to solvent, thereby increasing the number of interactions between the agonists and the receptor and stabilizing the closed VFT conformation. As known agonists and most antagonists are analogues of GABA or baclofen, all ligands selected as cluster representatives showed similar ligand-interaction patterns (Figure 3). The LB1 residues Ser130 and Ser153 formed hydrogen bonds with a carboxylic acid moiety present in all agonists and antagonists. The LB1 residue Tyr65 and the LB2 residue Tyr250 stabilized the agonists by forming π-stacks or π-cation interactions, while Glu349 formed a salt bridge or ionic interaction with the amine moiety present in the agonists (Figure 3). The LB2 residue Trp278 formed a π-cation interaction with the ligands selected from three of four agonist clusters. Interactions between antagonists and hydrophobic residues in LB2 such as Trp278 and Tyr250 were observed for the highest affinity antagonists. The GABA$_B$-R antagonists are bigger and more bulky than agonists and will most likely prohibit the VFT closing as previously described by Geng et al. [9].

The average docking scores of known agonists and antagonists (dataset of active compounds) were used as threshold values for evaluating the docking of inactive compounds and false positive DUD-E decoys from the pharmacophore mapping.

2.5.2. Docking of Inactive GABA$_B$-R Compounds

Docking the dataset of 97 inactive GABA$_R$-R compounds (Supplementary, Table S2) showed that 79 of 97 compounds docked into the agonist-induced VFT, while all of them could dock into the inactive antagonist-induced conformation. In total, 13 compounds scored better than the threshold for agonists (average score of the 42 agonists) in the agonist-induced conformation. The compounds scoring higher than threshold are baclofen analogues containing an aromatic ring with a halogen and an alkyl chain with amino and carboxylic end groups. In total, 10 from the set of inactive compounds scored better than the threshold for antagonists (average score of the 13 antagonists) in the open inactive antagonist-induced VFT conformation.

2.5.3. Docking of False Positive Compounds from the Ligand-Based Pharmacophore Mapping

The false positive DUD-E decoys from the pharmacophore mapping were docked into the X-ray crystal structures in order to reveal if a succeeding docking procedure could reduce the number of false positives in a VS campaign. Twenty-three of the 650 DUD-E decoys generated from antagonists were identified as false positives by pharmacophore mapping. All of them scored worse than the threshold value for known antagonists (−7.1 kcal/mol), and 11 scored better than the poorest scored known antagonist (−5.6 kcal/mol). As the average docking score was used as the threshold, none was applied for further investigation by LIA models.
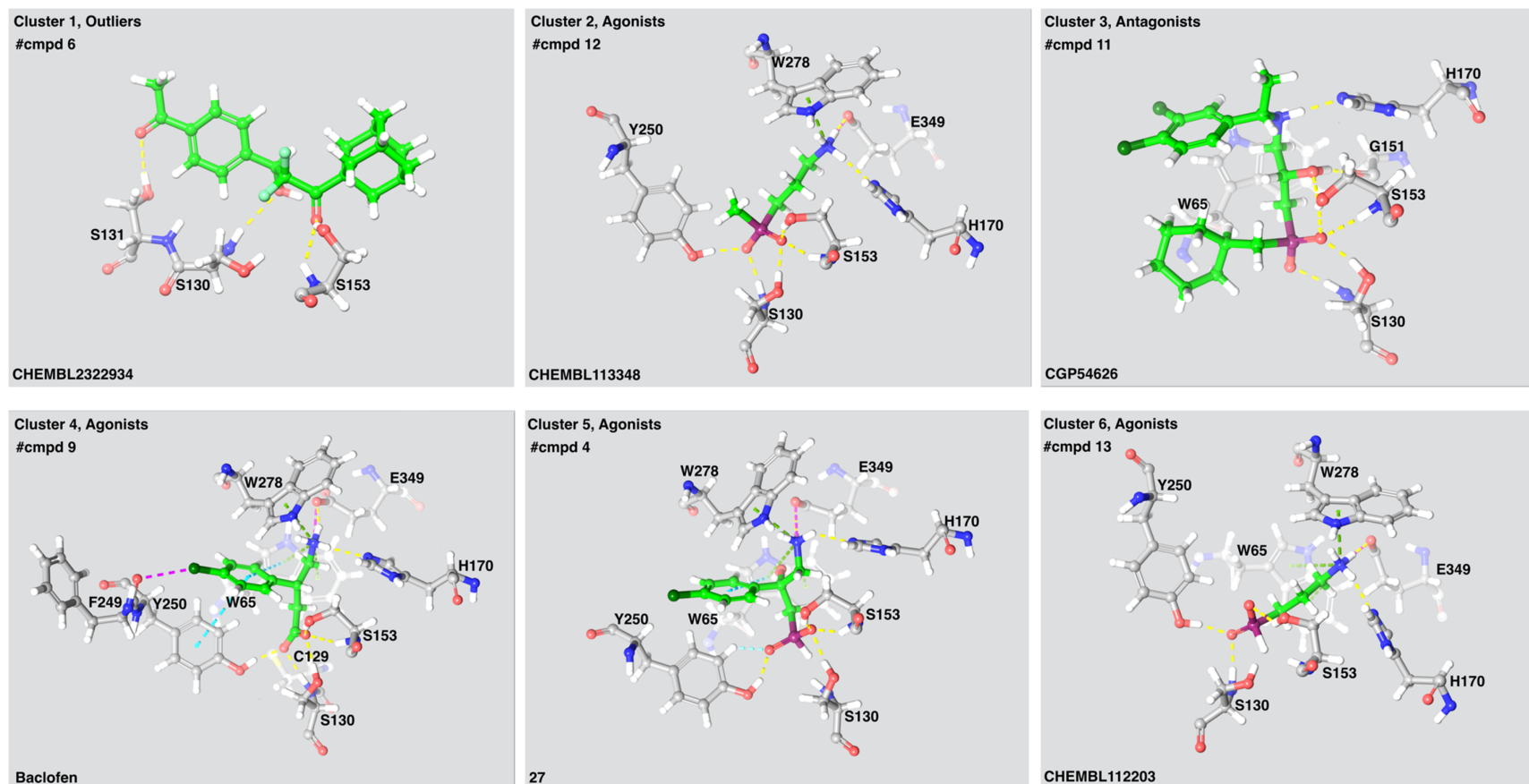
Figure 3. The ligand-receptor interactions of a selected compound from each cluster. Compound name is indicated in the lower left corner of each panel. The number of compounds (#cmpds) in each cluster and the intrinsic activity of the compounds is indicated. Cluster 1 consist of two antagonists and four agonists. Yellow lines: hydrogen bonds, green lines: Pi-cation interactions, Cyan lines: salt bridges, light blue lines: aromatic hydrogen bonds, magenta—halogen bond.

In total 116 DUD-E decoys generated from agonists were found to be false positive after pharmacophore mapping. Of these, five had a docking score better than the agonist threshold (−8.0 kcal/mol) and 72 out of the 116 gave a better score than the poorest scored agonist (−5.7 kcal/mol). The five compounds with docking score better than threshold were studied in the agonist LIA model to evaluate if the LIA method could identify the compounds as theoretically inactive DUD-E decoys.

2.6. Generation and Evaluation of LIA Models

The Liaison software in combination with Strike included in the Schrödinger package [36,37] were used for generating linear interaction approximation (LIA) models of agonists and antagonists and predicting ligand-receptor affinities using the LIA models. A training set of 11 agonists were used to construct the agonist LIA model, while a training set of eight antagonists were used to generate the antagonist LIA model. The models were evaluated by true positives from the pharmacophore mapping, but excluding those included in the training sets.

The LIA model generated for antagonists gave a R^2 value of 0.98 indicating that the predicted pIC_{50} values highly correlate to the fitted regression line of the experimental pIC_{50} values. The standard deviation was 0.41 with a P-value of 0.0044 (Table 2 and Figure 4). The LIA model generated for agonists gave a R^2 value of 0.61, which indicates that the predicted pIC_{50} values correlate to the fitted regression line of the experimental pIC_{50} values. The standard deviation was calculated to be 0.32 with a *p*-value of 0.074 (Table 2), and applying the LIA model to predict the pIC_{50} values of the true positive from the pharmacophore screening, gave less accurate results for agonists then for antagonists (Figure 4).

The agonist LIA model was applied to the five false positive DUD-E decoys from docking. Only one out of the false positives had a predicted pIC_{50} value < 5. Five is normally considered as the threshold pIC_{50} value for activity, and the agonist LIA model could therefore identify only one of the five compounds as a false positive.

Table 2. The statistical values and LIA parameters (α, β and γ) of the LIA models for agonists and antagonists.

LIA Model	R^2	Standard Deviation	p	α	β	γ
Agonist	0.61	0.322	0.074	−0.015	−0.0012	0.34
Antagonist	0.98	0.41	0.00445	−0.1707	0.0073	−0.842
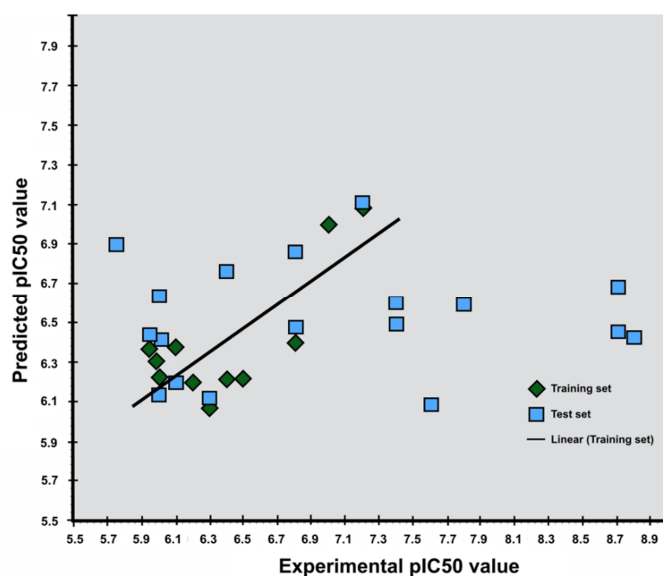
Figure 4. *Cont.*
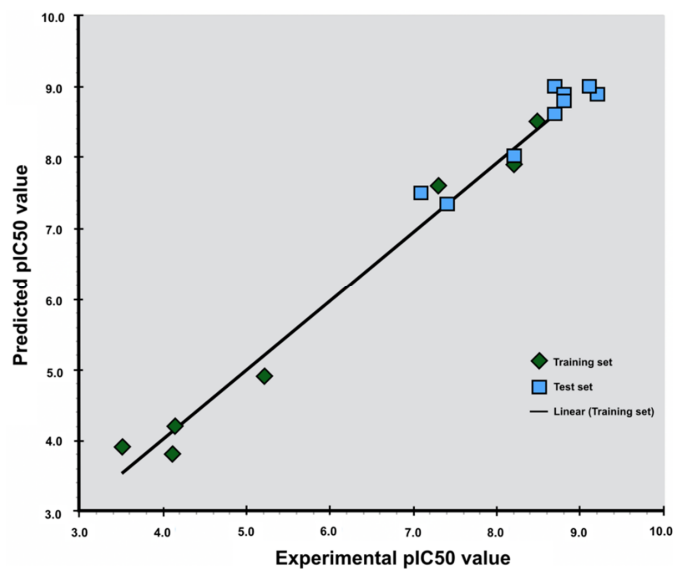
Figure 4. Scatter diagram of experimental and predicted pIC$_{50}$ values using the LIA method for agonists (**top**) and antagonists (**below**). The green squares are the ligands of the training set used to generate the parameters for predicting pIC$_{50}$ value of the ligands of the test set (blue squares).

3. Discussion

The GABA$_B$-R has a large potential as a target for new drugs. The number of known compounds is limited and most of them are analogues of the endogenous compound GABA and the therapeutically used agonist baclofen. Known compounds represent a quite small conformational space that complicates the understanding of molecular descriptors contributing to differences in affinity and intrinsic activity, and it is a challenge to identify new and improved orthosteric GABA$_B$-R compounds.

Our dataset of active compounds consists of compounds from experimental studies using different assay conditions (Supplementary Material, Table S1), which is a challenge for the robustness of the dataset since binding data from different assays are not necessary directly comparable. However, in order to get an acceptable number of compounds for the ligand-based approaches it was necessary to include compounds that had been evaluated using different experimental procedures. We used threshold values for experimental activity to discriminate between active and inactive compound datasets in order to reduce the influence of low affinity compounds on our in silico models. The dataset of inactive compounds therefore contained not only inactive compounds, but also compounds with low GABA$_B$-R activity. The compounds with highest affinity in the set of inactive compounds were four antagonists also used to generate LIA models (Supplementary Material, Table S1). Other low affinity/activity compounds in the set of inactive compounds had activity values far below these antagonists. The low affinity compounds are also structural analogues of GABA and baclofen, which complicates the present study since the datasets of active and inactive compounds both contains GABA and baclofen analogues. Discriminating between the active and inactive datasets by the LBDD and SBDD in silico methods in the present study is therefore challenging.

3.1. Ligand-Based Screening

3.1.1. Fingerprinting, Clustering and Modal Fingerprints

Average fingerprints for each cluster failed to recognise the compounds from which the fingerprints were generated in front of active compounds from other clusters, and in addition, they did not discriminate between actives and DUD-E decoys. This was not a surprise due to the structural similarities between clusters. Selecting more structurally divergent compounds was not possible.

Using fingerprinting alone in a VS campaign for new orthosteric compounds would therefore most likely not identify novel GABA$_B$-R compounds.

3.1.2. Ligand-Based Pharmacophore Modelling

One pharmacophore hypothesis per cluster was selected after statistical evaluation (Table 1). Ideally, a higher number of pharmacophores would be preferable for screening to account for structural diversity, but this was not possible due to structural similarities between the clusters. The pharmacophores for cluster 1, 2 and 5 gave poor discrimination between actives and DUD-E decoys, and identified many false positive compounds. In these models, the hypothesis composition was very general with repetitive features able to align with multiple compound structures. Low discrimination and retrieval of many false positives is not necessarily negative in a VS workflow, as also these models could contribute to discovery of new structural scaffolds.

A pharmacophore model of only three features can be problematic as several compounds may fit to the model, and the models may select many false positives during VS. The GABA$_B$-R agonists are small with few functional groups, which gives few pharmacophore features in the hypothesis. Changing the intersection distance constraints from 2 Å to 1.5 Å (for cluster 5 and 6) gave demanding hypotheses, i.e., an amine group with two hydrogen bond donating features, whereas the default intersection distance (2 Å) would generate only one hydrogen bond donor or preferably a positive charged site, as seen for two of the clusters. A main purpose of generating cluster-based pharmacophore models was to increase the possibility of retrieving new chemotypes. Decreasing the intersection distance to avoid repetitive feature composition as most of the actives contains a positive- and a negative charged group in the same positions, could also contribute to new chemotypes.

Known antagonists are larger than agonists, and may give a higher number of features in pharmacophores than agonists. However, there are only 13 known high affinity antagonists for the GABA$_B$-R. Of these, 11 were grouped into the same structural cluster (cluster 3) when applying the similarity metric and thereby only one pharmacophore model was generated. In a VS approach this hypothesis would be considered as accurate due to selectivity towards active ligands, and it is not too strict in terms of feature composition.

Mapping the inactive set of compounds to the pharmacophores also confirms the high structural similarity between the active and inactive compound datasets (Supplementary, Tables S1 and S2) as 61 out of the 97 could be mapped to the models.

3.2. Structure-Based Screening

3.2.1. Structure-Based e-Pharmacophore Models

E-Pharmacophores can be applied for VS and compound optimization (e.g., hit-to-lead and lead optimization). Using fragments that cover a wide range of functional groups to map the binding pocket gives new insight into the properties of the binding pocket. This knowledge can be used to guide ligand growing into areas of the pocket where specific ligand features are beneficial, as suggested for the areas discovered in the inactive VFT structure. This possibility can be more restricted when applying active ligands for e-Pharmacophore development, especially if the information about active ligands is limited, as for the GABA$_B$-R.

The antagonist-based e-Pharmacophore identified an aromatic feature in the LB2 moiety close to Tyr250 and Tyr278. In both the X-ray complexes and our docking studies, interactions are seen only for high affinity antagonists at this site [9], indicating that this feature is important for high affinity antagonist binding. In addition, both a hydrogen bond donor and a hydrogen bond acceptor feature located in this area were unexplored in our docking studies, despite being within the generated grid map (Figure 2). These sites could be further explored by growing antagonists anchored in LB1 towards these points using fragments complementary to the discovered features. As described, amino acids in LB1 are essential anchoring points for antagonists and the features located in this site were not

unexpected. In the LB1, a negatively charged feature, a hydrogen donor and one hydrogen bonding accepting feature were identified which represents serine residues that are necessary for both agonist and antagonist binding. None of the identified features in the agonist-induced active VFT conformation revealed any areas not already identified in our docking studies.

3.2.2. Docking

Visual inspection of the GABA$_B$-R VFT co-crystalized with agonists or antagonists showed that most of the α-acid groups formed interactions with residues in LB1 such as His170, Trp65, Ser130 and Glu349. Amino acid located in LB2 such as Tyr250 and Trp278 interact with the agonists in all complexes. Trp65 forms van der Waals interactions with all antagonists. An interesting observation was a ~180° flip of Trp278 in the structure co-crystalized with baclofen compared with the other agonist bound VFT 3D structures [9]. This flip is probably necessary for stabilizing the aromatic ring of baclofen. Visual inspection of selected inactive and low affinity compounds that scored better than threshold in both receptor conformations showed similar binding patterns as the active compounds, which also was expected due to structural similarities.

None of the 23 false positive antagonist-like DUD-E decoys from the pharmacophore mapping scored better than the average score of active antagonists when docking into the antagonist-induced conformation. In the agonist-induced VFT, the number of false positive agonist-like DUD-E decoys was reduced from 116 to five when using the average score of active agonists as threshold. This indicates that using average docking scores of active compounds as a threshold in combined ligand- and structure-based VS for orthosteric GABA$_B$-R compounds may have filtered out most of the false positives from the pharmacophore mapping. Identification of ligands with high affinity is desirable and to ensure fulfilling this criterion, the threshold for evaluating docking pose should be set to the average value instead of the value of the poorest scored active ligand in a VS campaign. By using the average value as threshold, it is of course a possibility of overlooking putative compounds, but most probably high affinity compounds would be identified. Using average docking scores may also account for the inaccuracy obtained by assuming similar activity of all generated enantiomers of a compound when the active form(s) is/are not known (Section 4.1).

Only two of nine available VFT structures were used in our docking. Ideally, the ligands should have been docked into multiple VFT conformations in order to account for the structural flexibility of the binding process [38]. However, the available X-ray crystal structures of the VFT are very similar. The RMSD between the binding site residues of the agonist bound VFTs is 0.26 Å, while the corresponding average value between six antagonists' bound is 0.27 Å. The overall Cα-RMSD between agonist-induced VFTs was 2 Å, while corresponding RMSDs between antagonist-induced VFTs were in the range of 0.75 to 2 Å. Visual investigation showed that the main differences were in regions other than the binding pocket, and available VFT X-ray crystal structures were therefore not encountered as conformational distinct.

The necessity of docking as a step in a VS protocol for identifying GABA$_B$-R compounds is clearly shown by the present study, but also the difficulty to differentiate between very similar compounds as shown by the docking of the false positives from the ligand-based pharmacophore screening. Ligand-based methods are more time- and cost-effective than docking and scoring, and in VS for new GABA$_B$-R compounds, ligand-based methods may remove some compounds in the library that definitely do not bind, before a docking step reduces the number of remaining false positives.

3.3. Generation and Evaluation of LIA Models

The methodology for predicting ligand-protein free energies by comparing the bound complex to the free ligand-receptor state using an explicit-solvent for building a model to predict/correlate binding free energies, was first suggested by Åqvist [39,40]. Their approach is computationally demanding as it uses molecular dynamic simulations with an explicit water model for sampling conformations. Using this approach for screening of a large number of compounds is therefore problematic. In the

present study, we have therefore evaluated the LIA method, which generates thermodynamic averages by using minimization as sampling method for the different molecular systems instead of MD. In contrast to the original Linear Interaction Energy (LIE) method by Åqvist et al., we have also used an implicit water model to speed up the calculations.

Åqvist found that the coefficients α = 0.18 and β = 0.5 (given a charged ligand) were sufficient to give results in agreement with experimental values for several protein systems. Later others reported that the values could be changed and still make intuitively sense [41]. However, our simplifications may affect the accuracy of the method, and may create coefficients different from the Åqvist LIE method. When a full simulation is not performed, the displacement of the water molecules from the receptor and placement of ligand in the pocket that is partly hydrophobic, is not necessarily satisfying in terms of calculating the energy and/or entropy.

Some coefficients obtained in the present study have negative values (Table 2). When using the OPLS2005 force field it is considered as acceptable if the γ value is negative due to changes in the cavity term [42]. Negative α and β coefficients, indicates that the van der Waals (vdW) and electrostatic forces favours the unbound state, but as previously discussed, the background of the LIE theory does not correspond completely with the methodology applied for calculating the Liaison parameters. Alman et al. applied the method for calculating the binding affinity of podophyllotoxin analogous for tubulin using MD for sampling, and got negative α, β and γ coefficients, but a significant squared correlation coefficient ($R^2 = 0.73$) [43].

The *p*-value of the LIA model for agonists was slightly higher than the normally accepted p-value (<0.05), but was tolerated due to the correlation coefficient and low standard deviation. The LIA model for predicting pIC$_{50}$ values for antagonists, performed well with a correlation coefficient of 0.98. The agonists have in general a lower pIC$_{50}$ value than antagonists, and the threshold must be set accordingly. Totally four DUD-E decoys generated from agonist structures were considered as actives after pIC$_{50}$ predictions by the agonist LIA model. DUD-E decoys generated from cluster 1 of outliers were included in the decoy set of both agonists and antagonists, and may have contributed to a lower accuracy.

The statistics of the agonist LIA model were significantly less specific than the model for antagonists. The results for prediction of pIC$_{50}$ value of false positives were therefore not unexpected, but it cannot be ruled out that these compounds are actually binders as they are only assumed non-binders with physicochemical properties resembling known binders. The assumption that enantiomers have identical experimental values may significantly affect the accuracy of the agonist LIA model. Stereochemistry plays a major role in target selectivity and pharmacokinetics. Chiral drugs can behave very differently in a system, which points out the inaccuracy with assuming an identical pIC$_{50}$ for enantiomers [44,45].

4. Materials and Methods

4.1. Datasets

All ChEMBL (version 24_1) compounds tested for GABA$_B$-R binding were downloaded and used to generate compound sets of active and inactive compounds. The activity threshold values for being including in the set of active compounds were: IC$_{50}$ < 4100 nM, K$_i$ < 1500 nM, EC$_{50}$ < 25 μM, or fold changes/inhibition indicating higher activity than GABA, and that they have been tested on assays of cloned or native human or rat GABA$_B$-R. The dataset of actives contained 13 antagonists and 42 agonists, including enantiomers (assuming same activity measurement for enantiomers when not specified) [33,46–50]. MOLPRINT 2D (M2D) chemical fingerprints of all 55 active compounds were generated, before Hierarchical clustering using Tanimoto similarity matrix was performed in Canvas [51]. The number of clusters was set to 10, but after manual modifications and merging of singletons and doubletons, the total number of clusters was reduced to six (Supplementary, Table S1). The clustering method separated agonists from the antagonists, giving 1 cluster with antagonists

and 4 clusters with agonists, in addition a cluster of outliers that merged singletons and doubletons from the initial clustering (4 agonists and 2 antagonists). The DUD-E methodology [52] was used to generate DUD-E decoys, using the structure of active compounds (agonists and antagonists) as input. Fifty DUD-E decoys per active ligand were generated. The compound structures were prepared by LigPrep [53] at a pH of 7.4. Tautomers were generated and the specified chirality of compounds was retained.

Phase Databases

Phase is an engine that is used in pharmacophore modelling [35]. The engine can also be used to generate and modify databases. A Phase databases were generated for each cluster of agonists and antagonist. In addition, a Phase database containing all 55 actives, and two DUD-E decoys databases one containing agonist-like decoys and one containing antagonist-like decoys were also generated. Default settings with generation of up to 50 conformers per ligand were used.

4.2. Ligand-Based Methods

4.2.1. Fingerprinting

Modal fingerprints for each cluster were generated by averaging the M2D fingerprints of ligands in each cluster into cluster based modal fingerprints, representing each of the six clusters [54]. The fingerprints selectivity were evaluated by their ability to identify true actives from DUD-E decoys by Tanimoto similarity metric.

4.2.2. Ligand-Based Pharmacophore Modelling

Pharmacophore models for each cluster of active compounds were generated in Schrödinger's Phase [55] using all compounds in each cluster as input. The pharmacophore models were generated with default parameters: 10 conformers per rotatable bond, maximum 100 conformers per compound, 2 Å RMSD tolerance level for match [55,56]. As the compounds are very similar, the intersite distance for cluster 5 and 6, i.e., the distances between pairs of potential features in the pharmacophore composition were changed from default 2 Å to 1.5 Å to produce more variable hypotheses, including additional features than by default (Table 2). Selection of pharmacophore features was conducted automatically. Any manual selection of features (or constraints) [57] was not applied due to the limited number of active compounds available. A pharmacophore model was considered valid when the model mapped and matched at least 50% of the compounds used to generate that particular pharmacophore model. Mapping and matching were performed by representing each feature of a pharmacophore composition as a distance vector that must overlap with that of the mapped ligand in order to be considered as a match. The pharmacophore hypothesis from each cluster were also evaluated by mapping their respective database of DUD-E decoys generated by the DUD-E methodology [58].

After mapping the respective databases of DUD-E decoys and actives to the pharmacophore models, the accuracy of the models was evaluated by calculating the Matthews correlation coefficient (MCC) (Equation (1)) and "Goodness of Hits" score (GH) (Equation (2)). MCC and GH are calculated from the number of true positives (TP), false positives (FP), true negatives (TN) and false negatives (FN). The compound had to match all features specified for a model to be classified as active, with the exception of the cluster with outliners where the threshold was set to match four out of five features:

$$MCC = \frac{TP{\cdot}TN - FP{\cdot}FN}{\sqrt{(TP + FP)(TP + FN)(TN + FP)(TN + FN)}} \tag{1}$$

$$GH = \left(\frac{Ha(3A + Ht)}{4HtA}\right) \cdot \left(1 - \frac{Ht - Ha}{D}\right) \tag{2}$$

where Ha = TN, Ht = TP + FP, A = TP + FN and D = DUD-E decoys.

The last step in the evaluation, was mapping all active and inactive compounds across clusters to all generated models. MCC gives a correlation between the observed and predicted classifications, in this case actual active and false positive compounds. MCC can be used even if the number of compounds in each class differ [59]. The value can range from −1 to 1, where 1 represents a perfect prediction, 0 indicates a random prediction and −1 represents an inverse prediction [60]. GH scoring function takes into account the sensitivity, specificity and enrichment. The GH scoring thereby gives a good indication of model quality by compromising the yield and actives retrieved and by taking into account the hit list size in comparison with the library size. The score ranges from 0 to 1, where a score of 1 represents the ideal model that perfectly separates active and inactive compounds [61].

4.3. Structure-Based Methods

4.3.1. Protein Preparation

Two crystal structure complexes of GABA$_B$-R VFT with agonists (PDB IDs: 4MS3, 4MS4) and six with antagonists (PDB IDs: 4MR7, 4MR8, 4MR9, 4MS1, 4MRM, 4MQF) are present in the PDB-database. The PBD ID 4MR7 in complex with the antagonist CGP54626 with a resolution of 2.15 Å, and the PDB ID 4MS4 in complex with the agonist baclofen with a resolution of 1.9 Å were used for the structure-based studies. They were selected to represent the active agonist and inactive antagonist-induced VFT structures due to the resolution. The structures were pre-processed in Schrödinger Protein Preparation wizard with default settings; Hydrogen bonds were assigned with a PROPKA pH of 7. A restrained minimization was performed with converging heavy atoms at RMSD of 0.3 Å [62].

4.3.2. Structure-Based e-Pharmacophore Model

The Phase program [35] was used to generate e-Pharmacophores. Receptor binding sites were defined using the centroids of residues involved in ligand binding in all agonist-receptor complexes and most of the antagonist-receptor complexes. For agonists the centroid of Tyr250, Ser130, Ser153, Glu349 and Trp278 was used, while for antagonists the centroid of Ser130, Ser153, Tyr65, His170, Gly151 and Tyr250 was used. The features of each pocket was then found by mapping a library of 441 unique fragments [35] to the binding pocket. The library consisted of 1–7 ionization/tautomer variants of each fragment, and each fragment contained 6–37 atoms with molecular weight ranging from 32 to 226 Da. In total, the set consisted of 667 low energy fragments with ionic and tautomeric states and with metal state penalties for each fragment. The fragments were docked into both X-ray crystal structures by using the Glide XP docking protocol, before the pose viewer file was used to generate e-Pharmacophores. The maximum number of features was set to seven and the hydrogen bond donors were projected as points instead of the default vectors.

The models were screened against the generated databases of active and DUD-E decoys in order to evaluate the capability of the models to select the active from DUD-E decoys. The matching rate of features was set such that at least four out of the seven features should match for the antagonists and three out of seven for agonists. The maximum number of hits was kept at the default number of 1000. The results were evaluated by calculating the Matthews correlation coefficient (MCC) and "Goodness of Hits" score (GH) (Equations (1) and (2))).

4.3.3. Docking Studies

The docking was performed with the Glide program of the Schrödinger suit [63]. One grid map was generated per selected crystal structures, 4MS4 and 4MR7, by selecting the co-crystalized ligand as the centroid of the grid box. However, the grid size was increased by changing the inner box diameter from 10 Å to 15 Å such that larger compounds than the co-crystallized ligands could be docked. The remaining settings for the grid generation were kept at default values. A standard precision (SP) docking protocol in Glide was set up with enhanced sampling and generation of maximum 10 poses per ligand. Binding poses with Coulomb and van der Waals forces > 0 kcal/mol were by default

filtered away, while ligand poses with RMSD < 0.5 Å were treated as duplicates and one of them was removed. The scoring threshold for agonists and the antagonists were found by calculating the average docking score of 42 agonists and the 13 antagonists, respectively. A cross-docking where agonists were docked into in antagonist-induced VFT conformation and antagonists into the agonist-induced was also performed.

After the docking, one representative compound from each cluster was selected for analysis and description of the interaction patterns between known orthosteric GABA$_B$-R compounds and the VFT. The interactions between the selected ligands and the VFT were compared to identify potential differences in binding modes between the clusters and between agonists and antagonists. Cluster 1 was not included since it contains outliers of both agonists and antagonists. Known inactive and low activity compounds (compounds with IC$_{50}$, K$_i$ or EC$_{50}$ values higher than those used in the selection of actives) were also docked and scored in the VFT of both agonist and antagonist-induced VFT conformation (Supplementary, Table S2).

The false positive compounds from the pharmacophore screening were also docked using the standard precision (SP) docking protocol in Glide with the same settings as previously described, to evaluate if the docking could correctly assign these compounds as TN in contrast to the pharmacophore screening which predicted these compounds as active.

4.4. LIA Model Development and Evaluation

In LIA calculations, molecular mechanics (MM) simulations are used to calculate energy of ligand both in a bound and unbound state, using a continuum solvation model. The Liaison program used the following equation to predict the free energy of binding (ΔGbind):

$$\Delta Gbind = \alpha(\langle Ubvdw \rangle - \langle Ufvdw \rangle) + \beta(\langle Ubelec \rangle - \langle Ufelec \rangle) + \gamma(\langle Ubcav \rangle - \langle Ufcav \rangle) \qquad (3)$$

The brackets indicate that the calculation uses the average energy of conformations sampled during MM simulations. Uf describes the molecule free in solution and Ub describes the target-ligand complex. The energy terms are the van der Waals interactions (Uvdw), the electrostatic interactions (Uelec) and the cavity parameter (Ucav). A training set of compounds with known affinity is used to build an energy model by fitting three coefficients (α, β, and γ,) to their experimental free energy of binding. The models can then be used to predict affinities of ligands with unknown experimental affinity.

In total, 42 compounds (including enantiomers) were considered as highly active GABA$_B$-R agonists. Their experimental values were converted to IC$_{50}$ (assuming IC$_{50}$ = K$_i$ × 2) and then to pIC$_{50}$ [64]. Six agonists were excluded since their experimental values were incompatible with conversion to pIC$_{50}$ (Supplementary Material, Table S1). Without considering enantiomers, there were then 20 unique agonists and due to the low diversity in pIC$_{50}$ totally 11 out of the 20 compounds were included in the training set for generating the agonist LIA model (Supplementary Material, Table S1). The remaining nine compounds were used in the test set in addition to all true positives identified by the pharmacophore mapping, however, agonists used in the training set were removed but enantiomers of these were kept.

Based on the affinity values, 13 compounds were considered as highly active GABA$_B$-R antagonists. Three of these were selected for the training set, in addition 4 low affinity antagonists from the set of inactive were included in the training set (Supplementary Material, Table S1), to increase the structural diversity and the range of the pIC$_{50}$ value to give more useful LIA models for identification of antagonists in a VS approach. Two of the included low affinity antagonists were from the X-ray complexes 4MQF and 4MRM of the GABA$_B$-R VFTs. The test set consisted of true positives from the pharmacophore mapping which included eight of 10 remaining high affinity antagonists. Two of the high affinity antagonists were found to be false negatives as they were not retrieved by the

pharmacophore mapping and therefor excluded from the test set, resulting in totally eight compounds in the test set.

The training and test sets of agonists and antagonists were docked into their respective crystal structures (PDB ID: 4MR7 for antagonists and 4MS4 for agonists) [65] before a Truncated Newton minimization sampling was performed with the maximum number of sampling steps set to 1000 (default settings). The flexible region of the receptor included the amino acids in the binding pocket. A similar sampling minimization procedure was also performed for the unbound ligand and receptor. The sampling simulations were performed in an implicit water model (default settings) [36,37]. The three necessary energy descriptors (van der Waals, electrostatic and a cavity term energies of bound and unbound states), were calculated from the simulations of the training sets. Together with the experimentally obtained activity values these energy values were used to derive the coefficients α, β, and γ, and for making linear regression models and statistical evaluation by comparing the predicted pIC_{50} values of the test set to the provided experimental values. The models were also applied to the false positive agonists retrieved by the docking protocol, to evaluate the predictability of the models.

5. Conclusions

The low number of available active ligands towards the $GABA_B$-R complicates and limits the use of both ligand-based and structure-based approaches. The quality of ligand-based methods and validation of the predictability of structure-based models are dependent on both the number and diversity of active ligands. Fingerprinting methods were used and evaluated, but did not give reliable results. The pharmacophore models combined with docking on the other hand, showed a discrimination between actives and DUD-E decoys acceptable for a VS process. The pharmacophore mapping gave false positives, but docking reduced this number. The present study indicates that the use of LIA models only slightly will affect the outcome of a VS campaign as only one DUD-E agonist decoy from docking was recognised as a false positive by the agonist LIA model. The structural analysis of X-ray structure complexes and docking showed that certain LB1 interactions are necessary for anchoring the ligands in the crevice of the VFT, and that the interactions with residues of LB2 will impact the function of the ligand and the affinity. On the background of previously mentioned studies and in light of the results in this study, there is a strong correlation with the specific ligand features and the number of interactions with key residues in both LB1 and LB2. In circumstances where a low number of actives is known, exhaustive structure-based methods in combination with pharmacophore modelling may lead to identification of novel compounds.

References

1. Coudrat, T.; Simms, J.; Christopoulos, A.; Wootten, D.; Sexton, P.M. Improving virtual screening of G protein-coupled receptors via ligand-directed modeling. *PLoS Comput. Biol.* **2017**, *13*, e1005819. [CrossRef] [PubMed]

2. Aparoy, P.; Kumar Reddy, K.; Reddanna, P. Structure and Ligand Based Drug Design Strategies in the Development of Novel 5-LOX Inhibitors. *Curr. Med. Chem.* **2012**, *19*, 3763–3778. [CrossRef] [PubMed]

3. Evers, A.; Klabunde, T. Structure-based Drug Discovery Using GPCR Homology Modeling: Successful Virtual Screening for Antagonists of the Alpha1A Adrenergic Receptor. *J. Med. Chem.* **2005**, *48*, 1088–1097. [CrossRef] [PubMed]

4. Gabrielsen, M.; Kurczab, R.; Siwek, A.; Wolak, M.; Ravna, A.W.; Kristiansen, K.; Kufareva, I.; Abagyan, R.; Nowak, G.; Chilmonczyk, Z.; et al. Identification of Novel Serotonin Transporter Compounds by Virtual Screening. *J. Chem. Inf. Model.* **2014**, *54*, 933–943. [CrossRef] [PubMed]

5. Kurczab, R.; Nowak, M.; Chilmonczyk, Z.; Sylte, I.; Bojarski, A.J. The development and validation of a novel virtual screening cascade protocol to identify potential serotonin 5-HT7R antagonists. *Bioorg. Med. Chem. Lett.* **2010**, *20*, 2465–2468. [CrossRef] [PubMed]

6. Ripphausen, P.; Nisius, B.; Peltason, L.; Bajorath, J. Quo Vadis, Virtual Screening? A Comprehensive Survey of Prospective Applications. *J. Med. Chem.* **2010**, *53*, 8461–8467. [CrossRef] [PubMed]

7. Pin, J.-P.; Prezeau, L. Allosteric Modulators of GABAB Receptors: Mechanism of Action and Therapeutic Perspective. *Curr. Neuropharmacol.* **2007**, *5*, 195–201. [CrossRef] [PubMed]

8. Calver, A.R.; Medhurst, A.D.; Robbins, M.J.; Charles, K.J.; Evans, M.L.; Harrison, D.C.; Stammers, M.; Hughes, S.A.; Hervieu, G.; Couve, A.; et al. The expression of GABAB1 and GABAB2 receptor subunits in the cNS differs from that in peripheral tissues. *Neuroscience* **2000**, *100*, 155–170. [CrossRef]

9. Geng, Y.; Bush, M.; Mosyak, L.; Wang, F.; Fan, Q.R. Structural mechanism of ligand activation in human GABAB receptor. *Nature* **2013**, *504*, 254–259. [CrossRef] [PubMed]

10. Jones, K.A.; Borowsky, B.; Tamm, J.A.; Craig, D.A.; Durkin, M.M.; Dai, M.; Yao, W.-J.; Johnson, M.; Gunwaldsen, C.; Huang, L.-Y.; et al. GABAB receptors function as a heteromeric assembly of the subunits GABABR1 and GABABR2. *Nature* **1998**, *396*, 674–679. [CrossRef] [PubMed]

11. Kniazeff, J.; Galvez, T.; Labesse, G.; Pin, J.-P. No Ligand Binding in the GB2 Subunit of the GABA B Receptor Is Required for Activation and Allosteric Interaction between the Subunits. *J. Neurosci.* **2002**, *22*, 7352–7361. [CrossRef] [PubMed]

12. Binet, V.; Brajon, C.; Le Corre, L.; Acher, F.; Pin, J.-P.; Prézeau, L. The Heptahelical Domain of GABA B2 Is Activated Directly by CGP7930, a Positive Allosteric Modulator of the GABA B Receptor. *J. Biol. Chem.* **2004**, *279*, 29085–29091. [CrossRef] [PubMed]

13. Eswar, N.; Webb, B.; Marti-Renom, M.A.; Madhusudhan, M.S.; Eramian, D.; Shen, M.; Pieper, U.; Sali, A. Comparative Protein Structure Modeling Using Modeller. In *Current Protocols in Bioinformatics*; Bateman, A., Pearson, W.R., Stein, L.D., Stormo, G.D., Yates, J.R., Eds.; John Wiley & Sons, Inc.: Hoboken, NJ, USA, 2006; pp. 5.6.1–5.6.30. ISBN 978-0-471-25095-1.

14. Pin, J.-P.; Parmentier, M.-L.; Prézeau, L. Positive Allosteric Modulators for γ-Aminobutyric Acid B Receptors Open New Routes for the Development of Drugs Targeting Family 3 G-Protein-Coupled Receptors. *Mol. Pharmacol.* **2001**, *60*, 881–884. [CrossRef] [PubMed]

15. Heaney, C.F.; Kinney, J.W. Role of GABAB receptors in learning and memory and neurological disorders. *Neurosci. Biobehav. Rev.* **2016**, *63*, 1–28. [CrossRef] [PubMed]

16. Tyacke, R.J.; Lingford-Hughes, A.; Reed, L.J.; Nutt, D.J. GABAB Receptors in Addiction and Its Treatment. In *Advances in Pharmacology*; Elsevier: Amsterdam, The Netherlands, 2010; Volume 58, pp. 373–396. ISBN 978-0-12-378647-0.

17. Varani, A.P.; Pedrón, V.T.; Aon, A.J.; Höcht, C.; Acosta, G.B.; Bettler, B.; Balerio, G.N. Nicotine-induced molecular alterations are modulated by GABAB receptor activity: GABAB receptors and nicotine. *Addict. Biol.* **2018**, *23*, 230–246. [CrossRef] [PubMed]

18. Pilc, A.; Nowak, G. GABA-ergic hypotheses of anxiety and depression: Focus on GABA-B receptor. *Drugs Today* **2005**, *41*, 755. [CrossRef] [PubMed]

19. Hedley, D.W.; Maroun, J.A.; Espir, M.L. Evaluation of baclofen (Lioresal) for spasticity in multiple sclerosis. *Postgrad. Med. J.* **1975**, *51*, 615–618. [CrossRef] [PubMed]

20. McIntyre, A.; Mays, R.; Mehta, S.; Janzen, S.; Townson, A.; Hsieh, J.; Wolfe, D.; Teasell, R. Examining the effectiveness of intrathecal baclofen on spasticity in individuals with chronic spinal cord injury: A systematic review. *J. Spinal Cord Med.* **2014**, *37*, 11–18. [CrossRef] [PubMed]

21. D'Aleo, G.; Cammaroto, S.; Rifici, C.; Marra, G.; Sessa, E.; Bramanti, P.; Di Bella, P. Hallucinations after abrupt withdrawal of oral and intrathecal baclofen. *Funct. Neurol.* **2007**, *22*, 81–88. [PubMed]

22. Farokhnia, M.; Schwandt, M.L.; Lee, M.R.; Bollinger, J.W.; Farinelli, L.A.; Amodio, J.P.; Sewell, L.; Lionetti, T.A.; Spero, D.E.; Leggio, L. Biobehavioral effects of baclofen in anxious alcohol-dependent individuals: A randomized, double-blind, placebo-controlled, laboratory study. *Transl. Psychiatry* **2017**, *7*, e1108. [CrossRef] [PubMed]

23. Reynaud, M.; Aubin, H.-J.; Trinquet, F.; Zakine, B.; Dano, C.; Dematteis, M.; Trojak, B.; Paille, F.; Detilleux, M. A Randomized, Placebo-Controlled Study of High-Dose Baclofen in Alcohol-Dependent Patients—The ALPADIR Study. *Alcohol Alcohol.* **2017**, *52*, 439–446. [CrossRef] [PubMed]

24. Varani, A.P.; Aso, E.; Moutinho, L.M.; Maldonado, R.; Balerio, G.N. Attenuation by baclofen of nicotine rewarding properties and nicotine withdrawal manifestations. *Psychopharmacology* **2014**, *231*, 3031–3040. [CrossRef] [PubMed]

25. Augier, E.; Dulman, R.S.; Damadzic, R.; Pilling, A.; Hamilton, J.P.; Heilig, M. The GABAB Positive Allosteric Modulator ADX71441 Attenuates Alcohol Self-Administration and Relapse to Alcohol Seeking in Rats. *Neuropsychopharmacology* **2017**, *42*, 1789–1799. [CrossRef] [PubMed]

26. Andrews, N.; File, S.E. Handling history of rats modifies behavioural effects of drugs in the elevated plus-maze test of anxiety. *Eur. J. Pharmacol.* **1993**, *235*, 109–112. [CrossRef]

27. Pizzo, R.; O'Leary, O.F.; Cryan, J.F. Elucidation of the neural circuits activated by a GABA B receptor positive modulator: Relevance to anxiety. *Neuropharmacology* **2018**, *136*, 129–145. [CrossRef] [PubMed]

28. Cryan, J.F.; Slattery, D.A. GABAB Receptors and Depression: Current Status. In *Advances in Pharmacology*; Elsevier: Amsterdam, The Netherlands, 2010; Volume 58, pp. 427–451. ISBN 978-0-12-378647-0.

29. Ghose, S.; Winter, M.K.; McCarson, K.E.; Tamminga, C.A.; Enna, S.J. The GABAB receptor as a target for antidepressant drug action: GABAB receptor expression and depression. *Br. J. Pharmacol.* **2011**, *162*, 1–17. [CrossRef] [PubMed]

30. Nakagawa, Y.; Ishima, T.; Ishibashi, Y.; Tsuji, M.; Takashima, T. Involvement of GABAB receptor systems in action of antidepressants. II: Baclofen attenuates the effect of desipramine whereas muscimol has no effect in learned helplessness paradigm in rats. *Brain Res.* **1996**, *728*, 225–230. [CrossRef]

31. Bowery, N. GABAB receptor: A site of therapeutic benefit. *Curr. Opin. Pharmacol.* **2006**, *6*, 37–43. [CrossRef] [PubMed]

32. Pin, J.-P.; Bettler, B. Organization and functions of mGlu and GABAB receptor complexes. *Nature* **2016**, *540*, 60–68. [CrossRef] [PubMed]

33. Hersey, A. *CHEMBL Database Release 21*; EMBL-EBI: Hinxton, Cambridgeshire, UK, 2016.

34. Cornish-Bowden, A. *Fundamentals of Enzyme Kinetics*, 4th ed.; Wiley-Blackwell: Weinheim, Germany, 2012; ISBN 978-3-527-33074-4.

35. *Phase Schrödinger Release 2017-4*; Schrödinger, LLC: New York, NY, USA, 2017.

36. *Liaison Schrödinger Release 2015-3*; Schrödinger, LLC: New York, NY, USA, 2015.

37. *Strike Version 2.2 Schrödinger Release 2015-3*; Schrödinger, LLC: New York, NY, USA, 2015.

38. Totrov, M.; Abagyan, R. Flexible ligand docking to multiple receptor conformations: A practical alternative. *Curr. Opin. Struct. Biol.* **2008**, *18*, 178–184. [CrossRef] [PubMed]

39. Aqvist, J.; Medina, C.; Samuelsson, J.E. A new method for predicting binding affinity in computer-aided drug design. *Protein Eng.* **1994**, *7*, 385–391. [CrossRef] [PubMed]

40. Aqvist, J.; Marelius, J. The Linear Interaction Energy Method for Predicting Ligand Binding Free Energies. *Comb. Chem. High Throughput Screen.* **2001**, *4*, 613–626. [CrossRef] [PubMed]

41. Gassmann, M.; Bettler, B. Regulation of neuronal GABAB receptor functions by subunit composition. *Nat. Rev. Neurosci.* **2012**, *13*, 380–394. [CrossRef] [PubMed]

42. *Liaison Manual 5.8 Schrödinger Release 2015-3*; Schrödinger, LLC: New York, NY, USA, 2015.

43. Alam, M.A.; Naik, P.K. Applying linear interaction energy method for binding affinity calculations of podophyllotoxin analogues with tubulin using continuum solvent model and prediction of cytotoxic activity. *J. Mol. Graph. Model.* **2009**, *27*, 930–943. [CrossRef] [PubMed]

44. Caldwell, J. The importance of stereochemistry in drug action and disposition. *J. Clin. Pharmacol.* **1992**, *32*, 925–929. [PubMed]

45. McConathy, J.; Owens, M.J. Stereochemistry in Drug Action. *Prim. Care Companion J. Clin. Psychiatry* **2003**, *5*, 70–73. [CrossRef] [PubMed]

46. Froestl, W.; Mickel, S.J.; Hall, R.G.; von Sprecher, G.; Strub, D.; Baumann, P.A.; Brugger, F.; Gentsch, C.; Jaekel, J. Phosphinic Acid Analogs of GABA. 1. New Potent and Selective GABAB Agonists. *J. Med. Chem.* **1995**, *38*, 3297–3312. [CrossRef] [PubMed]

47. Froestl, W.; Mickel, S.J.; von Sprecher, G.; Diel, P.J.; Hall, R.G.; Maier, L.; Strub, D.; Melillo, V.; Baumann, P.A. Phosphinic Acid Analogs of GABA. 2. Selective, Orally Active GABAB Antagonists. *J. Med. Chem.* **1995**, *38*, 3313–3331. [CrossRef] [PubMed]

48. Kaupmann, K.; Huggel, K.; Heid, J.; Flor, P.J.; Bischoff, S.; Mickel, S.J.; McMaster, G.; Angst, C.; Bittiger, H.; Froestl, W.; et al. Expression cloning of GABAB receptors uncovers similarity to metabotropic glutamate receptors. *Nature* **1997**, *386*, 239–246. [CrossRef] [PubMed]

49. Locock, K.E.S.; Yamamoto, I.; Tran, P.; Hanrahan, J.R.; Chebib, M.; Johnston, G.A.R.; Allan, R.D. γ-Aminobutyric Acid(C) (GABA C) Selective Antagonists Derived from the Bioisosteric Modification of 4-Aminocyclopent-1-enecarboxylic Acid: Amides and Hydroxamates. *J. Med. Chem.* **2013**, *56*, 5626–5630. [CrossRef] [PubMed]

50. Blackburn, T. *GABAb Receptor Pharmacology: A Tribute to Norman Bowery*, 1st ed.; Advances in Pharmacology (Book 58); Academic Press: Cambridge, MA, USA, 2010; Volume 54, ISBN 978-0-12-378647-0.

51. *Canvas Schrödinger Release 2017-4*; Schrödinger, LLC: New York, NY, USA, 2017.

52. Mysinger, M.M.; Carchia, M.; Irwin, J.J.; Shoichet, B.K. Directory of Useful Decoys, Enhanced (DUD-E): Better Ligands and Decoys for Better Benchmarking. *J. Med. Chem.* **2012**, *55*, 6582–6594. [CrossRef] [PubMed]

53. *LigPrep*; Schrödinger, LLC: New York, NY, USA, 2017.

54. Duan, J.; Dixon, S.L.; Lowrie, J.F.; Sherman, W. Analysis and comparison of 2D fingerprints: Insights into database screening performance using eight fingerprint methods. *J. Mol. Graph. Model.* **2010**, *29*, 157–170. [CrossRef] [PubMed]

55. Dixon, S.L.; Smondyrev, A.M.; Knoll, E.H.; Rao, S.N.; Shaw, D.E.; Friesner, R.A. PHASE: A new engine for pharmacophore perception, 3D QSAR model development, and 3D database screening: 1. Methodology and preliminary results. *J. Comput. Aided Mol. Des.* **2006**, *20*, 647–671. [CrossRef] [PubMed]

56. Khan, M.F.; Verma, G.; Akhtar, W.; Shaquiquzzaman, M.; Akhter, M.; Rizvi, M.A.; Alam, M.M. Pharmacophore modeling, 3D-QSAR, docking study and ADME prediction of acyl 1,3,4-thiadiazole amides and sulfonamides as antitubulin agents. *Arab. J. Chem.* **2016**. [CrossRef]

57. Warszycki, D.; Mordalski, S.; Kristiansen, K.; Kafel, R.; Sylte, I.; Chilmonczyk, Z.; Bojarski, A.J. A linear combination of pharmacophore hypotheses as a new tool in search of new active compounds—An application for 5-HT1A receptor ligands. *PLoS ONE* **2013**, *8*, e84510. [CrossRef] [PubMed]

58. Huang, N.; Shoichet, B.K.; Irwin, J.J. Benchmarking Sets for Molecular Docking. *J. Med. Chem.* **2006**, *49*, 6789–6801. [CrossRef] [PubMed]

59. Matthews, B.W. Comparison of the predicted and observed secondary structure of T4 phage lysozyme. *Biochim. Biophys. Acta* **1975**, *405*, 442–451. [CrossRef]

60. Shimizu, K.; Hirose, S.; Noguchi, T. POODLE-S: Web application for predicting protein disorder by using physicochemical features and reduced amino acid set of a position-specific scoring matrix. *Bioinformatics* **2007**, *23*, 2337–2338. [CrossRef] [PubMed]

61. Seal, A.; Yogeeswari, P.; Sriram, D.; Consortium, O.; Wild, D.J. Enhanced ranking of PknB Inhibitors using data fusion methods. *J. Cheminform.* **2013**, *5*, 2. [CrossRef] [PubMed]

62. Madhavi Sastry, G.; Adzhigirey, M.; Day, T.; Annabhimoju, R.; Sherman, W. Protein and ligand preparation: Parameters, protocols, and influence on virtual screening enrichments. *J. Comput. Aided Mol. Des.* **2013**, *27*, 221–234. [CrossRef] [PubMed]

63. *Glide Schrödinger Release 2017-4*; Schrödinger, LLC: New York, NY, USA, 2017.

64. Haupt, L.J.; Kazmi, F.; Ogilvie, B.W.; Buckley, D.B.; Smith, B.D.; Leatherman, S.; Paris, B.; Parkinson, O.; Parkinson, A. The Reliability of Estimating Ki Values for Direct, Reversible Inhibition of Cytochrome P450 Enzymes from Corresponding IC50 Values: A Retrospective Analysis of 343 Experiments. *Drug Metab. Dispos.* **2015**, *43*, 1744–1750. [CrossRef] [PubMed]
65. *Glide Schrödinger Release 2015-3*; Schrödinger, LLC: New York, NY, USA, 2015.

Sample Availability: Not Available.

In Silico Methods for the Discovery of Orthosteric GABAB Receptor Compounds

Linn M. Evenseth [1], Dawid Warszycki [2], Andrzej J. Bojarski [2], Mari Gabrielsen [1] and Ingebrigt Sylte [1],*

[1] Molecular Pharmacology and Toxicology, Department of Medical Biology, Faculty of Health Sciences, UiT —The Arctic University of Norway, NO-9037 Tromsø, Norway; linn.evenseth@uit.no (L.M.E.); mari.gabrielsen@uit.no (M.G.)

[2] Department of Medicinal Chemistry, Institute of Pharmacology, Polish Academy of Science, Smetna 12, 31-343 Kraków, Poland; warszyc@if-pan.krakow.pl (D.W.); bojarski@if-pan.krakow.pl (A.J.B.)

* Correspondence: ingebrigt.sylte@uit.no; Tel.: +47-77-64-4705

Table S1 - **Biological data.** The table shows the dataset of active GABAB-R compounds. Threshold values for being including in the set of active compounds were: $IC_{50} < 4100$ nM, $K_i < 1500$ nM, $EC_{50} < 25$ μM, or fold changes/inhibition indicating higher activity than GABA. Compounds were structurally clustered into six clusters based on fingerprints. The compounds are shown with activity values and the source of the data (reference). Cluster 1: four agonists and two antagonists. Cluster 2: 12 agonists. Cluster 3: 11 antagonists. Cluster 4: nine agonists. Cluster 5: four agonists. Cluster 6: 13 agonists.

Compound		Activity		Source
Structure	Name	Type	Value	
Cluster 1				
	CGP52432*	IC_{50}	0.055 μM	[1]
	SCH50911	IC_{50}	1.100 μM	[2]
	CHEMBL 2322934 (S)	EC_{50}	24.90 μM	[3]
	CHEMBL 2322934 (R)	EC_{50}	24.90 μM	[3]

Table S1. *Cont.*
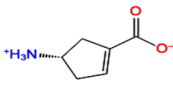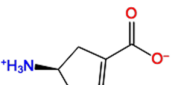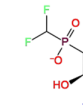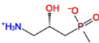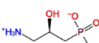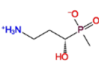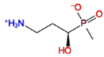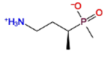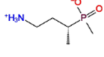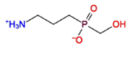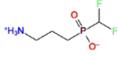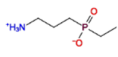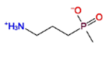
	CHEMBL239812 1 (S)	Max. response	75.3%	[4]
	CHEMBL239812 1 (R)	Max. response	75.3%	[4]

1. *GABA B receptor pharmacology: a tribute to Norman Bowery*; Blackburn, T.P., Bowery, N., Eds.; Advances in Pharmacology; Elsevier, Acad. Press: Amsterdam, The Netherlands, 2010; ISBN 978-0-12-378647-0. Inhibition of binding of [^{3}H]CGP27492

2. Bolser, D.C.; Blythin, D.J.; Chapman, R.W.; Egan, R.W.; Hey, J.A.; Rizzo, C.; Kuo, S.C.; Kreutner, W. The pharmacology of SCH 50911: a novel, orally-active GABA-beta receptor antagonist. *J. Pharmacol. Exp. Ther.* **1995**, *274*, 1393–1398. Inhibition of the binding of 5 nM [3H]GABA.

3. Han, C.; Salyer, A.E.; Kim, E.H.; Jiang, X.; Jarrard, R.E.; Powers, M.S.; Kirchhoff, A.M.; Salvador, T.K.; Chester, J.A.; Hockerman, G.H.; et al. Evaluation of Difluoromethyl Ketones as Agonists of the γ-Aminobutyric Acid Type B (GABA B Receptor). *J. Med. Chem.* **2013**, *56*, 2456–2465. Inhibition of forskolin stimulated (10 μM) cAMP production.

4. Locock, K.E.S.; Yamamoto, I.; Tran, P.; Hanrahan, J.R.; Chebib, M.; Johnston, G.A.R.; Allan, R.D. γ-Aminobutyric Acid(C) (GABA C) Selective Antagonists Derived from the Bioisosteric Modification of 4-Aminocyclopent-1-enecarboxylic Acid: Amides and Hydroxamates. *J. Med. Chem.* **2013**, *56*, 5626–5630. Percent of maximum GABA (300 μM) response at a concentration of 300 μM of tested compound.

Cluster 2

	56 (R)[+]	IC$_{50}$	0.213 μM	[5]
	56 (S)	IC$_{50}$	0.213 μM	[5]
	55 (R)	IC$_{50}$	0.077 μM	[5]
	55 (S)	IC$_{50}$	0.077 μM	[5]
	52 (S)	IC$_{50}$	1.160 μM	[5]

Table S1. *Cont.*

	52 (R) [+]	IC$_{50}$	1.160 μM	[5]
	45 (S)	IC$_{50}$	0.140 μM	[5]
	45 (R)	IC$_{50}$	0.140 μM	[5]
	44	IC$_{50}$	1.050 μM	[5]
	43 [+]	IC$_{50}$	0.089 μM	[5]
	ChEMBL325921	IC$_{50}$	1.350 μM (*)	[5]
	ChEMBL112710	IC$_{50}$	0.0066 μM (*)	[5]

5. Froestl, W.; Mickel, S.J.; Hall, R.G.; von Sprecher, G.; Strub, D.; Baumann, P.A.; Brugger, F.; Gentsch, C.; Jaekel, J. Phosphinic Acid Analogs of GABA. 1. New Potent and Selective GABAB Agonists. *J. Med. Chem.* **1995**, *38*, 3297–3312.: Inhibition of binding of 10nM [³H]Baclofen (*) or 2 nM [3H]CGP 27492 to GABA$_B$ receptors from rat cortex.

Cluster 3
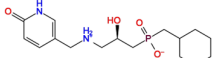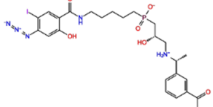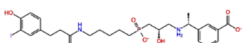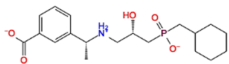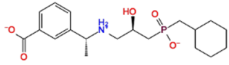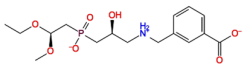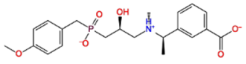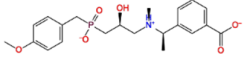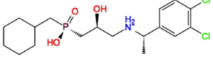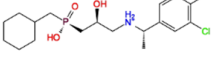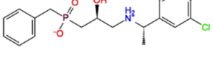
	CGP63360	IC$_{50}$	0.0390 μM	[1]
	CGP71782	IC$_{50}$	0.0024 μM	[6]
	CGP64213*	IC$_{50}$	0.002 μM	[6]
	CGP56999	IC$_{50}$	0.0004 μM	[6]
	CGP56433	IC$_{50}$	0.080 μM	[1]

Table S1. *Cont.*

	CGP61334	IC$_{50}$	0.036 μM	[1]
	CGP62349(S)	IC$_{50}$	0.002 μM	[1]
	CGP62349(R)	IC$_{50}$	0.002 μM	[1]
	CGP54626(S)	IC$_{50}$	0.002 μM	[6]
	CGP54626(R)	IC$_{50}$	0.002 μM	[6]
	CGP55845*	IC$_{50}$	0.006 μM	[1]

1. *GABA B receptor pharmacology: a tribute to Norman Bowery*; Blackburn, T.P., Bowery, N., Eds.; Advances in pharmacology; Elsevier, Academic Press: Amsterdam, The Netherlands, 2010; ISBN 978-0-12-378647-0. Inhibition of binding of [³H]CGP27492

6. Kaupmann, K.; Huggel, K.; Heid, J.; Flor, P.J.; Bischoff, S.; Mickel, S.J.; McMaster, G.; Angst, C.; Bittiger, H.; Froestl, W.; et al. Expression cloning of GABA(B) receptors uncovers similarity to metabotropic glutamate receptors. *Nature* **1997**, *386*, 239–246. Inhibition of binding of 0.1 nM [¹²⁵I]CGP64213

Cluster 4
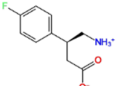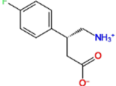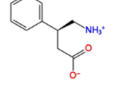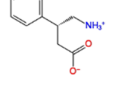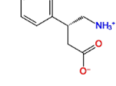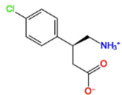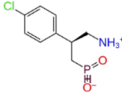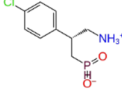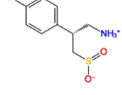
	13(S)	IC$_{50}$	0.360 μM	[5]
	13(R)⁺	IC$_{50}$	0.360 μM	[5]
	14(S)	IC$_{50}$	0.880 μM	[5]
	14(R)⁺	IC$_{50}$	0.880 μM	[5]
	R-Baclofen	IC$_{50}$	0.015 μM	[5]
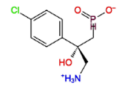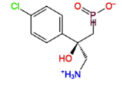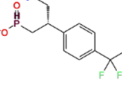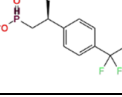
Table S1. *Cont.*

	S-Baclofen	IC$_{50}$	1.770 μM	[5]
	12(S)	IC$_{50}$	0.039 μM	[5]
	12(R)	IC$_{50}$	0.039 μM	[5]
	ChEMBL312675	IC$_{50}$	0.200 μM	[7]

5. Froestl, W.; Mickel, S.J.; Hall, R.G.; von Sprecher, G.; Strub, D.; Baumann, P.A.; Brugger, F.; Gentsch, C.; Jaekel, J. Phosphinic Acid Analogs of GABA. 1. New Potent and Selective GABAB Agonists. *J. Med. Chem.* **1995**, *38*, 3297–3312. Inhibition of binding of the binding 10nM [³H]Baclofen to GABA$_B$ receptor from rat cortex.

7. Carruthers, N.I.; Spitler, J.M.; Shing-Chun Wong; Blythin, D.J.; Xiao Chen; Ho-Jane Shue; Mittelman, S. Synthesis and resolution of β-(aminomethyl)-4-chlorobenzeneethanesulfinic acid a potent gabaB receptor ligand. *Bioorg. Med. Chem. Lett.* **1995**, *5*, 237–240. Not specified

Cluster 5

	27(S)	IC$_{50}$	0.065 μM	[5]
	27(R)[+]	IC$_{50}$	0.065 μM	[5]
	ChEMBL325507(R)	Inhibition	66%	[5]
	ChEMBL325507(S)	Inhibition	66%	[5]

5. Froestl, W.; Mickel, S.J.; Hall, R.G.; von Sprecher, G.; Strub, D.; Baumann, P.A.; Brugger, F.; Gentsch, C.; Jaekel, J. Phosphinic Acid Analogs of GABA. 1. New Potent and Selective GABAB Agonists. *J. Med. Chem.* **1995**, *38*, 3297–3312. Inhibition of binding of 10nM [³H]Baclofen

Cluster 6

	GABA	IC$_{50}$	0.025 μM	[5]

Table S1. *Cont.*
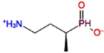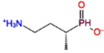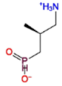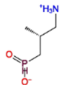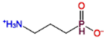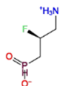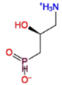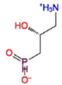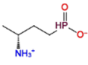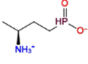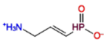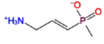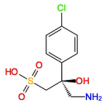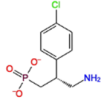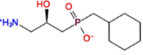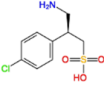
	7(S)	IC$_{50}$	0.920 μM	[5]
	7(R)[+]	IC$_{50}$	0.920 μM	[5]
	8(S)	IC$_{50}$	0.780 μM	[5]
	8(R)[+]	IC$_{50}$	0.780 μM	[5]
	ChEMBL112203	IC$_{50}$	0.0024 μM	[5]
	ChEMBL448343	K$_i$	0.0051 μM	[8]
	16(S)	IC$_{50}$	0.018 μM	[5]
	16(R)	IC$_{50}$	0.018 μM	[5]
	9(S)	IC$_{50}$	0.5 μM	[5]
	9(R[+])	IC$_{50}$	0.5 μM	[5]
	29[+]	IC$_{50}$	0.280 μM	[5]
	68[+]	IC$_{50}$	0.665 μM (*)	[5]

Table S1. *Cont.*

5. Froestl, W.; Mickel, S.J.; Hall, R.G.; von Sprecher, G.; Strub, D.; Baumann, P.A.; Brugger, F.; Gentsch, C.; Jaekel, J. Phosphinic Acid Analogs of GABA. 1. New Potent and Selective GABAB Agonists. *J. Med. Chem.* **1995**, *38*, 3297–3312. Inhibition of binding of 10nM [³H]Baclofen or 2 nM [3H]CGP 27492 (*) to GABA$_B$ receptors from rat cortex.

8. Alstermark, C.; Amin, K.; Dinn, S.R.; Elebring, T.; Fjellström, O.; Fitzpatrick, K.; Geiss, W.B.; Gottfries, J.; Guzzo, P.R.; Harding, J.P.; et al. Synthesis and Pharmacological Evaluation of Novel γ-Aminobutyric Acid Type B (GABAB) Receptor Agonists as Gastroesophageal Reflux Inhibitors. *J. Med. Chem.* **2008**, *51*, 4315–4320. Displacement of [³H]GABA.

Low affinity antagonists added for LIA modelling

	2-hydroxy-saclofen	pIC50	4.1M	Guidetopharmacology. org
	phaclofen	pIC50	4.1M	Guidetopharmacology. org
	CGP51776	IC50	6 μM	[1]
	saclofen	pIC50	3.5M	Guidetopharmacology. org

1. *GABA B receptor pharmacology: a tribute to Norman Bowery*; Blackburn, T.P., Bowery, N., Eds.; Advances in pharmacology; Elsevier, Academic Press: Amsterdam, The Netherlands 2010; ISBN 978-0-12-378647-0. Inhibition of binding of   [³H]CGP27492

⁺Agonists included in the test set used to calculate the LIA coefficients

*Antagonists included in the test set used to calculate the LIA coefficients

Table S2 - **Inactive compounds.** The structure of the inactive compounds. The dataset contains totally inactive and low affinity/activity GABA_B-R compounds.
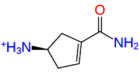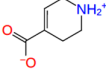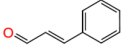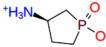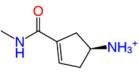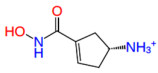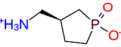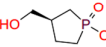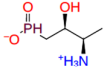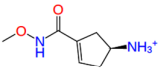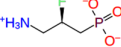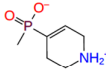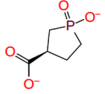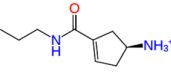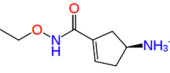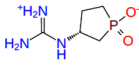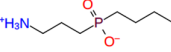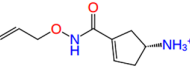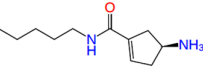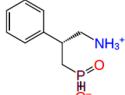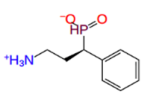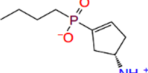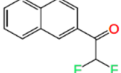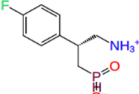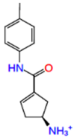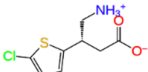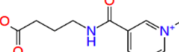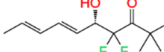
title: C6H10N2O

title: C6H9NO2

title: C9H8O

title: C4H10NO2P

title: C7H12N2O

title: C6H10N2O2

title: C5H12NO2P

title: C5H11O3P

title: C4H11NO3P

title: C7H12N2O2

title: C3H9FNO3P

title: C6H12NO2P

title: C5H9O4P

title: C9H16N2O

title: C8H14N2O2

title: C5H12N3O2P

title: C7H18NO2P

title: C9H14N2O2

title: C11H20N2O

title: C9H13NO2P

title: C9H13NO2P

title: C9H18NO2P

title: C12H8F2O

title: C9H12FNO2P

title: C13H16N2O

title: C8H10ClNO2S

title: C12H18N2O7S

title: C12H18F2O2

Table S2. *Cont.*
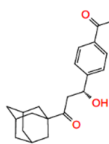
title: C21H26O3
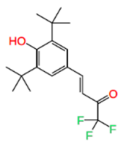
title: C18H23F3O2
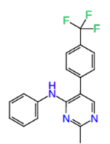
title: C18H14F3N3
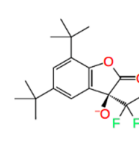
title: C17H21F3O3
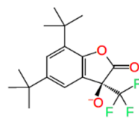
title: C17H21F3O3
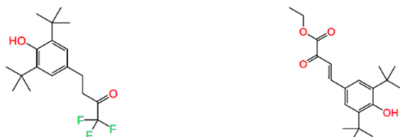
title: C18H25F3O2
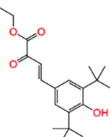
title: C20H28O4
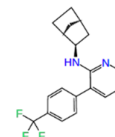
title: C18H18F3N3
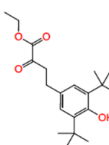
title: C20H30O4

title: C18H20F3N3
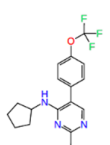
title: C17H18F3N3O
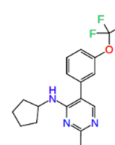
title: C17H18F3N3O
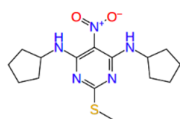
title: C15H23N5O2S
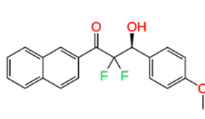
title: C20H16F2O3
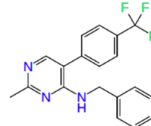
title: C19H16F3N3
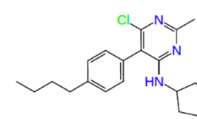
title: C20H26ClN3
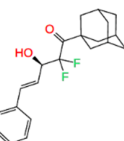
title: C21H24F2O2
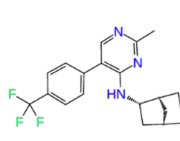
title: C19H20F3N3
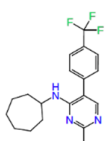
title: C19H22F3N3
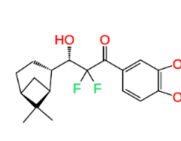
title: C19H22F2O4
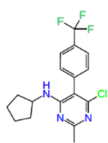
title: C17H17ClF3N3
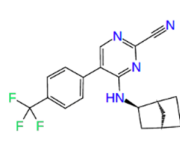
title: C19H17F3N4
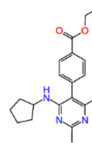
title: C19H22ClN3O2
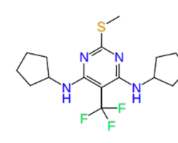
title: C16H23F3N4S
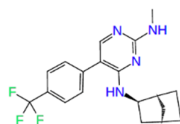
title: C19H21F3N4
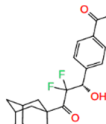
title: C21H24F2O3
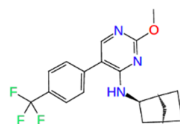
title: C19H20F3N3O
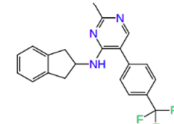
title: C21H18F3N3

Table S2. *Cont.*
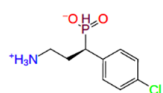
title: C9H12ClNO2P
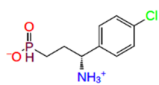
title: C9H12ClNO2P
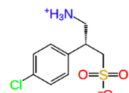
title: C9H12ClNO3S
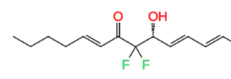
title: C14H20F2O2
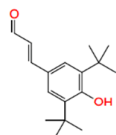
title: C17H24O2
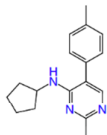
title: C17H21N3
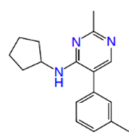
title: C17H21N3
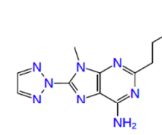
title: C12H16N8
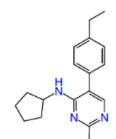
title: C18H23N3
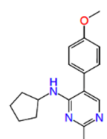
title: C17H21N3O
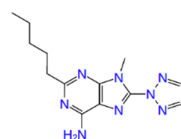
title: C13H18N8
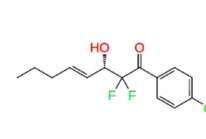
title: C14H15ClF2O2
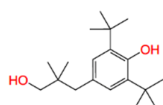
title: C19H32O2
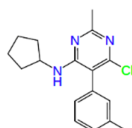
title: C17H20ClN3
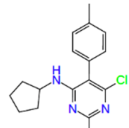
title: C17H20ClN3
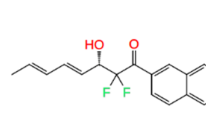
title: C18H16F2O2
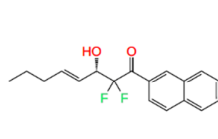
title: C18H18F2O2
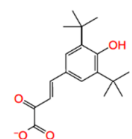
title: C18H24O4
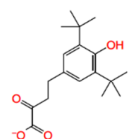
title: C18H26O4
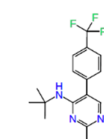
title: C16H18F3N3
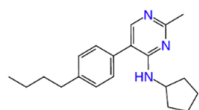
title: C20H27N3
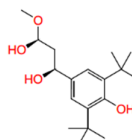
title: C18H30O4

title: C11H13ClF3N3S
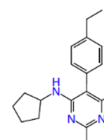
title: C18H22ClN3
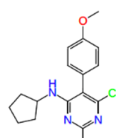
title: C17H20ClN3O
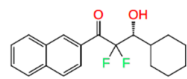
title: C19H20F2O2
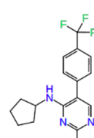
title: C17H18F3N3
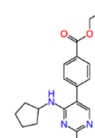
title: C19H23N3O2

Table S2. *Cont.*

title: C17H17ClF3N3O
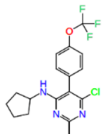
title: C17H17ClF3N3O
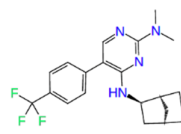
title: C20H23F3N4
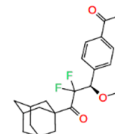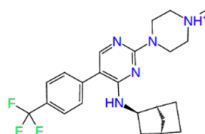
title: C22H26F2O3
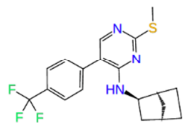
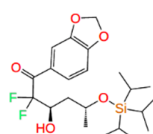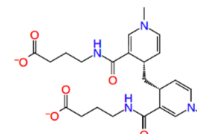title: C19H20F3N3S
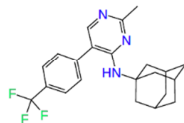
title: C22H24F3N3
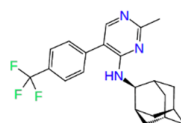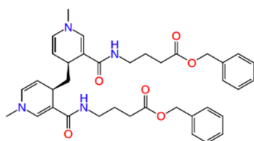
title: C22H24F3N3
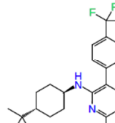
title: C22H28F3N3
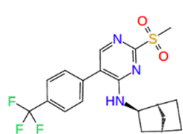
title: C19H20F3N3O2S

title: C23H28F3N5

title: C22H34F2O5Si

title: C23H30N4Na2O6

title: C37H44N4O6

Paper II

Paper III